Thesis

on

DEVELOPMENT OF AUTOMATIC MOVEMENT SETUP FOR GAS METAL ARC WELDING AND INVESTIGATION ON WELDING ASPECTS OF AISI 304 AND AISI 316

Submitted in partial fulfillment of the requirements for the award of degree of

MASTER OF ENGINEERING

IN

PRODUCTION AND INDUSTRIAL ENGINEERING

Submitted by:

VINOD KUMAR

ROLL NO: 821082005

Under the guidance of

ANIRBAN BHATTACHARYA

Assistant Professor
Mechanical Engineering Department
Thapar University, Patiala

MECHANICAL ENGINEERING DEPARTMENT
THAPAR UNIVERSITY
PATIALA-147004, INDIA
DECEMBER- 2013

CERTIFICATE

I hereby declare that the dissertation entitled "**DEVELOPMENT OF AUTOMATIC MOVEMENT SETUP FOR GAS METAL ARC WELDING AND INVESTIGATION ON WELDING ASPECTS OF AISI 304 AND AISI 316**" is an authentic record of my own work carried out in partial fulfillment of the requirement for the award of degree of **Master of Engineering** in **PRODUCTION AND INDUSTRIAL EINGINEERING** under the guidance of **ANIRBAN BHATTACHARYA**, Assistant Professor, MED, Thapar University, Patiala.

Vinod Kumar

Date: 03-1-2014

VINOD KUMAR

(821082005)

This is to certify that the above statement made by the candidate is correct and true to the best of my knowledge.

Anirban Bhattacharya 03/01/2014

ANIRBAN BHATTACHARYA
Assistant Professor
Mechanical Engineering Department
Thapar University, Patiala-147004

Countersigned By:-

Dr. Ajay Batish
Professor and Head
Mechanical Engineering Department
Thapar University, Patiala-147004

Dr. S. K. Mohapatra
Dean of Academic Affairs
Thapar University, Patiala-147004

ACKNOWLEDGEMENT

Though only my name appears on the cover of this dissertation, a lot of people have contributed to its completion. I owe my gratitude to all those people who have made this dissertation possible and because of whom my post graduate experience has been one that I will cherish forever.

My deepest gratitude is to my supervisor **Anirban Bhattacharya**. I have been amazingly fortunate to have an advisor who gave me the freedom to explore on my own and at the same time the guidance to recover when my steps faltered. He taught me how to question thoughts and express ideas. I am grateful to him for holding me to high research standards and enforcing strict validations for each research result and thus teaching me how to do research.

I thank our head of department Dr. Ajay Batish, whose excellent leadership and administration made this research project very convenient in terms of required staff and nice working conditions. I am extremely thankful to members of distinguished faculty.

I express my sincere thanks to Dr. Harpreet Singh, HOD SMMEE at Indian Institute of Technology, Ropar for allowing me to use the infrastructure of the institute to carry out my research work.

Many friends have helped me stay sane through these years. Their support and care helped me overcome setbacks and keep me centered on my study. I greatly worth their friendship and I deeply appreciate their belief in me.

Most significantly, none of this would have been possible without the love and patience of my family. I would like to express my heartfelt gratitude to my family for their support.

Vinod Kumar

VINOD KUMAR

ABSTRACT

Gas Metal Arc Welding process is leading in the development in arc welding process which is higher productivity and good in quality. An automatic GMAW setup is designed and fabricated to improve the weld quality. The setup is capable of producing straight, neat, uniform width and deposition rate with low spatters.The present study has been done to study the effect of different input parameters on the desired responses in the gas metal arc welding process. The welding aspects like microhardness, impact strength, crystal structure and microstructure of stainless steel (AISI 304 and AISI 316) during GMAW using the three levels of welding current, voltage, gas flow rate and travelling speed to optimize the process following Taguchi experimental design. An automatic gas metal arc welding setup was fabricated to control the speed of welding gun at different levels. The effect of various input parameters on output responses have been analyzed using Analysis of Variance (ANOVA). Surface composition was determined by X-ray diffraction (XRD) analysis and Scanning Electron Microscopy was carried out to study the microstructural properties. Impact test results for AISI 304 stain steel shows that toughness at room temperature mainly depends on the value of welding speed. Toughness is increases with the increase of voltage value up to the highest voltage for AISI 316 stainless steel. Welding speed is the most important parameter in effecting the value of microhardness for AISI 316 stainless steel.

TABLE OF CONTENTS

LIST OF TABLES

LIST OF FIGURES

ABBREVIATIONS

AC	Alternating current
AISI	American Iron and Steel Institute
ANOVA	Analysis of variance
AWS	American welding society
BM	Base metal
DC	Direct current
DCEN	Direct current with negatively charged electrode
DCEP	Direct current with positively charged electrode
GMAW	Gas metal arc welding
GTAW	Gas tungsten arc welding
HAZ	Heat affected zone
HVN	Vickers hardness number
ISO	International organization for standardization
SAW	Submerged arc welding
SEM	Scanning Electron Microscopy
TIG	Tungsten inert gas welding
WM	Weld metal
XRD	X-Ray Diffraction

CHAPTER 1

INTRODUCTION

1.1 INTRODUCTION

Welding is a type of manufacturing process which is primarily used for joining metal parts especially larger lengths of standard sections when several pieces are to be joined together to fabricate a desired structure.

Welding is the art of joining metals and plastics by such methods which do not employ fasteners and adhesives.

Welding can be defined as ‘a process of joining two similar or dissimilar metals by fusion, with or without the application of pressure and with or without the use of filler metal’ [1]. The fusion of metal takes place by means of heat and is obtained from electric arc, electric resistance, chemical reaction, friction or radiant energy. The result is a continuity of homogeneous material of the composition and characteristics of two parts which are being joined together as shown in the figure 1.1.

Figure 1.1: Welding process [2]

1.2 CLASSIFICATION OF WELDING PROCESSES

Most of the welding processes utilize heat and/or pressure for making a weld joint. Based on the method of heat generation and its application the welding processes can be grouped into two main classes. Under these classes there are a number of welding processes with special characteristics and fields of applications. Figure 1.2 shows all significant welding and allied processes which are used in the industry.

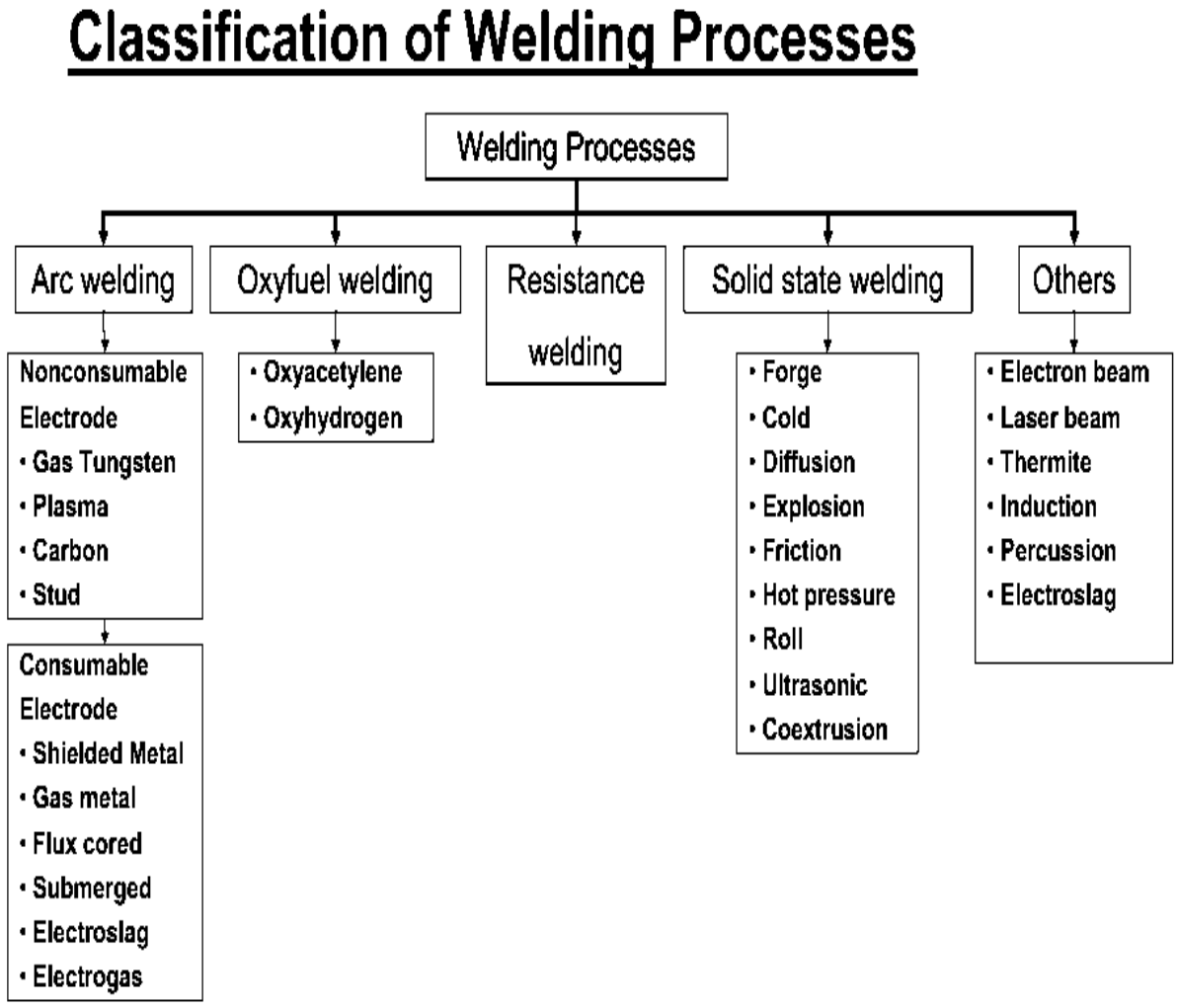

Figure 1.2: Classification of welding processes [3]

1.3 GAS METAL ARC WELDING

Gas metal arc welding (GMAW or Metal Inert Gas, MIG welding) is an electric arc welding process which joins metals by heating them with an arc established between a continuous filler metal (consumable) electrode and the work. Shielding of the arc and molten weld pool

is obtained entirely from an externally supplied gas or gas mixture as shown in figure 1.3. The process is sometimes referred to as MIG or CO_2 welding. Recent developments in the process include operation at low current densities and pulsed direct current, application to a broader range of materials, and the use of reactive gases, particularly CO_2, or gas mixtures. This latter development has led to the formal acceptance of the term GMAW for the process because both inert and reactive gases are used. The term MIG welding is still more commonly used.

Figure 1.3: Gas metal arc welding [2]

MIG welding is operated in semiautomatic, machine, and automatic modes. It is utilized particularly in high production welding operations. All commercially important metals such as carbon steel, stainless steel, aluminum, and copper can be welded with this process in all positions by choosing the appropriate shielding gas, electrode, and welding conditions.

1.4 HISTORY

Many different energy sources can be used for welding, including a gas flame, an electric arc, a laser, an electron beam, friction, and ultrasound. While often an industrial process, welding may be performed in many different environments, including open air, under water and in outer space. Welding is a potentially hazardous undertaking and precautions are required to avoid burns, electric shock, vision damage, inhalation of poisonous gases and fumes, and exposure to intense ultraviolet radiation. Until the end of the 19^{th} century, the only welding process was forge welding, which blacksmiths had used for centuries to join iron and steel by

heating and hammering. Arc welding and oxyfuel welding were among the first processes to develop late in the century, and electric resistance welding followed soon after. Welding technology advanced quickly during the early 20th century as World War I and World War II drove the demand for reliable and inexpensive joining methods. Following the wars, several modern welding techniques were developed, including manual methods like shielded metal arc welding, now one of the most popular welding methods, as well as semi-automatic and automatic processes such as gas metal arc welding, submerged arc welding, flux-cored arc welding and electroslag welding. Developments continued with the invention of laser beam welding, electron beam welding, electromagnetic pulse welding and friction stir welding in the latter half of the century. Today, the science continues to advance. Robot welding is commonplace in industrial settings, and researchers continue to develop new welding methods and gain greater understanding of weld quality.

1.5 EQUIPMENT FOR GMAW

Gas metal arc welding equipment consists of a welding gun, a power supply, a shielding gas supply, and a wire-drive system which pulls the wire electrode from a spool and pushes it through a welding gun (see figure 1.4). A source of cooling water may be required for the welding gun. In passing through the gun, the wire becomes energized by contact with a copper contact tube, which transfers current from a power source to the arc. While simple in principle, a system of accurate controls is employed to initiate and terminate the shielding gas and cooling water, operate the welding contactor, and control electrode feed speed as required. The basic features of MIG welding equipment are shown in figure. The MIG process is used for semiautomatic, machine, and automatic welding. Semiautomatic MIG welding is often referred to as manual welding.

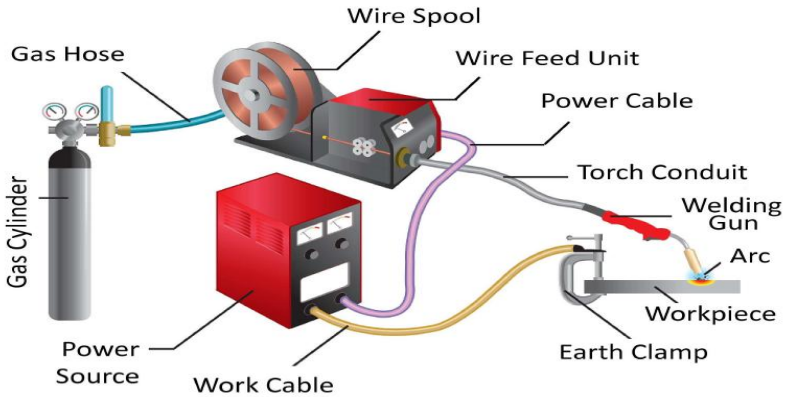

Figure 1.4: Gas metal arc welding setup [4]

Two types of power sources are used for MIG welding: constant current and constant voltage.

Constant current power supply: With this type, the welding current is established by the appropriate setting on the power supply. Arc length (voltage) is controlled by the automatic adjustment of the electrode feed rate. This type of welding is best suited to large diameter electrodes and machine or automatic welding, where very rapid change of electrode feed rate is not required. Most constant current power sources have a drooping volt-ampere output characteristic. However, true constant current machines are available. Constant current power sources are not normally selected for MIG welding because of the control needed for electrode feed speed. The systems are not self-regulating.

Constant voltage power supply: The arc voltage is established by setting the output voltage on the power supply (see figure 1.5). The power source will supply the necessary amperage to melt the welding electrode at the rate required to maintain the present voltage or relative arc length. The speed of the electrode drive is used to control the average welding current. This characteristic is generally preferred for the welding of all metals. The use of this type of power supply in conjunction with a constant wire electrode feed results in a self-correcting arc length system.

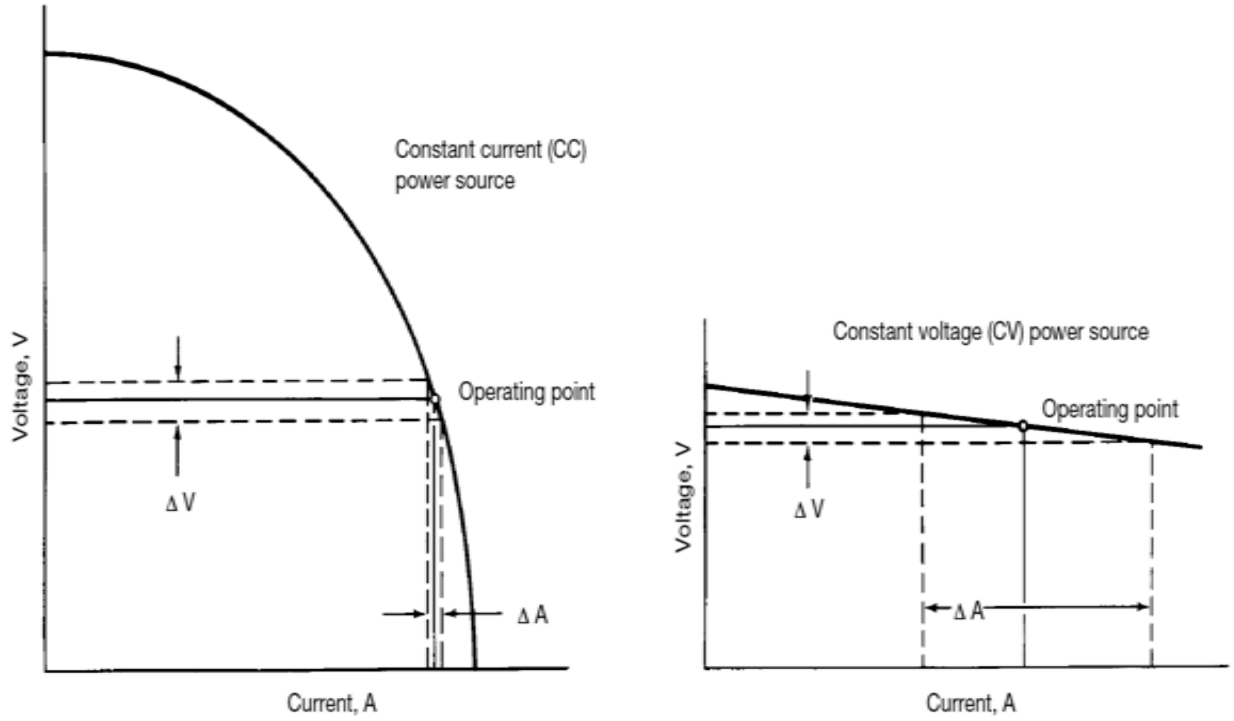

Figure 1.5: Static volt-ampere characteristics [5]

Welding Guns: Welding guns for MIG welding are available for manual manipulation (semiautomatic welding) and for machine or automatic welding. Because the electrode is fed continuously, a welding gun must have a sliding electrical contact to transmit the welding current to the electrode. The gun must also have a gas passage and a nozzle to direct the shielding gas around the arc and the molten weld pool. Cooling is required to remove the heat generated within the gun and radiated from the welding arc and the molten weld metal. Shielding gas, internal circulating water, or both, is used for cooling. An electrical switch is needed to start and stop the welding current, the electrode feed system, and shielding gas flow.

Semiautomatic Guns: Semiautomatic, hand-held guns are usually similar to a pistol in shape. Sometimes they are shaped similar to an oxyacetylene torch, with electrode wire fed through the barrel or handle as shown in the figure 1.6. In some versions of the pistol design, where the most cooling is necessary, water is directed through passages in the gun to cool both the contact tube and the metal shielding gas nozzle. The curved gun uses a curved current-carrying body at the front end, through which the shielding gas is brought to the nozzle. This type of gun is designed for small diameter wires and is flexible and maneuverable. It is suited for welding in tight, hard to reach corners and other confined places. Guns are equipped with metal nozzles of various internal diameters to ensure adequate gas shielding.

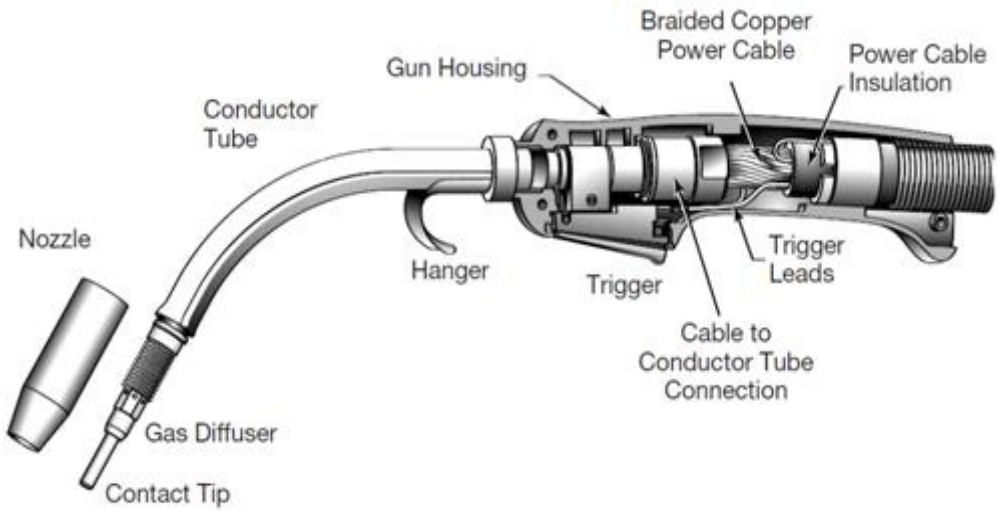

Figure 1.6: GMAW torch cut section [5]

Air cooled Guns: Air-cooled guns are available for applications where water is not readily obtainable as a cooling medium. These guns are available for service up to 600 amperes, intermittent duty, with carbon dioxide shielding gas. However, they are usually limited to 200 amperes with argon or helium shielding. The holder is generally pistol-like and its operation is similar to the water-cooled type. Three general types of air-cooled guns are available.

Water Cooled Guns: Water-cooled guns for manual MIG welding similar to gas-cooled types with the addition of water cooling ducts. The ducts circulate water around the contact tube and the gas nozzle. Water cooling permits the gun to operate continuously at rated capacity and at lower temperatures. Water-coded guns are used for applications requiring 200 to 750 amperes. The water in and out lines to the gun add weight and reduce maneuverability of the gun for welding.

1.6 MODES OF METAL TRANSFER IN GMAW

Filler metal can be transferred from the electrode to the work in two ways: when the electrode contacts the molten weld pool, thereby establishing a short circuit, which is known as short circuiting transfer (short circuiting arc welding); and when discrete drops are moved across the arc gap under the influence of gravity or electromagnetic forces. Drop transfer can be either globular or spray type.

Shape, size, direction of drops (axial or non-axial), and type of transfer are determined by a number of factors. The factors having the most influence are:

1. Magnitude and type of welding current.

2. Current density.

3. Electrode composition.

4. Electrode extension.

5. Shielding gas.

6. Power supply characteristics.

Axially directed transfer refers to the movement of drops along a line that is a continuation of the longitudinal axis of the electrode. Non-axially directed transfer refers to movement in any other direction.

1.6.1 Short Circuiting Transfer

Short circuiting arc welding uses the lowest range of welding currents and electrode diameters associated with MIG welding. This type of transfer produces a small, fast-freezing weld pool that is generally suited for the joining of thin sections, out-of-position welding, and filling of large root openings. When weld heat input is extremely low, plate distortion is small. Metal is transferred from the electrode to the work only during a period when the electrode is in contact with the weld pool. There is no metal transfer across the arc gap.

1.6.2 Globular Transfer

With a positive electrode (dcrp), globular transfer takes place when the current density is relatively low, regardless of the type of shielding gas. However, carbon dioxide (CO_2) shielding yields this type of transfer at all usable welding currents. Globular transfer is characterized by a drop size of greater diameter than that of the electrode.

Globular, axially directed transfer can be achieved in a substantially inert gas shield without spatter. The arc length must be long enough to assure detachment of the drop before it contacts the molten metal. However, the resulting weld is likely to be unacceptable because of lack of fusion, insufficient penetration, and excessive reinforcement.

1.6.3 Axial Spray Transfer

In a gas shield of at least 80 percent argon or helium, filler metal transfer changes from globular to spray type as welding current increases for a given size electrode. For all metals, the change takes place at a current value called the globular-to-spray transition current.

Spray type transfer has a typical fine arc column and pointed wire tip associated with it. Molten filler metal transfers across the arc as fine droplets. The droplet diameter is equal to or less than the electrode diameter. The metal spray is axially directed. The reduction in droplet size is also accompanied by an increase in the rate of droplet detachment. Metal transfer rate may range from less than 100 to several hundred droplets per second as the electrode feed rate increases from approximately 42 to 339 mm/s.

1.6.4 Pulsed Spray Transfer

Pulsed spray metal transfer, known by the acronym GMAW-P is a highly controlled variant of axial spray transfer, in which the welding current is cycled between a high peak current to a low background current level. Metal transfer occurs during the high energy peak level in the form of a single molten droplet.

This mode employs electrode diameters from 0.8-1.6 mm solid wire electrodes. The welding current alternates between a peak current and a lower background current, and this controlled dynamics of the results in a lower average current than is found with axial spray transfer. The time which include the peak current and the background current, is a period, and the period is known as a cycle (Hz).

1.7 WELDING PARAMETERS

During a manual welding operation, the welder has to have control over the welding variables, which affect the weld penetration, bead geometry and the overall weld quality. A proper selection of welding variables will increase the chances of producing welds of a satisfactory quality. However, these variables are not completely independent and changing one variable generally requires the changing of some of the others in order to achieve the desired result. When all these variables are in proper balance, the welder can deposit higher quality weld metal and produce sound welds. The selection of the welding variables should be made after the base metal, filler metal and joint design have been determined. The welding process variables mainly affect the geometry of the weld bead such as the penetration, bead reinforcement, bead width and the deposition rate, which is the weight of the metal deposited per unit of time. These variables are as follows:

a) Welding Current
b) Welding Voltage
c) Travel Speed
d) Wire Electrode Size
e) Type of Shielding Gas
f) Electrode Extension
g) Electrode Angle
h) Weld Joint Position

1.7.1 Welding Current

The value of welding current used in MIG has the greatest effect on the deposition rate, the weld bead size, shape and the penetration. In MIG welding, metals are generally welded with direct current polarity electrode positive (DCEP, opposite to TIG welding), because it provides the maximum heat input to the work and therefore a relatively deep penetration can be obtained. The oxide removal effect of the DCEP, which is very important in the welding of aluminium and magnesium alloys, contributes to clean the weld deposit. When all the other welding parameters are held constant, increasing the current will increase the depth and the width of the weld penetration and the size of the weld bead. In a constant voltage system, the wire feed speed and welding current is controlled by the same knob. As the wire feed speed is increased the welding current also increases, resulting in increases in the wire melt-off rate and the rate of deposition. Each electrode wire size and type has a minimum and maximum current range to give the best results. An excessively low welding current for a given electrode size produces a poor penetration and the pileup of the weld metal on the surface of the base metal transfer by the arc is sluggish, the bead is rough and reinforcement high. If the current is too high, the size of the weld bead is large and the excessive deep penetration that wastes the filler metal causes burn-through and undercut. Too high or too low welding current also affects the mechanical properties of the weld metal and the tensile strength. The ductility is reduced and porosity, excessive oxides and impurities can be seen in the weld metal.

1.7.2 Welding Voltage (Arc Length)

The arc length is one of the most important variables in MIG that must be held under control. When all the variables such as the electrode composition and sizes, the type of shielding gas and the welding technique are held constant, the arc length is directly related to the arc voltage. For example, normal arc voltage in carbon dioxide and helium is much higher than those obtained in argon. A long arc length disturbs the gas shield; the arc tends to wander and thus affects the bead surface of the bead and the penetration. In MIG the arc voltage has a decided effect upon the penetration, the bead reinforcement and bead width. By increasing the arc voltage the weld bead becomes flatter and wider, the penetration increases until an optimum value of the voltage is reached, at which time it begins to decrease. High and low voltages cause an unstable arc. Excessive voltage causes the formation of excessive spatter and porosity, in fillet welds it increases undercut and produces concave fillet welds subject to

cracking. Low voltage produces narrower beads with greater convexity (high crown), but an excessive low voltage may cause porosity and overlapping at the edges of the weld bead.

1.7.3 Travel Speed

The travel speed is the rate at which the arc travels along the work-piece. It is controlled by the welder in semiautomatic welding and by the machine in automatic welding. The effects of the travel speed are just about similar to the effects of the arc voltage. The penetration is maximum at a certain value and decreases as the arc speed is varied. For a constant given current, slower travel speeds proportionally provide larger beads and higher heat input to the base metal because of the longer heating time. The high heat input increases the weld penetration and the weld metal deposit per unit length and consequently results in a wider bead contour. If the travel speed is too slow, unusual weld build-up occurs, which causes poor fusion, lower penetration, porosity, slag inclusions and a rough uneven bead. Increasing the travel speed shows opposite effects: Less weld metal gets deposited with lower heat input that produces a narrower bead with less penetration. Excessively high speeds cause high spatter and undercutting and the beads show an irregular form because of very little weld metal deposit per unit length of weld. The travel speed, which is an important variable in MIG, just like the wire speed (current) and the arc voltage, is chosen by the operator according to the thickness of the metal being welded, the joint design, joint fit-up and welding position.

1.7.4 Electrode Size

The electrode diameter influences the weld bead configuration (such as the size), the depth of penetration, bead reinforcement and bead width and has a consequent effect on the travel speed of welding. As a general rule, for the same welding current (wire feed speed setting) the arc becomes more penetrating as the electrode diameter decreases. A larger electrode in general requires a higher minimum current for the same characteristics. To get the maximum deposition rate at a given current, one should have the smallest wire possible that provides the necessary penetration of the weld. The larger electrode diameters create welds with less penetration but wider in width. The choice of the wire electrode diameter depends on the thickness of the work-piece to be welded, the required weld penetration, the desired weld profile and deposition rate, the position of welding and the cost of electrode wire. For many purposes small diameter wires are good for thin sections and for welding in vertical and overhead positions. Large diameter wires are desirable for heavy sections and hard surfacing and built-up works with low current applications because of less weld penetration.

1.7.5 Type of Shielding Gas

The range of viable shielding gas options is limited by the need to satisfy the criteria listed above. Some of the common gases are listed below.

Argon

Argon is one of the most widely used shielding gases for GTAW welding. It is totally inert and has a high density relative to air. The low ionization potential facilitates arc striking and stability.

Helium

Helium is chemically inert, has a lower density than air and requires a higher arc voltage (at the same current and arc length) than argon. The resultant increase in power produces increased heat input and fusion area although lower depth-to-width ratios are normally experienced. The cost of helium is considerably higher than that of argon, but the welding speeds that are usually obtained make it a viable option, particularly for high-conductivity materials.

Carbon dioxide

Carbon dioxide is chemically active, but has a higher density than air. It can dissociate in the arc to release oxygen and carbon monoxide and this can result in a reduction in the weld metal content of elements such as silicon, manganese and titanium and an increase in carbon. Because of its chemical activity its use is restricted to GMAW welding of steel. The arc voltage is 1–2 V higher in CO_2 (for an equivalent current and arc length) than that found in argon-based mixtures and the heat input is slightly higher resulting in increased fusion. Transfer behaviour, operating tolerances and arc stability are generally poor, especially at high currents.

Oxygen

Oxygen is not used as a shielding medium, but is an important constituent of many gas mixtures. When added to argon it improves arc stability, reduces the surface tension of steel and improves arc root behaviour. The reduced surface tension improves metal transfer and bead shape. Like CO_2, the use of oxygen will decrease the recovery of the more reactive alloying elements.

Hydrogen

Hydrogen increases the arc voltage and heat input when mixed with argon. Its use is usually restricted to the GTAW and plasma processes, and to materials that do not suffer any adverse chemical or physical changes in its presence. Its chemically reducing properties may be used to advantage on austenitic stainless steels where it promotes wetting and produces improved weld bead finish.

As mentioned before, different types of shielding gases are used in the MIG process, and the melting rate, bead profile and penetration of weld changes due to gas type. At the same time, the type of the shielding gas affects the spattering, welding speed and the mode of metal transfer and thus the overall mechanical properties of the weld metal. Pure carbon dioxide or argon-carbon dioxide and argon-oxygen mixed gases are generally used for welding of iron based metals. For the same welding current the high melting rate, greater penetration, large and convex weld profile will be obtained when carbon dioxide is chosen as a shielding gas. When pure carbon dioxide shielding is used, a complex interaction of forces occurs around the metal droplets at the wire tip. These unbalanced forces cause large, unstable droplets to grow and transfer to the molten metal in a random action. This is the reason for an increase in spatter along the weld bead. Also pure carbon dioxide generates more fumes. Argon, helium and argon-helium mixtures are used in many applications for welding non-ferrous metals and alloys. These inert gas mixtures provide lower melting rate, smaller penetration and narrow bead contour. Argon is cheaper than helium and helium-argon mixtures and it also produces fewer spatters. Unlike argon, helium improves the weld bead penetration profile (higher melting rate, deeper penetration and convex surface profile). But, when helium is used, welding voltage rises for the same arc length and the consumption of shielding gas increases more than when argon is used.

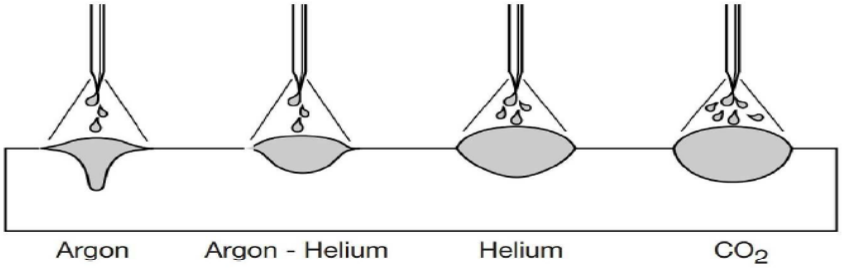

Figure 1.7: Effect of different gases on weld bead geometry [5]

1.7.6 Electrode Extension (Stickout)

The electrode extension or stickout is the length of the filler wire between the end of the contact tip and the end of the electrode. This is the only section of the wire electrode which conducts the welding current. Therefore an increase of the extension results in an increase of its electrical resistance and also causes the electrode temperature to rise because of the resistance heating. This preheat can reach a temperature value approaching the melting point of the electrode so that an arc heat of small intensity will be enough for it to become molten at the point of welding.

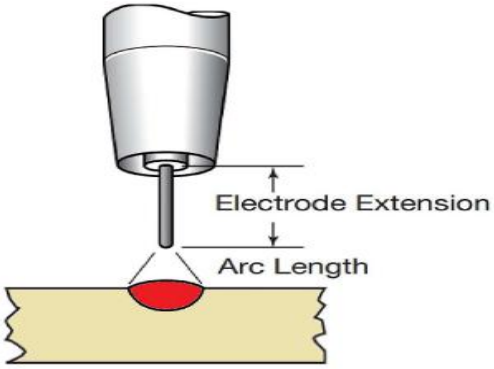

Figure 1.8: Electrode extension [5]

In a constant voltage power source, the increase of the resistance of the stickout produces a greater voltage drop from the contact tip to the work. The CV power source compensates for the higher voltage drop by decreasing the current, which produces a smaller arc resulting in a narrow, high-crowned weld bead with shallow penetration. Decreasing the stickout shows just the opposite effect, preheating of the wire is reduced, the voltage drop is not as high and the power source provides more current than the heat input to work-piece which causes an increase in the penetration. Typical electrode extensions range from 6 to 13 mm for short circuiting transfers and from 13 to 25 mm for other types of metal transfers. Longer extensions are used for flux cored electrodes. The welder can increase the electrode extension, which reduces the welding current and the penetration to make adjustments in the characteristic of the weld bead to compensate for changes over a short length of the weld such as an area where the root opening is excessively wide or narrow.

1.7.7 Electrode Position

The position of the wire electrode with respect to the weld joint, affects the weld bead shape and the penetration to a greater extent than the arc voltage and the travel speed. The position of the wire electrodes is defined by means of two angles which are called ‘work’ and ‘travel’ angles.

1.8 WELDABILITY

The **weldability**, also known as **joinability**, of a material refers to its ability to be welded. Many metals and thermoplastics can be welded, but some are easier to weld than others.

A material's weldability is used to determine the welding process and to compare the final weld quality to other materials.

Weldability is often hard to define quantitatively, so most standards define it qualitatively. For instance the International Organization for Standardization (ISO) defines weldability in ISO standard 581-1980 as: ‘Metallic material is considered to be susceptible to welding to an established extent with given processes and for given purposes when welding provides metal integrity by a corresponding technological process for welded parts to meet technical requirements as to their own qualities as well as to their influence on a structure they form’.

1.9 STAINLESS STEEL

They are also known as Corrosion Resistant Steels. Their principal alloying element is chromium while some other elements like nickel, manganese etc. can also be present in small amounts. Since substantial amount of chromium is present in them they cannot be considered as low alloy steels. It is seen that an addition of just 4 to 6 percent chromium to low carbon steels renders them fairly required to be highly corrosion resistant with very superior appearance, a very high percentage of chromium (usually > 12 %) is added. The chromium reacts with the oxygen to form a strong layer of Chromium Oxide on the surface of the metal which is responsible for offering the resistance to corrosion. Stainless steels carrying more than 12 % chromium are known as True Stainless Steels.

1.9.1 Welding of stainless steels

Stainless steels can be classified according to the structure of their matrix, thus

- Austenitic stainless steels
- Ferritic stainless steels
- Martensitic stainless steels
- Precipitation hardening stainless steels
- Duplex stainless steels

Heat conductivity of Cr-Ni steels is about 50 percent less than that of mild steel. Hence concentration of heat is obtained resulting in less heat input for a given job. As a general rule about 10 per cent less current is used with stainless steel electrodes as compared to mild steel.

Melt off rates of stainless steel electrodes are higher than the rates for M.S. electrodes. This is another reason for slightly lower current being used in stainless steel welding. Thermal expansion of Cr-Ni steels is about 50 percent greater than for M.S. This will increase the chance of warping and buckling. Thus suitable fixture must be used while welding stainless steels. Electrical resistance is 6 to 12 times higher than that of M.S. and hence this may cause over heating in the electrodes. Therefore shorter electrodes are normally used to reduce electrode heating.

We will concentrate our discussion regarding weldability of only austenitic stainless steel which is the object of this experimental work.

1.9.2 Austenitic stainless steels

Standard austenitic stainless steels contain chromium in the range of 16 to 26 percent and nickel 6 to 22 percent. Typical AISI types of stainless steel and their compositions are given in table 1.1.

Table 1.1: Typical AISI type of stainless steels. (Wt %) [8]

Type→ Composition↓	301	302	304	310	316	321	347	201	202
C%	0.15	0.08	0.08	0.25	0.08	0.08	0.08	0.15	0.15
Cr	16-18	17-19	11-20	24-26	16-18	17-19	17-19	16-18	17-19
Ni	6-8	8-10	8-12	19-22	10-14	9-12	9-13	3-6	4-6
N	0.03	0.03	0.03	0.03	0.03	0.03	0.03	0.25	0.25
Ti	-	-	-	-	-	5C	-	-	-
Nb	-	-	-	-	-	-	10C	-	-
Mo	-	-	-	-	2-3	-	-	-	-
Mn	-	-	-	-	-	-	-	6-8	8-10

1.9.3 Difficulty in welding of Stainless steel

- **Low thermal conductivity and high electrical resistance**: It is a big problem as overheating of SS may result in diffusion of metal. It may be overcome by using low values of current and using electrode of shorter lengths.
- **Carbide Precipitation**: The austenitic grades are non-hardening type and welding normally does not adversely affect the strength and ductility of the deposit. However, one detrimental effect of heating of a Cr – Ni steel is carbide precipitation at the grain boundaries, resulting in reduced corrosion resistance. A fine film of Cr-rich carbides containing as much as 90 % Cr, taken from the layer of metal next to the grain boundary will get precipitated along the grain boundary. Precipitation of intergranular chromium carbides is accelerated by an increase in temperature within the sensitized range and by an increase in time at that temperature. Carbide precipitation can be controlled by using stabilized steels by adding columbium and titanium which have greater affinity for carbon than chromium.

  Rapid quench may minimize the carbide precipitation: however, this may not be possible in all cases, especially in thick sections.

  Limiting the carbon content to a maximum of 0.03 %, known as extra low carbon stainless steel, can help avoiding the harmful carbide precipitation.

  Post weld solution annealing – it puts carbide back into solution and restores corrosion resistance. Austenitic stainless steel stabilized with niobium plus tantalum or titanium and welded with stabilized filler metal gives good strength and corrosion properties.

- **Cracking:** Interdendritic cracking in the weld area that occurs before the weld cools to room temperature is known as hot cracking or microfissuring. When metal with a wholly austenitic structure is more susceptible to microfissuring that weld metals with a duplex structure of delta ferrite in austenite. Susceptibility can be reduced by a small increase in carbon or nitrogen content or by a substantial increase in manganese content.

  Cracking can be avoided: Weld metal should have a ferrite content of atleast 3 to 5 ferrite number (FN) and hence filler metal of suitable composition is to be selected. To determine suitable composition and the corresponding ferrite number the Schaeffler diagram is made use of which is as shown below:

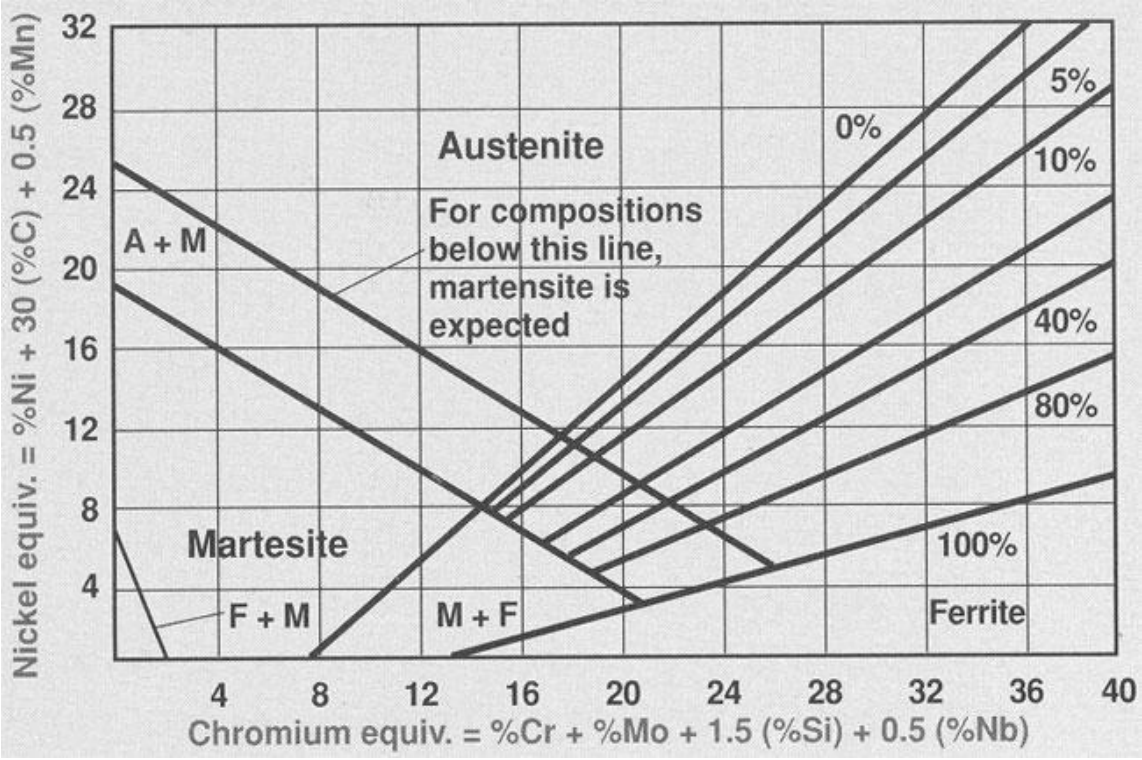

Figure 1.9: Schaeffler diagram [6]

Nitrogen acts as a solid solution strengthener and increases the annealed yield strength to approximately twice that of the conventional austenitic steels. Specific attention should be paid to the control of nitrogen when welding these grades. A significant reduction in nitrogen will result in a loss of strength and corrosion resistance. An increase in the nitrogen content is likely to result in weld porosity or weld hot cracking.

CHAPTER 2
LITERATURE SURVEY

A lot of research work has been carried out to investigate the strength and other mechanical properties of different kinds of steel welded by GMAW process. In this chapter literatures on GMAW are presented in four categories as given under-

1. Influence of process parameters
2. Study of mechanical properties and microstructure
3. Effect of different metal transfer modes
4. Effect of shielding gas

2.1 INFLUENCE OF PROCESS PARAMETERS

Kannan et al. [10] carried out an experimental study to develop mathematical models to predict clad bead geometry and its shape during GMAW of austenitic stainless steel deposited. They conducted experiments using four-factor, five-level central composite rotatable design with full replication technique. The mathematical models were developed using multiple regression method. Their study concluded that weld bead width, height of reinforcement and depth of penetration increases with increase in wire feed rate and decreases with the increase in welding speed.

Ibrahim et al. [11] studied the effects of different parameters on welding penetration, microstructural and hardness measurement in mild steel of 6 mm thick using the robotic gas metal arc welding. Arc voltage, welding current and welding speed were varied to study the effect on penetration, microstructure and hardness. Shielding of CO_2 gas was used with 1.2 mm diameter electrode wire and 12 mm nozzle to work distance. The depth of penetration increases with increase of welding current. They conclude that voltage and welding speed also effects the penetration. The value of hardness is decreases with the increase of welding current at weld bead.

Karadeniz et al. [12] studied the effect of various welding parameters on penetration of steel by robotics gas metal arc welding. The welding current, welding voltage and welding speed

were three variable parameters. They observed increase in welding current increases the depth of penetration.

Grad et al. [13] studied the acoustic waves produce by the GMAW which contains information about the behavior of arc column, the molten pool and droplet transfer. The pressure of produced sound increases with the arc length and welding current. Welding was performed by using consumable electrode of dia. 1.2 mm with two different shielding gases CO_2 and gas mixture (90% Ar and 10% CO_2). Acoustic waveforms were detected in the surrounding air by a microphone and in work piece was measured by a piezoelectric sensor. They concluded higher current, reignition produce louder sound due to which greater energy released in the arc column. The wire extension length has substantial influence only at lengths larger than 12 mm.

Modenesi et al. [14] used a numerical model to include the effects of the temperature on physical properties of the electrode wire. In this model they observed that temperature profile exhibits two characteristics region first longer one which corresponds to the bulk of wire and heated mainly due to electrical resistive heating. Second corresponds to a very narrow region close to the arc and mainly heated by it. At the end they concluded that the values of current were associated with heating of electrode by arc and fraction of filler material being molten which was vaporized by arc. The arc was observed through high speed video-cinematography.

Tham et al. [15] studied the correlation between welding parameters and bead geometry of 3F fillet joint welding by articulate robot GMAW in downhill position. A calculator was developed to display the values of weld bead geometry for any value of welding parameter. They observed that heat input is influenced by welding parameters and it is proportional to current and voltage, but inversely proportional to the welding speed.

Nansaarng et al. [16] studied the effect of process parameters of GMAW on microstructures and mechanical properties of stainless steel 304 with factorial design experiment. They concluded that current, welding speed and shielding gas affects the ultimate tensile strength, yield strength and hardness. The results revealed that microstructure of higher and lower ultimate tensile strength has columnar dendrite structure. The shape of dendrite and grain growth in the heat affected zone was smaller of higher on the ultimate tensile strength than lower on tensile strength. Chromium carbide ($Cr_{23}C_6$) presented in all conditions.

Kaewkuekool et al. [17] studied the different process parameters affecting the mechanical properties of dissimilar welding between AISI 304 and low carbon steel by GMAW. The results revealed that ultimate tensile strength and elongation for dissimilar welding significantly different for interaction affect of filler metal, welding speed and current at the level of 0.01. At end they concluded that current, welding speed and filler metal affected the mechanical properties of dissimilar welding between stainless steel and low carbon steel.

Sudhakaran et al. [18] established a relationship between welding input parameters and depth of penetration for gas tungsten arc welding of 202 grade stainless steel plates with five level four factor central composite rotatable design experiments. A mathematical model was developed to correlate the process parameters to depth of penetration and compared with the experimental results. The predicted depth of penetration was compared with the experimental results and the deviation falls within the accepted limit of 95% confidence level.

Giridharan et al. [19] carried out optimization of pulsed gas tungsten arc welding (pulsed GTAW) process parameters to obtain optimum weld bead geometry with full penetration in welding of stainless steel 304L sheets of 3 mm thickness. Optimum pulsed GTAW process and optimum weld bead parameters for welding of 3 mm thick stainless steel 304L sheets were found using a quasi-Newton numerical optimization technique. They concluded that welding speed and pulse current were the most important influencing process variable on bead parameters. While pulse current duration was the least important among the three process parameters considered in this study.

Vasudevan et al. [20] studied the process parameters that were varied to obtain partial penetration welds with different weld bead geometries and the process variables. An automatic GTAW machine with cold wire feeder was used for making partial penetration welds on 12 mm thick 316LN stainless steel plates. They concluded that good correlation can be obtained between the measured and the regression model predicted weld-bead shape parameters. Optimum process parameters were obtained by minimising the objective function.

2.2 STUDY OF MECHANICAL PROPERTIES AND MICROSTRUCTURE

Shang et al. [21] studied the Mg alloy and Al alloy are joined by using cold metal transfer welding with pure copper as the filler metal. The microstructure of the weld joint was study

by optical microscopy, scanning electron microscope (SEM), Energy dispersive X-ray (EDX), X-ray diffractive (XRD). Mg alloy side of the joint was etched in a solution of (1 ml oxalic acid, 1 ml nitric acid, 1 ml acetic and 150 ml distilled water). Similarly Al alloy side of the joint was etched in a solution of (2 ml hydrofluoric acid, 5 ml nitric acid and 95 ml distilled water). They conclude Mg/Al metals successfully by CMT welding using pure copper filler metal with welding current 129 A, voltage 12 V and wire feed speed 5.7 mm/s. Different Al-Cu intermetallic compounds i.e. AlCu, $CuAl_2$, Cu_9Al_4 were presented in the fusion zone of Al side and Cu based solid solution was generated in weld zone, while Cu_2Mg and Al-Cu-Mg ternary eutectic structure was formed in fusion zone of Mg side

Ruan et al. [22] studied twin wire Metal Inert Gas (MIG) arc welding employing 6 mm thick Al alloy plate partially with SiO_2 activating flux. The micro structural characteristics of the weld joint were investigated using optical, scanning microscopy and energy dispersive spectroscopy. Mechanical properties were studied for micro-hardness and tensile test. They concluded weld joint penetration with SiO_2 flux was about 26% deeper than without SiO_2 flux. There was no obvious difference from the microstructure of the joints with and without SiO_2 flux welded with twin wire MIG. SiO_2 flux did not have any obvious effect on the micro-hardness and strength of the weld joint.

Zumelzu et al. [23] studied the mechanical behavior of welded joints of AISI 316L by considering the effect of the amount of ferrite, phase changes and chemical heterogeneity. The hardness test was made cross sectional to the welded bead, and several points were measured on the ends and centre of coupons. SEM technique was used in order to characterize the morphology of the welding. They observed a direct correlation between the thermal contribution and tensile strength. They recommended combination of mechanical trails and microstructural characterization (SEM) are adequate tools to evaluate and predict the behaviour of welded joints.

Klimpel et al. [24] studied four iron and two cobalt based hard facing alloys used as GMAW cored wire surfaced to evaluate their low-stress abrasion resistance. The chemical composition (microstructure) was the most important variable in determining low stress abrasion resistance of the deposit. ASTM G 65 standard test method was used for measurement of abrasion using the dry sand/rubber wheel apparatus. They concluded that the layer one and three of high chromium cast iron and cobalt alloy based alloys had 2.5 times higher abrasion resistance than HARDOX 400 steel.

Torbati et al. [25] studied the autogenous (GTAW) and pulsed rapid arc welding (GMAW) of butting pipelines. GMAW was carried out from the outside of the pipe while GTAW is done from the inside to prevent lack of penetration. The bimetal pipe consists of a corrosion resisting pipe which was telescopically aligned inside a pipe in carbon-manganese material. The tight bonding between the two pipes was achieved by hydraulic expansion. GTAW and GMAW processes were used for this type of steel in oil and gas pipelines. They concluded that helium introduces more heat to the fusion zone and slightly increases penetration. And also observed the adding CO_2 to an argon/helium mix increased penetration, but caused rapid electrode deterioration and eventually arc wandering.

Yilmaz et al. [26] studied the mechanical properties such as tensile properties, hardness and impact properties of 304L and 316L austenitic stainless steel welded by GMAW and GTAW. The results shows that the yield and tensile strength, hardness and impact energy values of 304L and 316L stainless steels welded by GTAW are higher than that of welded by GMAW. The microstructural investigation showed the presence of some δ-ferrite in the weld metal and its ratio was determined by Schaeffer diagram which varied between 9% and 11%. In addition microstructure of the weld metal contained mixture of austenite and ferrite.

Sittichai et al. [27] studied the parameters affecting to mechanical property of austenitic stainless steel AISI 304 during GMAW. It was concluded that shield gas with combination 70% Ar + 25% CO_2 + 5% O_2 was the main factor that affected the ultimate tensile strength for austenitic stainless steel AISI 304. The highest value of elongation was observed significantly at interaction effect between shield gas 69.5% Ar + 25% CO_2 + 5% O_2 + 0.5% He and welding speed at 250 mm/min approximately at 47.94%.

Hung et al. [28] analysed the bead-on-plate by Electron back-scattered diffraction (EBSD) using GMAW welding of stainless steel SUS-304 and TRIP steel. The grain size, texture evolution, misorientation distributions, coincidence site lattice *(*CSL*)* grain boundary of weld metal, HAZ and base metal was observed at various welding conditions. They observed that with increase of heat input the grain size increased at weld metal. While increasing heat input no significant textural change was observed but the characteristics of misorientation distributions and the CSL grain boundary decreased.

Cabrera et al. [29] studied the effect of both the metallic transfer mode (pulsed arc or short circuit) and the O_2 content in the Ar/O_2 gas mixture on the fatigue life under uniaxial conditions of welded joints of 316L stainless steel using GMAW. It was concluded that the

mixture of the shielding gases affect the fatigue life in two different ways firstly through the modification of the radius of curvature at the joint between the welding toe and the base metal, secondly, through a more pronounced degree of oxidation of the alloying elements induced by a higher O_2 content in the mixture. The welded joints obtained under a pulsed arc mode showed a greater fatigue life in comparison with the joints obtained under short circuit for both gas mixtures.

Choi et al. [30] analysed a finite element thermo-mechanical model for temperature and stress with solidification model using GMAW. The effects of welding process parameters on these welding fields were analysed and reported. They concluded that the specific welding energy (welding power/welding speed) controlled the welding process in determining the three weld fields. The increasing the welding power and welding speed showed the same results as decreasing the welding power and welding speed in the thermal, stress and microstructure distributions.

Aval et al. [31] studied temperature field and weld pool geometry by solving the governing equations of heat transfer and fluid flow under quasi-steady state conditions during gas tungsten arc welding of 304 stainless steel. It is concluded that the weld pool geometry predicted by the proposed model was reasonable agreement with experimentally results. The solidification behaviour of the weld pool can be predicted properly by the model predictions. Support of copper backing plate effectively altered the solidified microstructures and cooling rate.

Aval et al. [32] studied the thermal cycles and the grain structure in the weld heat-affected zone (HAZ). A combined heat transfer and fluid flow model was employed to assess the temperature fields during and after welding 304 stainless steel. Then grain structure was observed using the predicted temperature distribution and an analytical model of grain growth. They concluded that the average grain size near the fusion plane was about two to four times larger than the average grain size in the base plate depending on the applied heat input.

2.3 EFFECT OF DIFFERENT METAL TRANSFER MODES

Feng et al. [33] studied the influence of welding velocity on impact behaviour of the globular metal transfer by high speed video photography. The results indicated that the impact location of a droplet depended strongly on the welding velocity. They examined that there was a

critical welding velocity (0.4 m/min) when the welding velocity was lower than this value the droplet impacted inside the weld pool, while the welding velocity was higher than this value the droplet impacted outside the weld pool. When a droplet impacted outside the weld pool, rebounded away from the workpiece surface and formed weld spatters resulting in discontinuous weld appearance.

Ghosh et al. [34] studied the variation in arc characteristics, stability in shielding of arc environment and behavior of metal transfer with a change in pulse parameters by high speed video photography. A comparative study of similar nature was carried out during gas metal arc (GMA) weld deposition in globular and spray transfer modes. The effect of pulse parameters were studied by considering their hypothetically proposed summarized factors Φ. Hypothetical factor Φ defined as a summarized influence of pulse parameters to control the behaviour of arc and metal transfer in pulsed-GMAW process. Then they concluded that increase in Φ from 0.05 to 0.27 enhance the arc length, root, projected diameters of arc and droplet diameter. On the other hand it reduces the arc pressure and velocity of droplet.

Luksa [35] studied two signals momentary arc power and momentary arc resistance. The analysis and the results of analysis were compared with the results of statistic analysis of welding current and voltage. Three forces which control the equilibrium in the arc region were surface tension force, electromagnetic force and gravitational force. During study he tested five artificial disturbances lack of shielding gas, layer of gases on the top surface of joint, layer of paint on the top surface of joint, too narrow root gap and too wide root gap. He observed two types of disturbances that meet the mentioned requirements, imperfection that affects the gas shield of the welding arc and length of wire extension.

2.4 EFFECT OF SHIELDING GAS

Gulenc et al. [36] investigated the mechanical and microstructure properties of the 304L stainless steel welded by MIG welding. Welding was carried out under different shielding gases like argon and varying amount of hydrogen in Ar. Impact test revealed that toughness of the welding increases with increasing hydrogen amount in Ar and welding current. They concluded that addition of hydrogen significantly increases the volume of molten material in the weld pool due to the higher thermal conductivity of argon-hydrogen mixture at temperature at which molecules of hydrogen dissociate.

Kang et al. [37] studied a new technology capable of achieving better quality and high efficiency using the physical properties of weld arc, which is produced by the periodical alternate supply of shielding gases in weld zone. The apparatus called KR301 is used for alternate supply of pure argon and pure helium. The equipment was composed of two parts. One was the electronic part, which controlled the flow rate and supplied frequency of shielding gases and the other is the valve that operated by electromagnetic force for alternate supply of shielding gasses. To evaluate weld shape a 100 mm x 200 mm x 12 mm was prepared and welded using welding conditions under a shielding gas atmosphere supplying (Ar) and (Ar + 67% He) by conventional method and supplying alternately (Ar and He) by alternate method. Specimen end faces are polished and etched using keller solution. They concluded new method produced lowest degree of weld porosity, deepest and broadest weld penetration under the same welding conditions.

Trevisan et al. [38] studied the effect of the pulsed mean welding current and the nitrogen gas concentration on the solidification cracks during the welding of AISI 316L austenitic stainless steels. Welding was done by the flux cored arc welding process with arc pulsing. They concluded that the total length of the solidification cracks reduces with the increase in the level of nitrogen in the deposited metal. As the concentration of nitrogen added to the CO_2 increases, it causes an increase in the level of this element in the deposited metal.

2.5 SUMMARY OF LITERATURE SURVEY

The summary of literature survey carried out during the present work are presented in the tabular form and given in table 2.1.

Table 2.1: Summary of literature survey

AUTHOR [Ref. No.]	INPUT PARAMETERS	WORKPIECE MATERIAL/ PROCESS	OUTPUT
Kannan et al. [10]	Electrode dia-1.2 mm Welding speed- 160, 170, 180 mm/min. Gas - 98% Ar + 2% O_2 Gas flow rate – 16.5 l/min. Thickness- 20 mm Electrode extension- 18, 20, 22, 24, 26 mm Wire feed rate -4, 5, 6, 7, 8 m/min	Low carbon Structural steel/ GMAW	Mathematical model to predict the clad bead geometry
Ibrahim et al. [11]	Electrode dia-1.2 mm Current –90, 150, 210 A Voltage – 22, 26, 30 V Welding speed- 20, 40, 60 cm/min. Gas - CO_2 Gas flow rate – 15 l/min. Thickness- 6 mm Electrode extension- 12 mm Welding robot used	Mild Steel/ GMAW	Microstructure, Vickers hardness,
Karadeniz et al. [12]	Electrode dia-1 mm Current – 95, 105, 115 A Voltage – 22, 24, 26 V Welding speed- 40, 60, 80 cm/min. Gas - 82% Ar + 18% CO_2 Gas flow rate – 15 l/min. Thickness- 2.5 mm Electrode extension- 15 mm Welding robot used	Steel/ GMAW	Microstructure
Grad et al. [13]	Electrode dia-1.2 mm Current – 110-130 A Voltage – 19-21 V Welding speed- 35-40 mm/sec. Gas - CO_2, 90% Ar + 10% CO_2 Gas flow rate – 15 l/min. Thickness- 3 mm	Low carbon steel and medium carbon Steel/ GMAW	Acoustic signals
Modenesi et al. [14]	Electrode dia.- 1.0, 1.2 mm Current –140-340 A Gas - pure argon, Ar-4% CO_2 and Ar-2% CO_2. Flow rate – 12 l/min. Thickness- 12 mm Electrode extension- 13-20 mm	Carbon steel plates/ GMAW	Model for melting rate

AUTHOR [Ref. No.]	INPUT PARAMETERS	WORKPIECE MATERIAL/ PROCESS	OUTPUT
Tham et al. [15]	Electrode dia-1.2 mm Current – 100-250 A Voltage – 18-30 V Welding speed- 15-72 cm/min. Gas - CO_2 at 15 l/min Electrode extension- 13 mm	Carbon steel plates/ GMAW (Articulated welding robot used)	A calculator developed to display value of weld bead geometry for any value of parameter.
Nansaarng et al. [16]	Electrode dia. - 0.8 mm Current - 90, 100, 110 A Welding speed-300, 400, 500 mm/min. GAS- mixture ($Ar+O_2+ H_2+ N_2$) Size-1270 x 1270 x 3 mm Single V shaped groove	AISI 304/ GMAW	Ultimate tensile strength, yield strength, elongation and hardness test.
Kaewkuekool et al. [17]	Current - 120, 150, 180 A Welding speed - 250, 350, 450 mm/min. Size- 60 x 150 x 5 mm	AISI 304 / Low carbon steel/ GMAW	Ultimate tensile strength, elongation
Sudhakaran et al. [18]	Current – 70, 80, 90, 100, 110 A Welding speed-170, 180, 190, 200, 210 mm/min Gas - Argon Size- 100 x 30 x 5 mm Welding gun angle - 50, 60, 70, 80, 90°	AISI 202/ GTAW	The mathematical model developed can be used to predict depth of penetration.
Giridharan et al. [19]	Tungsten electrode dia.- 2.4 mm Pulse current – 180, 188, 200, 212, 220 A Mean arc voltage – 14 V Arc length – 2 mm Welding speed- 11, 12.6, 15, 17.4, 19 cm/min Gas - Argon Size- 100 × 50 × 3 mm	AISI 304L / GTAW	Weld bead geometry
Vasudevan et al. [20]	Tungsten electrode dia-3.2 mm Welding current – 100, 250A Voltage – 13.2, 19.5 V Arc length – 3 mm Welding speed- 0.89, 4.95 mm/sec Gas - Argon Thickness- 12 mm	316LN Austenitic stainless steel/ GTAW	Optimising process parameters using genetic algorithm
Shang et al. [21]	Electrode dia-1.2 mm Current – 114, 125, 129, 134 A Voltage – 11.1, 11.6, 12.0, 12.4 V Welding speed- .45, .55, .65 m/min. Thickness- 3 mm Wire feed rate -5.1, 5.5, 5.7, 5.9 m/min	Al and Mg alloys/ GMAW	Microstructure, microhardness, tensile strength and fracture analysis

AUTHOR [Ref. No.]	INPUT PARAMETERS	WORKPIECE MATERIAL/ PROCESS	OUTPUT
Ruan et al. [22]	Electrode dia-1.2mm Current, former wire – 210, 220 A Current, rear wire – 150, 160 A Voltage Former wire – 19, 21 V Rear wire – 20, 22 V Welding speed- 120 cm/min.	Al alloy/ GMAW	Twin wire welding by robot, microhardness and tensile strength
Zumelzu et al. [23]	Electrode dia-1.2 mm	Stainless steel 316 L /GMAW, SMAW	Tensile strength, hardness, microstructure
Klimpel et al. [24]	Electrode dia-1.6 mm Current - 140, 145, 150, 160, 170 A Voltage – 18.5, 19, 19.5, 20, 20.5, 21, 22, 22.5 V Welding speed- 5 mm/sec. Gas - 97% Ar+2.5% CO_2 Gas flow rate – 18.01 l/min. Thickness- 10 mm Electrode extension- 22 mm Robotized GMA surfacing stand	Stainless steel/ GMAW	Abrasion resistance
Torbati et al. [25]	Electrode dia-1.2 mm Current – 170, 187, 188 A Voltage – 23.4, 23.1 V Welding speed- 200 mm/min. Gas - 75% He + 25% Ar Gas flow rate – 16 l/min. Wall thickness- 14 mm Electrode extension- 12 mm Wire feed rate -9.23, 9.25 m/min	Stainless steel /GTAW, GMAW	Bimetal pipes weld
Yilmaz et al. [26]	Electrode dia-1,1.6 mm Current - GTAW-100,120 A GMAW-150 A GAS- Argon, Ar+O_2 Size-120 x 140 x 5 mm Single v shaped groove One pass for GMAW, Two passes for GTAW	AISI 304L and 316L/ GMAW, GTAW	Tensile, hardness and impact test
Sittichai et al. [27]	Current - 80, 90, 100 A Welding speed- 250, 300, 350 mm/min. GAS- Mixture (Ar+CO_2+O_2) Size- 65 x 80 x 3 mm	AISI 304/ GMAW	Ultimate tensile strength, elongation
Hung Ha et al. [28]	Electrode dia-1.2 mm Current – 160, 180, 200 A Voltage – 23, 25 V Welding speed- 400, 450, 500 mm/min. GAS - Argon Size- 260 x 130 x 3 mm Electrode extension- 14 mm Wire feed rate -680 cm/min	SUS-304 stainless steel/ TRIP steel/ GMAW	Microstructure study

AUTHOR [Ref. No.]	INPUT PARAMETERS	WORKPIECE MATERIAL/ PROCESS	OUTPUT
Cabrera et al. [29]	Electrode dia-1.2 mm Current – 100, 300 A Welding speed- 400 mm/min. Gas - Argon + Oxygen Size -125 x 400 x 6 mm	AISI 316L/ GMAW	Fatigue life
Choi et al. [30]	Electrode dia-1.6 mm Current – 200 A Voltage – 30.3 V Welding speed- 3.387, 5.08, 7.62 mm/sec Gas - Argon + Oxygen Size- 254 x 25.4 x 5.8 mm Wire feed rate -55.5 mm/sec	AISI 304/ GMAW	Microstructure, and stresses
Aval et al. [31]	Current – 110, 150, 200A Voltage – 11.5,12.6,13.8 V Welding speed- 1.6,2.5 mm/sec Gas - Argon Size- 400×100×6 mm	AISI 304 / GTAW	Optical Metallography
Aval et al. [32]	Current – 110, 150, 200 A Voltage – 11.5,12.6,13.8 V Welding speed- 10, 15 cm/min Gas - Argon Size- 400×100×6 mm	AISI 304 /GTAW	Prediction of grain structure using mathematical model.
Feng et al. [33]	Electrode dia-1.2 mm Current – 180 A Voltage – 30 V Welding speed- 0.4, 0.8, 1.2, 1.6, 2.0 m/min. Gas - 80% Ar + 20% CO_2 Gas flow rate – 25 l/min. Thickness- 16 mm Electrode extension- 15 mm	Carbon steel/ GMAW	High speed video photography impact behaviour
Ghosh et al. [34]	Electrode dia. - 1.2 mm Current – 150, 157, 166, 170, 190, 195, 205 A Voltage – 23, 24, 25 V Welding speed- 400, 450, 500 mm/min. Gas - Argon Thickness- 10 mm Electrode extension- 12 mm Wire feed rate - 67, 83, 92, 100, 117, 158 cm/min	Stainless steel/ GMAW	Arc study
Luksa [35]	Wire dia. – 1.2 mm Current – 120, 130A Voltage – 18 V Welding speed – 266, 275 mm/min Thickness – 5 mm Electrode extension- 15 mm	Structural steel/ GMAW	Arc stability

AUTHOR [Ref. No.]	INPUT PARAMETERS	WORKPIECE MATERIAL/ PROCESS	OUTPUT
Gulenc et al. [36]	Electrode dia-1.2 mm Current – 140, 180, 240 A Welding speed- 50 mm/min. Gas - Argon + Hydrogen Size - 140x75x10 mm	AISI 304L/ GMAW	Tensile, Vickers hardness and impact bending test
Kang et al. [37]	Electrode dia. - 1.2 mm Voltage –25 V Welding speed- 40 cm/min. Gas - Ar, He, Ar + He Gas flow rate – 20 l/min. Thickness- 15 mm Electrode extension- 12 mm Wire feed rate – 13.4 m/min	Aluminum/ GMAW	Effect of alternate supply of shielding gas
Trevisan et al. [38]	Electrode dia-1.6 mm Current – 110,170,220,350 A Welding speed- 250 mm/min. Gas - $CO_2 + N_2$ Size -260 x 160 x 9.5 mm	AISI 316L/ GMAW	Metallographic tests

2.6 SCOPE AND OBJECTIVES OF THE PRESENT WORK

AISI 304 and AISI 316 are the two most common austenitic stainless steels being used widely in automobile, aerospace, medical and related industries. Joining of such steels has always been an issue due to the facts like carbide precipitation, cracks due to low thermal conductivity and high electrical resistance, distortion and residual stresses. Majority of the earlier studies involves manual travelling of welding gun while joining these materials by GMAW [10, 13, 14, 16-21, 23, 25-38]. Some authors [11, 12, 15, 22, 24] employed robotic movement for GMAW of steel, but they may require an expensive arrangement. Many others studied the effect of gas shielding while welding AISI304 and AISI 316 stainless steel [36, 37, 38]. Effects of welding speed on joint quality and mechanical strength have also been investigated by many researchers [11, 12, 13, 14, 15, 16, 17, 18, 19, 20]. As it can be well understood that an automatic movement of welding gun will lead to more precise welding with low spatter, a simple arrangement for automatic welding in GMAW may be helpful for good quality welding. Automatic movement of welding torch may also reduce the fluctuation in welding current due to the fact that a constant gap is possible to maintain with the help of automatic movement setup as compared to manual movement of welding torch in GMAW. This will offer more uniform depth of penetration and good welding appearance. Based on the above discussion, the following objectives are identified for the present work.

- Development of an automatic (single axis) movement setup for GMAW which will eliminate the human involvement of welding torch movement.
- Study of weld quality improvements using automatic welding movement setup for low carbon steel, two different graded of stainless steel (AISI 304, AISI 316).
- Investigate the effect of process parameters (welding current, voltage, travelling speed, gas flow rate) on welding behaviour of AISI 304 and AISI 316 during GMAW using the automatic movement setup.
- To study the relative significance of process parameters on impact strength (at room temperature and at -20 °C), microhardness and microstructure; Taguchi Design of Experiments (DOE) and analysis of variance (ANOVA) to optimize the process parameters.
- To obtain a relative comparison between the weldability aspects of AISI 304 and AISI 316.
- Following test and analysis were carried out after automatic welding of AISI 304 and AISI 316: Impact Test, Microhardness, metallurgical studies by Scanning Electron Microscopy and X-Ray Diffraction (XRD) analysis.

CHAPTER 3

DEVELOPMENT OF AUTOMATIC MOVEMENT SETUP FOR GMAW AND WELD QUALITY IMPROVEMENT

3.1 AUTOMATIC GMAW SETUP

Geometric modelling of various parts of the automatic movement setup for GMAW was modelled in CREO software. These parts were assembled to form the complete setup. The complete model of the setup is shown in figure 3.1.

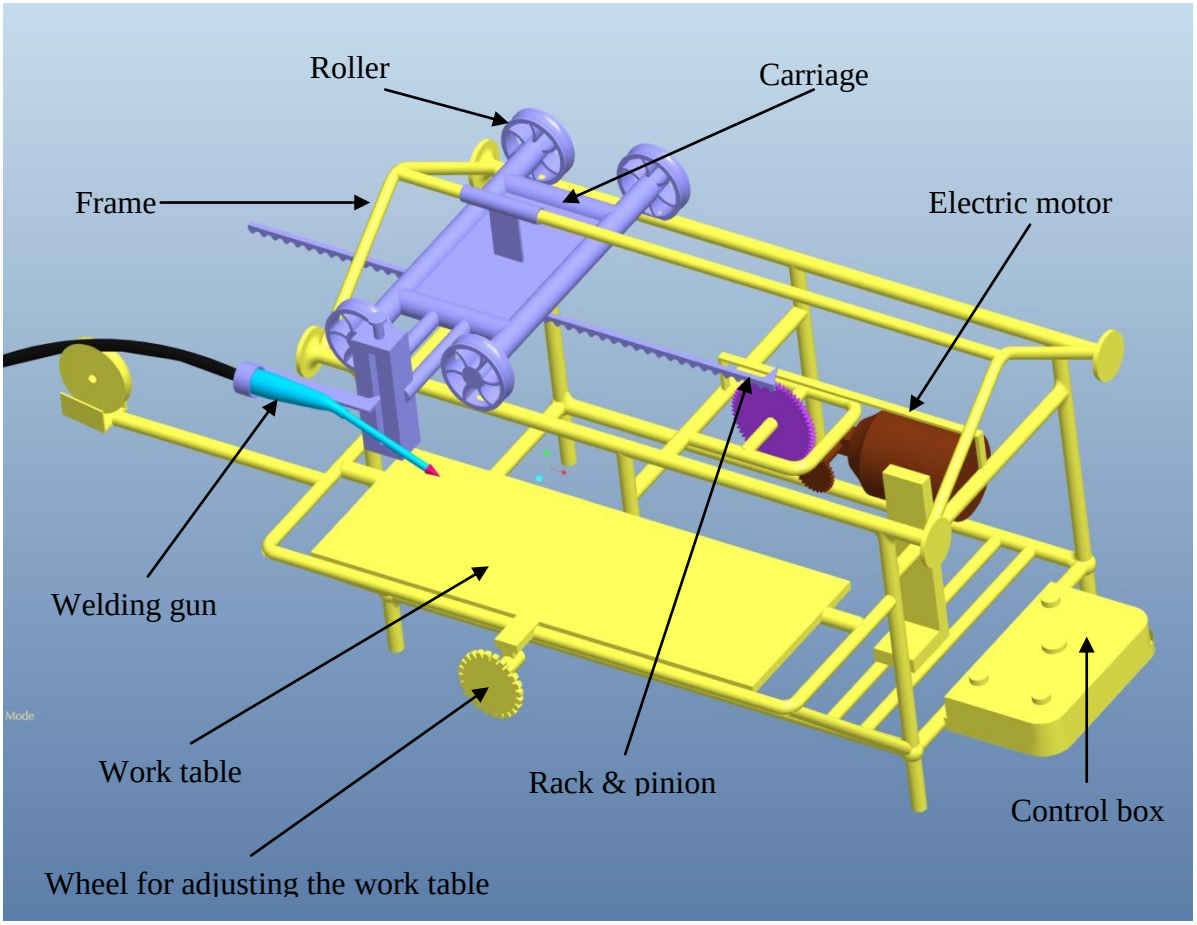

Figure 3.1: Geometric model of GMAW setup

Then modeled GMAW setup is fabricated in the welding shop, at Thapar University, Patiala. M.S. bar (ϕ 12 mm) is used for fabricating main frame of the setup. The dimensions of the

setup have been decided to accommodate only small jobs. The setup is rigid enough to carry weight of the welding gun, carriage and electrode cable. The assembled setup is shown in figure 3.2.

Figure 3.2: Gas metal arc welding fabricated setup

3.1.1 Actuator Motor

The speed of the welding gun is controlled by varying the speed of the electric motor through control box. An AC/DC electric motor with a reduction ratio of 228:1 is used to run the whole mechanism. The motor is permanently fixed to the main frame by nuts and bolts. The control box contains a regulator to provide the different speeds to the welding gun and a switch is used to reverse the motion of the electric motor (see the figure 3.3).

Figure 3.3: Motor used for drive movement in automatic GMAW

3.1.2 Transmission

A rack and pinion arrangement is used to move the welding gun for accomplishing the welding operation as shown in the figure 3.4. The rack and pinion arrangement is operated by the AC/DC electric motor which is fixed to the main frame. The rack is attached to a carriage which rolls over the main frame with the help of four grooved wheels. First of all the power is transfered from pinion (20 teeth) to the large intermediate gear (72 teeth), which is used to provide the speed reduction to the carriage. This intermediate gear is in mesh with the rack to transfer the motion to the carriage and hence welding gun.

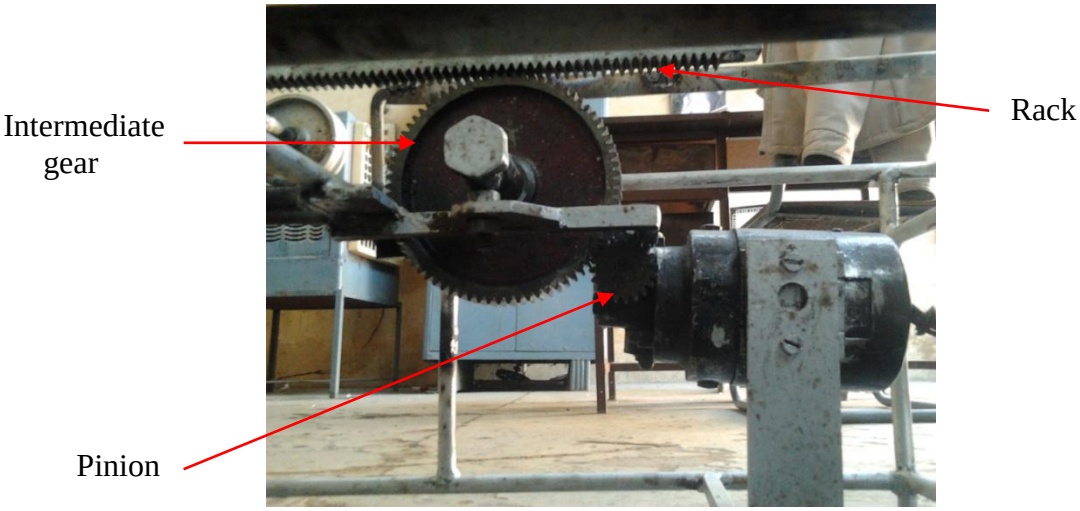

Figure 3.4: Transmission system of GMAW setup

3.1.3 Carriage

Carriage is the main part of the setup which holds the welding gun and moves over the main frame as shown in the figure 3.5. Carriage is attached to the main frame with the help of a rod which passes through a pipe which is welded over the carriage. Both the grooved wheels and rod passing through the pipe of main frame help keep the welding gun in straight direction while moving forward and backward.

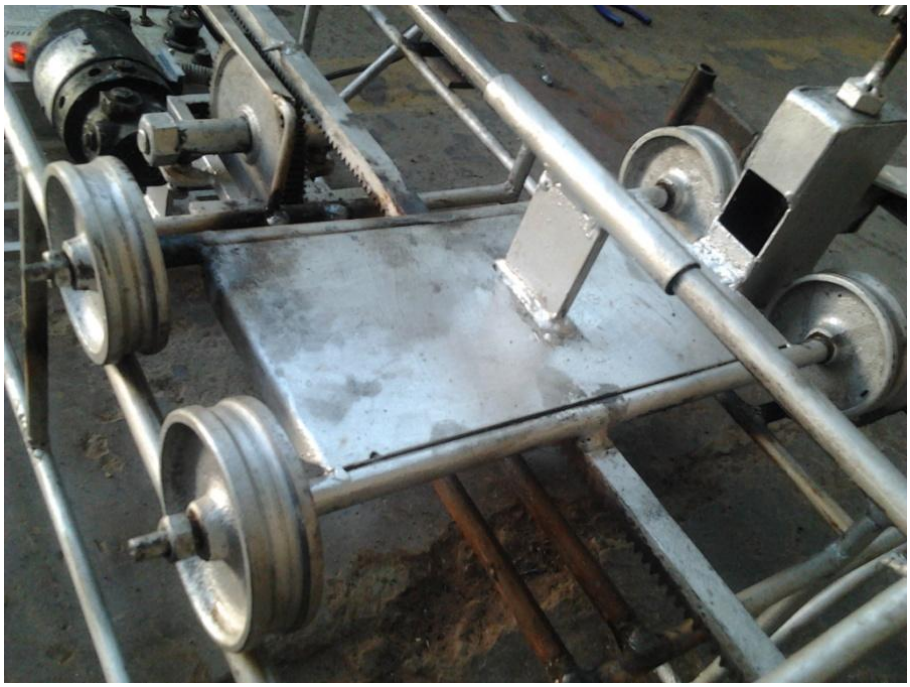

Figure 3.5: Carriage used for moving the welding gun

3.1.4 Arrangement for Holding Welding Gun

- **Vertical Up/Down Arrangement**

Welding gun is attached to the carriage with a nut and bolt mechanism. With the use of this mechanism we are able to adjust the height of welding gun over the bed (see figure 3.6). The up/down movement of the welding gun is very helpful in maintaining the proper gap between the nozzle and work for precise welding conditions.

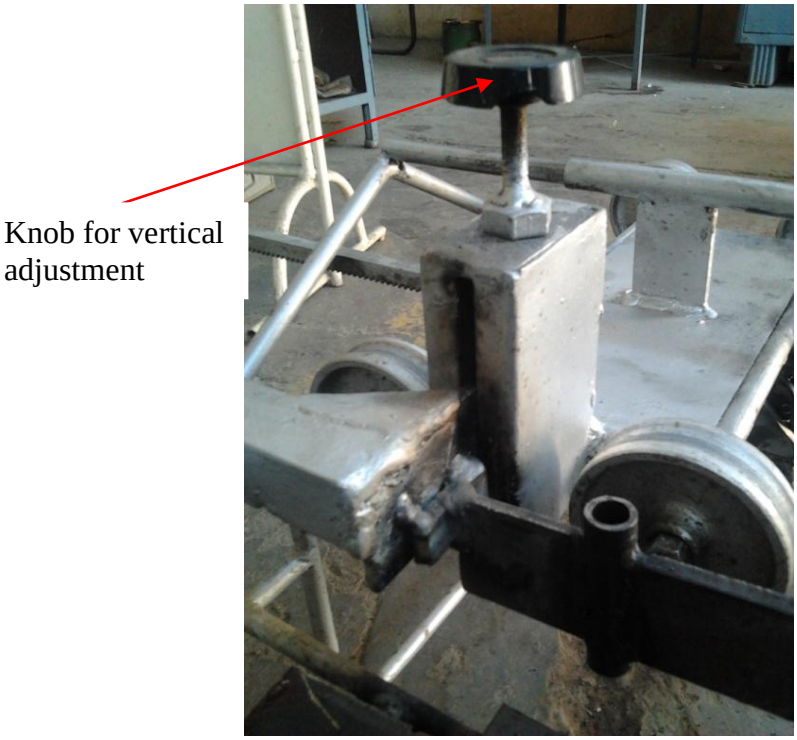

Figure 3.6: Vertical up/down arrangement

- **Clamping of Welding Gun**

A special hinged fixture is welded to the up/down mechanism for holding the welding gun in a particular position. With this hinged fixture we can position the welding gun in other than flat position also. An on-off switch is used for pressing the trigger of the welding gun while welding is performed. The actual welding gun attachment mechanism is shown in the figure 3.7.

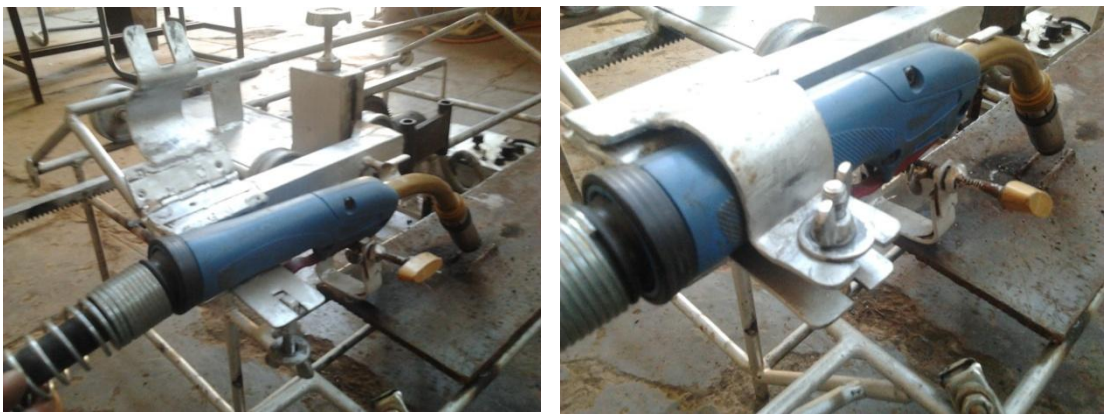

Figure 3.7: Welding gun holding mechanism

3.1.5 Work Table

Table is that part of the setup which accommodates the workpiece for welding operation. There is an arrangement beneath the plate, which is placed over the work table for adjusting the workpiece right and left for different welding positions as shown in the figure 3.8.

Figure 3.8: Work table for placing the welding specimens

3.2 WELD QUALITY IMPROVEMENT DURING AUTOMATIC SETUP

Comparison made in different workpieces like low carbon steel, AISI 304 and AISI 316 to observe the improvement in welding. The process condition and results using the present setup is discussed below.

3.2.1 Low Carbon Steel

A Comparison between manual and automatic welding using automatic GMAW setup was conducted on low carbon steel samples. All the welding parameters were kept constant during welding for both manual and automatic welding. Different welding parameters and their levels for each sample is given in the table 3.1.

Table 3.1: Welding parameters for comparison between manual and automatic welding for low carbon steel

Sample No.	Constant parameters	Variable parameters
1	Voltage = 20 V, Ar flow rate = 12 l/min., speed = 4 mm/s	Current = 140 A
2	Voltage = 20 V, Ar flow rate = 12 l/min., speed = 4 mm/s	Current = 160 A
3	Voltage = 20 V, Ar flow rate = 12 l/min., current = 140 A	Speed = 2.5 mm/s
4	Voltage = 20 V, Ar flow rate = 12 l/min., current = 140 A	Speed = 6 mm/s

From the sample it is very clear that the welding result of automatic GMAW setup are very fine and have good weld bead appearance (see figure 3.9). The weld bead is exactly uniform in a straight line by automatic setup than manual one. From the results of sample no. 3 of low carbon steel it can be concluded that the spatters get disappear with the use of automatic welding setup because there is a constant gap between nozzle and work during welding as shown in the figure 3.10. The metal deposition rate is constant in automatic welding. The weld bead is not regular with manual welding because it is not possible to maintain the constant gap and move straight without any reference. Consequently the weld bead with and the penetration affects with the change of these parameters. A significant increase in the amount of spatters was observed sample no. 1 with manual welding.

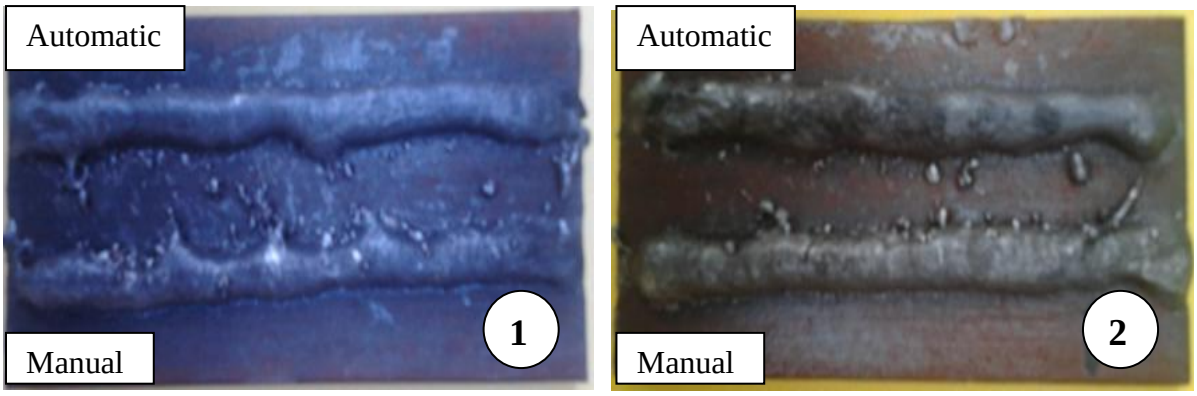

(a) 20 V, 12 l/min. Ar, 4 mm/s; 140 A (b) 20 V, 12 l/min. Ar, 4 mm/s; 160 A

Figure 3.9: Comparison between manual and automatic welding at different current values (a) 140 A and (b) 160 A

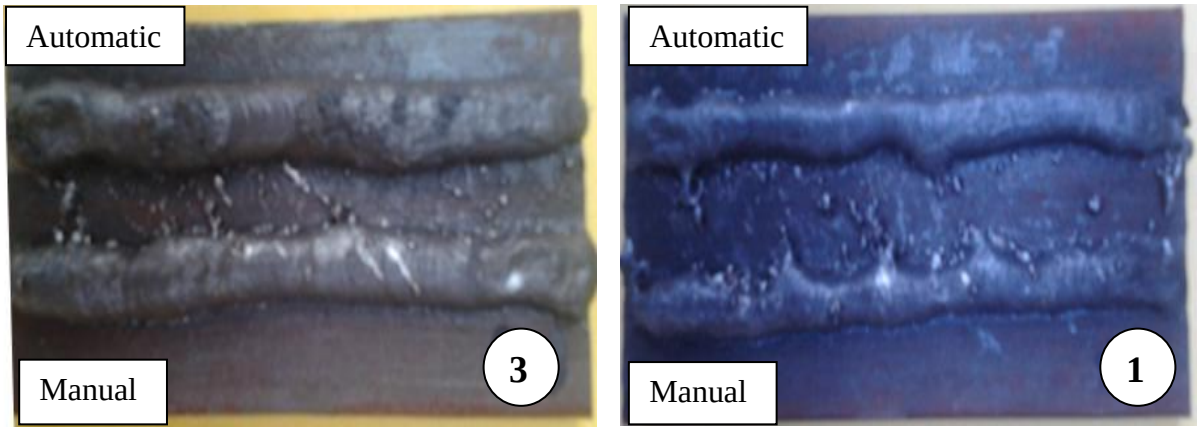

(a) 20 V, 12 l/min. Ar, 140 A; 2.5 mm/s (b) 20 V, 12 l/min. Ar, 140 A; 4 mm/s

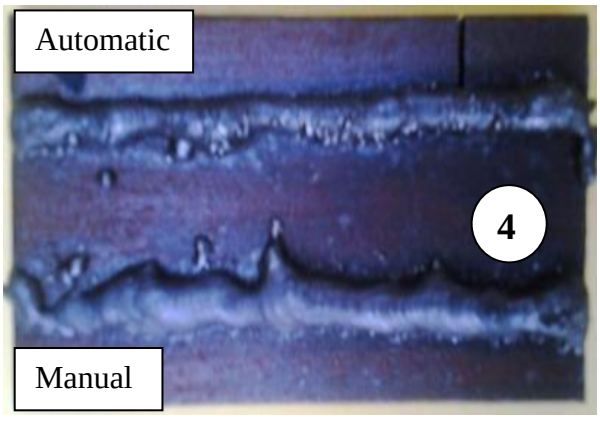

(c) 20 V, 12 l/min. Ar, 140 A; 6 mm/s

Figure 3.10: Comparison between manual and automatic welding at different welding speeds (a) 2.5 mm/s, (b) 4 mm/s and (c) 6 mm/s

3.2.2 AISI 304 Stainless Steel

A Comparison between manual and automatic welding using automatic GMAW setup was conducted on AISI 304 Stainless Steel samples. All the welding parameters were kept constant during welding for both manual and automatic welding. Different welding parameters and their levels for each sample is given in the table 3.2.

Table 3.2: Welding parameters for comparison between manual and automatic welding for AISI 304

Sample No.	Constant parameters	Variable parameters
1	Voltage = 20 V, Ar flow rate = 12 l/min., speed = 4 mm/s	Current = 140 A
2	Voltage = 20 V, Ar flow rate = 12 l/min., speed = 4 mm/s	Current = 180 A
3	Voltage = 20 V, Ar flow rate = 12 l/min., current = 140 A	Speed = 2.5 mm/s
4	Voltage = 20 V, Ar flow rate = 12 l/min., current = 140 A	Speed = 6 mm/s

Figure 3.11 depict clearly that the welding result of automatic GMAW setup are very fine and have good weld bead appearance. From the results it can be concluded that the spatters get disappear with the use of automatic welding setup because there is a constant gap between nozzle and work during welding as shown in the figure 3.12. Sample no. 1 shows the bead with consistent uniform ripples and a uniform bead width and height produced by automatic welding setup. The weld bead is exactly uniform in a straight line by automatic setup than manual one. The metal deposition rate is uniform in sample no. 2 of AISI 304 by automatic welding. Specimen no. 3 ranked highest in having the least amount of spatters. It can be concluded by seeing this sample that the bead weaving zig-zag with manual welding which gives poor appearance.

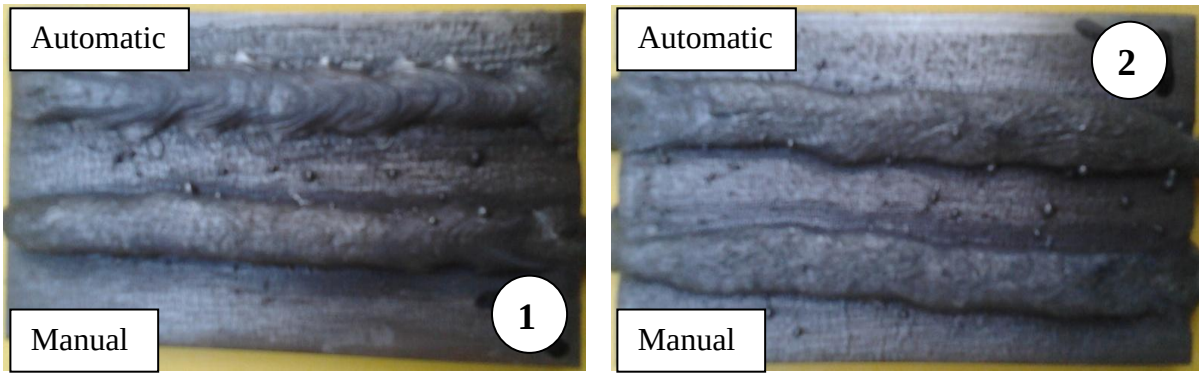

(a) 20 V, 12 l/min. Ar, 4 mm/s; 140 A (b) 20 V, 12 l/min. Ar, 4 mm/s; 180 A

Figure 3.11: Comparison between manual and automatic welding at different current values (a) 140 A and (b) 180 A

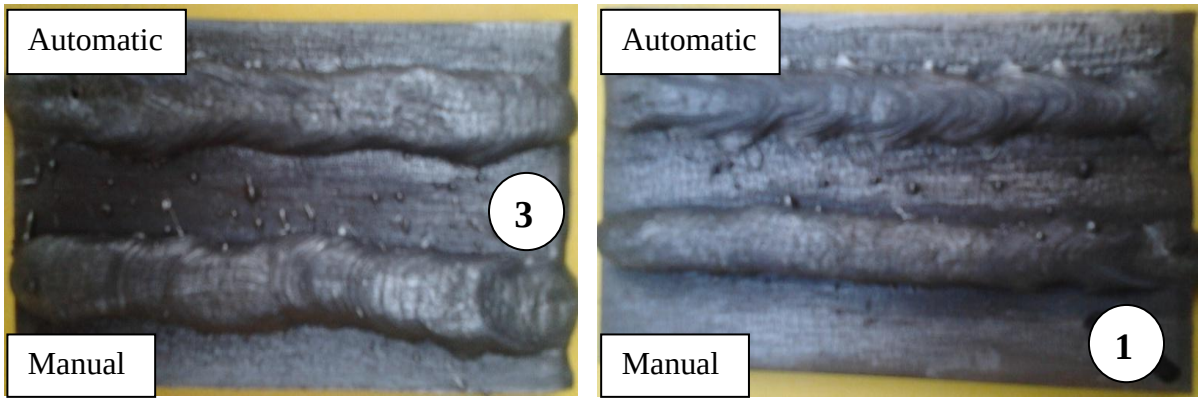

(a) 20 V, 12 l/min. Ar, 140 A; 2.5 mm/s (b) 20 V, 12 l/min. Ar, 140 A; 4 mm/s

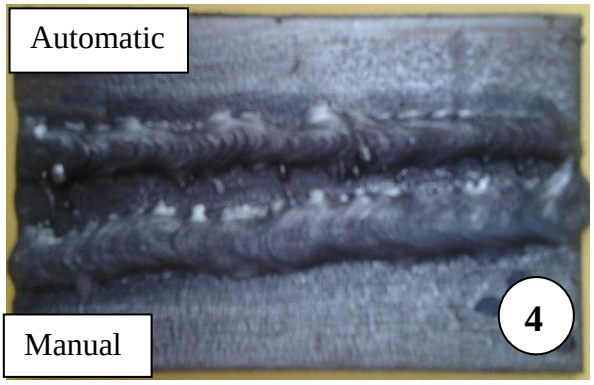

(c) 20 V, 12 l/min. Ar, 140 A; 6 mm/s

Figure 3.12: Comparison between manual and automatic welding at different welding speeds (a) 2.5 mm/s, (b) 4 mm/s and (c) 6 mm/s

3.2.3 AISI 316 Stainless Steel

A Comparison between manual and automatic welding using automatic GMAW setup was carried out on AISI 316 Stainless Steel samples. All the welding parameters were kept constant during welding for both manual and automatic welding. Different welding parameters and their levels for each sample is given in the table 3.3.

Table 3.3: Welding parameters for comparison between manual and automatic welding for AISI 316

Sample No.	Constant parameters	Variable parameters
1	Voltage = 20 V, Ar flow rate = 12 l/min., speed = 4 mm/s	Current = 160 A
2	Voltage = 20 V, Ar flow rate = 12 l/min., speed = 4 mm/s	Current = 200 A
3	Voltage = 20 V, Ar flow rate = 12 l/min., current = 160 A	Speed = 2.5 mm/s
4	Voltage = 20 V, Ar flow rate = 12 l/min., current = 160 A	Speed = 6 mm/s

From the sample it is very clear that the welding result of automatic GMAW setup are very fine and have good weld bead appearance. The weld bead is exactly uniform in a straight line by automatic setup than manual one. In sample no. 1 of AISI 316 stainless steel the weld bead is broader and has less face reinforcement with automatic setup than manual welding (see figure 3.13). The reason of broader bead and deep penetration in case of sample no. 1 is high current. From the results it can be concluded that the spatters get disappear with the use of automatic welding setup because there is a constant gap between nozzle and work during welding. The metal deposition rate is constant in automatic welding as shown the figure 3.14. Sample no. 4 depict that the weld bead profile and surface finish is excellent. As the welding gun moves at constant speed the deepest penetration is possible by controlling the speed.

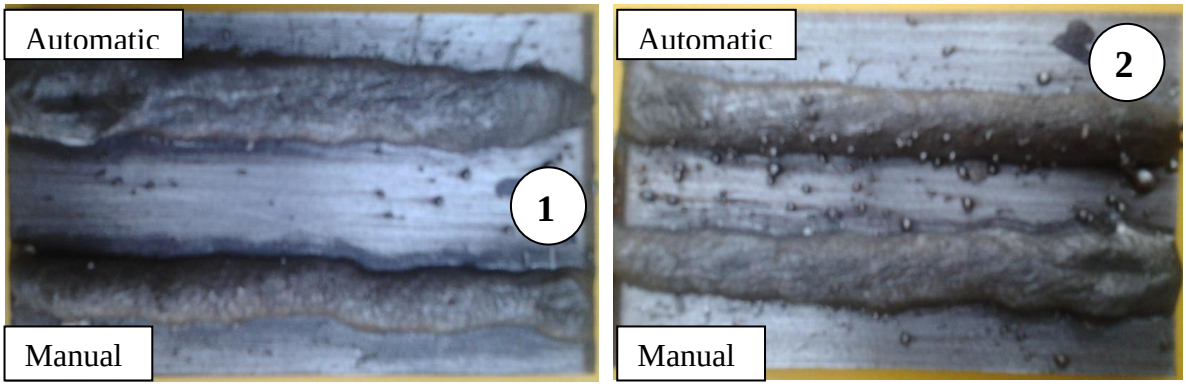

(a) 20 V, 12 l/min. Ar, 4 mm/s; 160 A (b) 20 V, 12 l/min. Ar, 4 mm/s; 200 A

Figure 3.13: Comparison between manual and automatic welding at different current values (a) 160 A and (b) 200 A

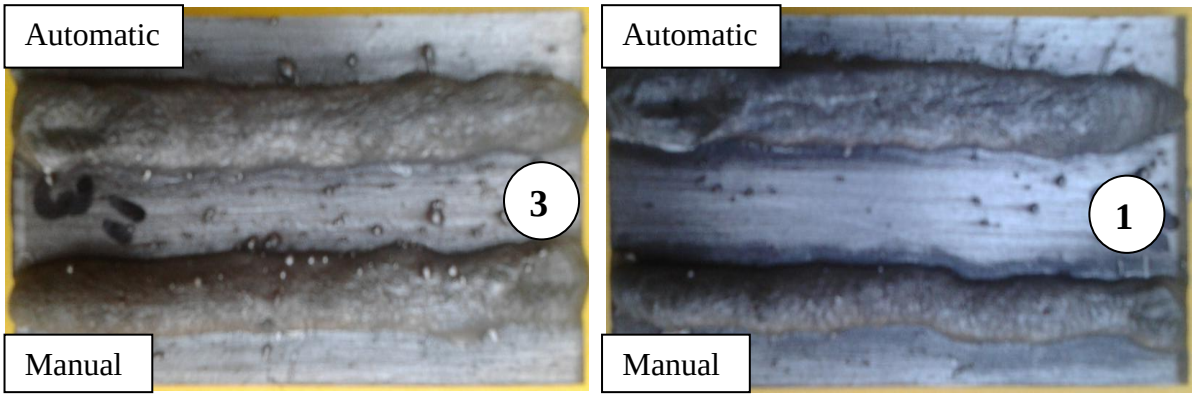

(a) 20 V, 12 l/min. Ar, 160 A; 2.5 mm/s (b) 20 V, 12 l/min. Ar, 160 A; 4 mm/s

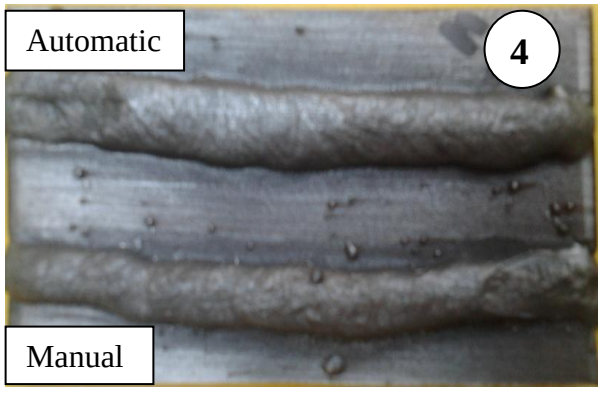

(c) 20 V, 12 l/min. Ar, 160 A; 6 mm/s

Figure 3.14: Comparison between manual and automatic welding at different welding speeds (a) 2.5 mm/s, (b) 4 mm/s and (c) 6 mm/s

CHAPTER 4

MATERIALS AND METHODS

4.1 WORKPIECE MATERIALS

After having literature review it is concluded that any change in parameters of Gas Metal Arc Welding affects the properties of the welding. Therefore in this study it has been proposed to find out the effects of changing different parameters like welding current, voltage, gas flow rate and travelling speed on weld properties using the presently developed automatic movement setup. The effects of changing parameters on impact strength, micro-hardness and microstructure and microstructural behaviour have been studied. The two grades of stainless steel AISI-304 and AISI-316 have been used to conduct these experiments.

4.1.1 AISI 304 Stainless Steel

The raw material for conducting the welding experiments and subsequently used for testing was AISI 304 stainless steel. The raw material was purchased from N. K. Steels, Chandigarh. The material was purchased in form of flat strip and then cut into small pieces (100 mm x 50 mm x 6 mm). The chemical composition of AISI 304 stainless steel as obtained from atomic absorption spectrometer (Make: WORLDWIDE ANALYTICAL SYSTEMS AG – FOUNDRY MASTER) is given in the table 4.1.

Table 4.1: Chemical composition of AISI 304 stainless steel

CHEMICAL COMPOSITION							
C	Mn	Si	Cr	Ni	P	S	Mo
0.064	1.821	0. 425	18.6	8.624	0.044	0.013	0.014

4.1.2 AISI 316 Stainless Steel

The other raw material used for conducting the welding experiments and subsequently for testing was AISI 316 stainless steel. The raw material was purchased from Kalson Impex Limited, Chandigarh. The material was purchased in form of flat strip and then cut into small pieces (100 mm x 50 mm x 6 mm). The chemical composition of AISI 316 stainless steel is given in the table 4.2.

Table 4.2: Chemical composition of AISI 316 stainless steel

CHEMICAL COMPOSITION							
C	Mn	Si	Cr	Ni	P	S	Mo
0.072	1.781	0.582	17.4	11.729	0.041	0.021	1.214

4.2 SELECTION OF DIFFERENT WELDING PARAMETERS

An automatic GMAW setup was fabricated and used to carry out the welding operation on two selected grades of stainless steel. A GMAW machine (Make: ADOR FONTECH LIMITED- TORNADO MIG 350) was used for performing welding experiments, available at central workshop, Thapar University, Patiala as shown in the figure 4.1.

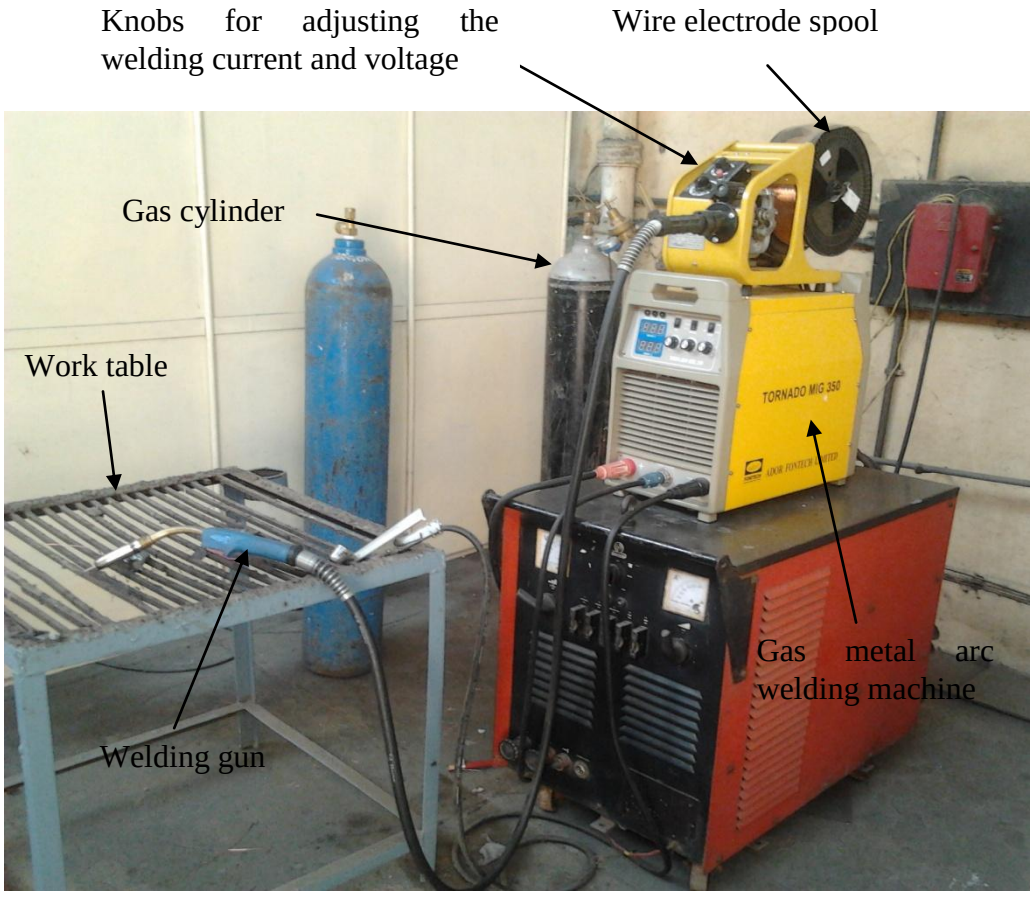

Figure 4.1: Gas metal arc welding setup
(**Courtesy:** Central Workshop, Thapar University, Patiala)

Table 4.3: Technical data of GMAW machine

S. No.	Welding parameter	Range
1.	Welding current	0-350 A
2.	Electrode diameter	0.8-1.2 mm
3.	Gas flow rate	0-25 l/min.

4.2.1 Pilot Study

Welding Current

Pilot study was carried out to identify the value of welding current as it is the most important parameter during GMAW by depositing beads on plates. The results revealed that the arc initiation and a proper weld bead was formed at 100 A. The current was raised in the steps of a 50 A till 250 A. It was observed that metal fused completely and deposited at the back of the plate because of high heat generated at this temperature in case of AISI 304 and AISI 316 stainless steel. Hence it was concluded that desirable range of the welding current was 100-200 A. On the basis of this study the values of current were chosen as 140, 160 and 180 A for AISI 304 stainless steel. The values of current chosen for AISI 316 stainless steel were 160, 180 and 200 A (see figures 4.2, 4.3).

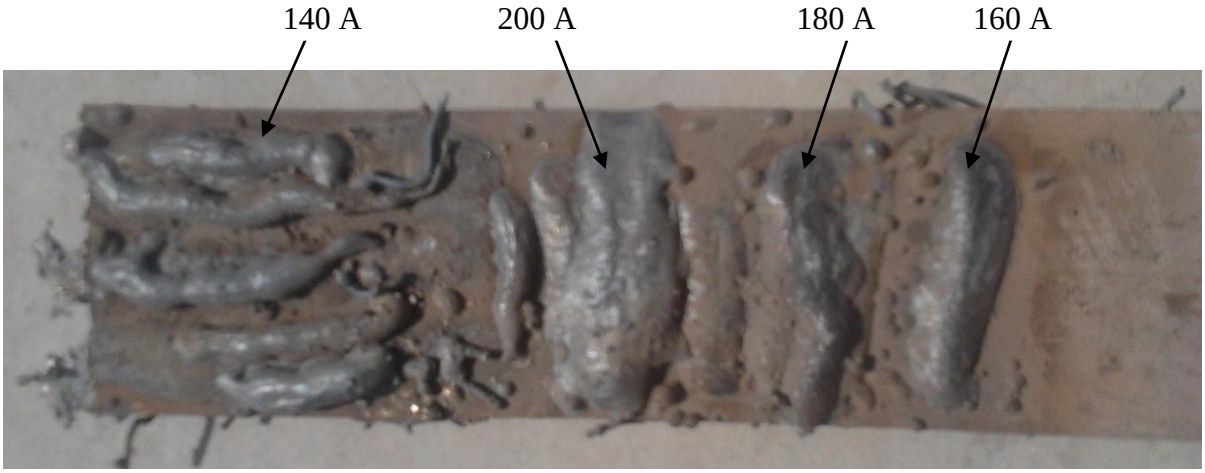

Figure 4.2: Pilot study for selecting the welding current manually
(Voltage = 20 V, gas = argon, flow rate = 12 l/min., work piece = AISI 304)

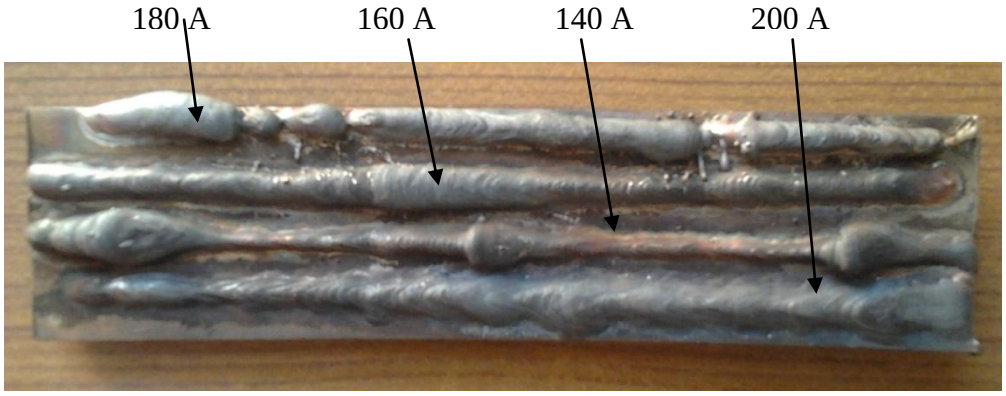

Figure 4.3: Pilot study for selecting the welding current on fabricated setup (Voltage = 23 V, gas = argon, flow rate = 12 l/min., work piece = AISI 316)

Welding Voltage

Pilot study was also carried out to know the effect of welding voltage during GMAW. Voltage play very important role in the geometry of weld bead (because GMAW works on the constant voltage characteristics). On the bases of pilot study the voltage range selected was 20 to 26 V.

Welding Speed

Pilot study for welding speed was completed to observe the effect of the weld deposition rate and consequently the strength of the joint by depositing weld bead on workpiece. The welding operation was carried out at different welding speeds on automatic GMAW setup. The pilot study for observing the effects of different welding speed at constant welding current 160 A and gas flow rate as 12 l/min was conducted.

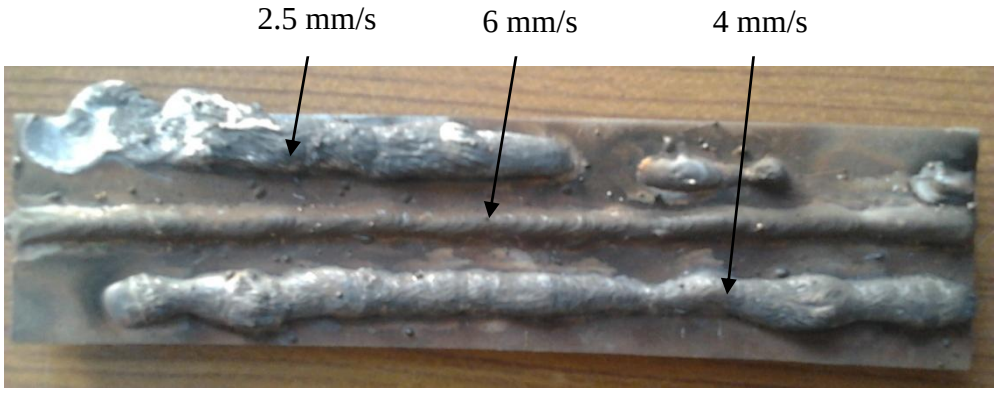

Figure 4.4: Pilot study for selecting the welding speed (Voltage = 20 V, gas = argon, flow rate = 12 l/min., work piece = AISI 304)

Shielding Gas for GMAW of Stainless Steel

Argon gas was used as shielding gas to protect the weld zone from environmental oxidation effect. Different gas flow rates were used to observe their effects on welding.

4.2.2 Selected Parameters

In the present experimental setup, there are four factors varied at 3-levels. Taguchi design has been used for the design of experiments, because it reduces the number of iterations and used to optimize the known parameters. The values of the input process parameters and their three levels for the automatic GMAW are as given in the table 4.4 and 4.5 for AISI 304 AISI 316 workpiece materials respectively.

Table 4.4: Parameters and their level for AISI 304 during automatic GMAW

S. No.	Materials parameters	Units	AISI 304 stainless steel		
1.	Welding current	A	140	160	180
2.	Welding voltage	V	20	22	24
3.	Gas flow rate	l/min.	8	12	16
4.	Welding speed	mm/s	2.5	4	6

Table 4.5: Parameters and their level for AISI 316 during automatic GMAW

S. No.	Materials parameters	Units	AISI 316 stainless steel		
1.	Welding current	A	160	180	200
2.	Welding voltage	V	20	23	26
3.	Gas flow rate	l/min.	8	12	16
4.	Welding speed	mm/s	2.5	4	6

4.3 DESIGN OF STUDY

To select an appropriate orthogonal array for experiments, the total degrees of freedom must be computed. The degrees of freedom are defined as the number of comparisons between process parameters that must be made to determine which level is better and, especially, how much better it is. For example, a two-level process parameter counts for one degree of freedom. The degrees of freedom associated with interaction between two process parameters are given by the product of the degrees of freedom for the two process parameters. In the present study, once the degrees of freedom are known, the next step is to select an appropriate

orthogonal array to fit the specific task. The degrees of freedom for the orthogonal should be greater than, or at least equal to, those for the process parameters. In this study, Taguchi L9 orthogonal array was used. Each welding parameter was assigned to a column and nine welding parameters combinations were tested. Therefore only nine experiments were required to study the entire welding parameter space using the L9 orthogonal array. The experimental layout for the welding parameters using the L9 orthogonal array is given in tables 4.6 and 4.7.

Table 4.6: Orthogonal array for experimentation on AISI 304 stainless steel

AISI 304 stainless steel				
Trial No.	Current (A)	Voltage (V)	Speed (mm/s)	Gas flow rate (l/min.)
1	140	20	2.5	8
2	140	22	4	12
3	140	24	6	16
4	160	20	4	16
5	160	22	6	8
6	160	24	2.5	12
7	180	20	6	12
8	180	22	2.5	16
9	180	24	4	8

Table 4.7: Orthogonal array for experimentation on AISI 316 stainless steel

AISI 316 stainless steel				
Trial No.	Current (A)	Voltage (V)	Speed (mm/s)	Gas flow rate (l/min.)
1	160	20	2.5	8
2	160	23	4	12
3	160	26	6	16
4	180	20	4	16
5	180	23	6	8
6	180	26	2.5	12
7	200	20	6	12
8	200	23	2.5	16
9	200	26	4	8

4.3.1 Selection of Orthogonal Array and Factors Assignment

In this experimental study, four factors were varied to three levels each. The degree of freedom (DOF) to a three level parameters is 2 (because DOF = number of levels-1), hence total DOF for the experiment is 8. So the orthogonal Array (OA) which could be used was L9. Degree of freedom allocated to various factors is given in table 4.8.

Table 4.8: DOF allocated to various factor combinations

S. No.	Parameter	Units	DOF
1.	Welding current	A	2
2.	Welding voltage	V	2
3.	Gas flow rate	l/min.	2
4.	Travelling speed	mm/s	2
	Total		8

4.4 EXPERIMENTAL METHODOLOGY

4.4.1 Edge Preparation of Stainless steel Specimen

Stainless steel flat of grade AISI 304 and AISI 316 were taken in the form of flat of sizes (100 mm x 50 mm x 6 mm) as shown in the figures 4.5 and 4.6.

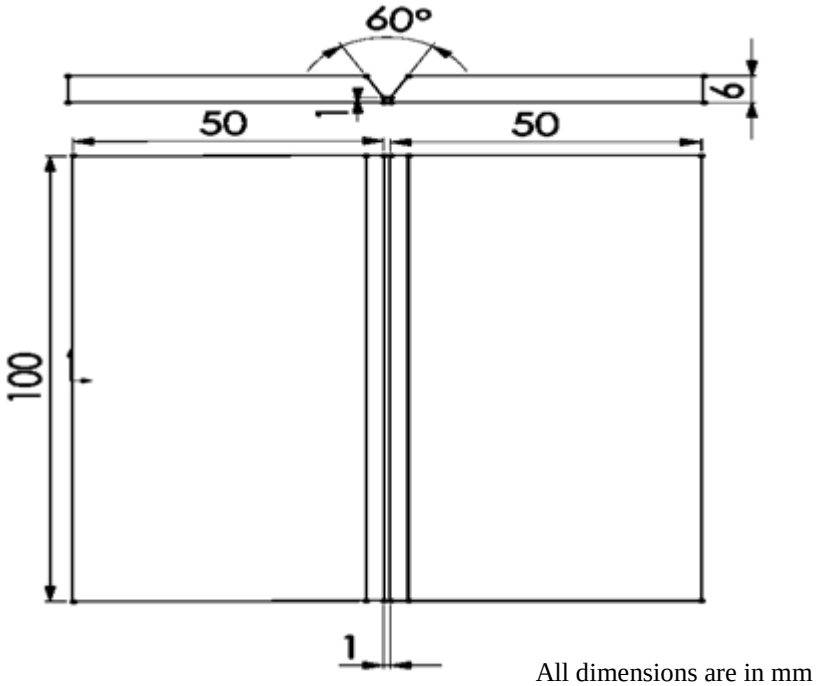

Figure 4.5: Edge preparation for GMAW

Figure 4.6: Specimens after edge preparation

4.4.2 Tacking of Welding Specimens

After edge preparation tacking was done at three points on the specimens using GMAW by properly clamping in the jaws to ensure their proper alignment and no mismatch. The specimen after tacking on the back side is shown in the figure 4.7.

Figure 4.7: Tacking of the welding specimens using GMAW

4.4.3 Welding of Specimens

As discussed previously that L9 orthogonal array was chosen and welding on specimens was carried out by fabricated setup with the help of GMAW machine (see figure 4.8). All the necessary precautions for the operator like helmet with shield and leather apron were used. The various welding speeds were precisely controlled by using regulator on control box during welding.

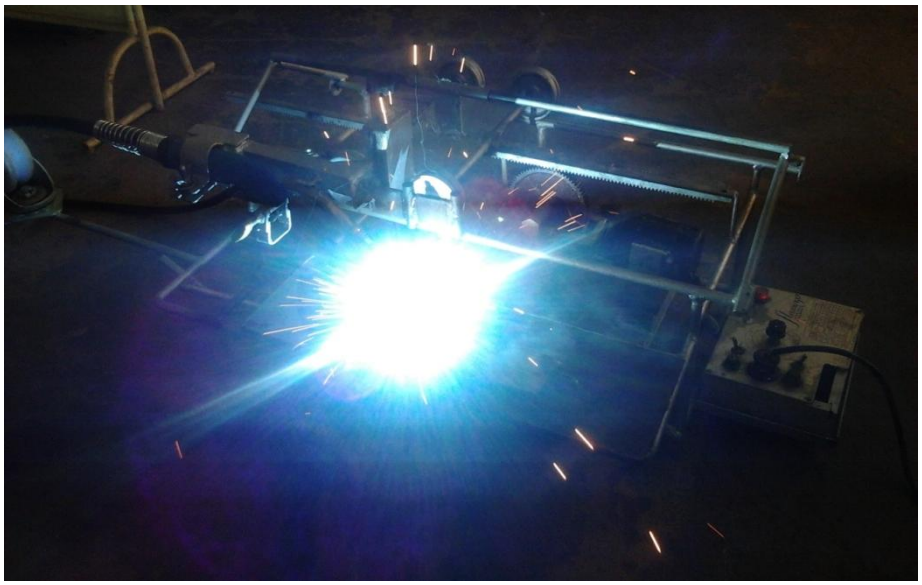

Figure 4.8: Welding of specimens on automatic GMAW setup

All specimens of AISI 304 stainless steel after welding are shown in the figure 4.9.

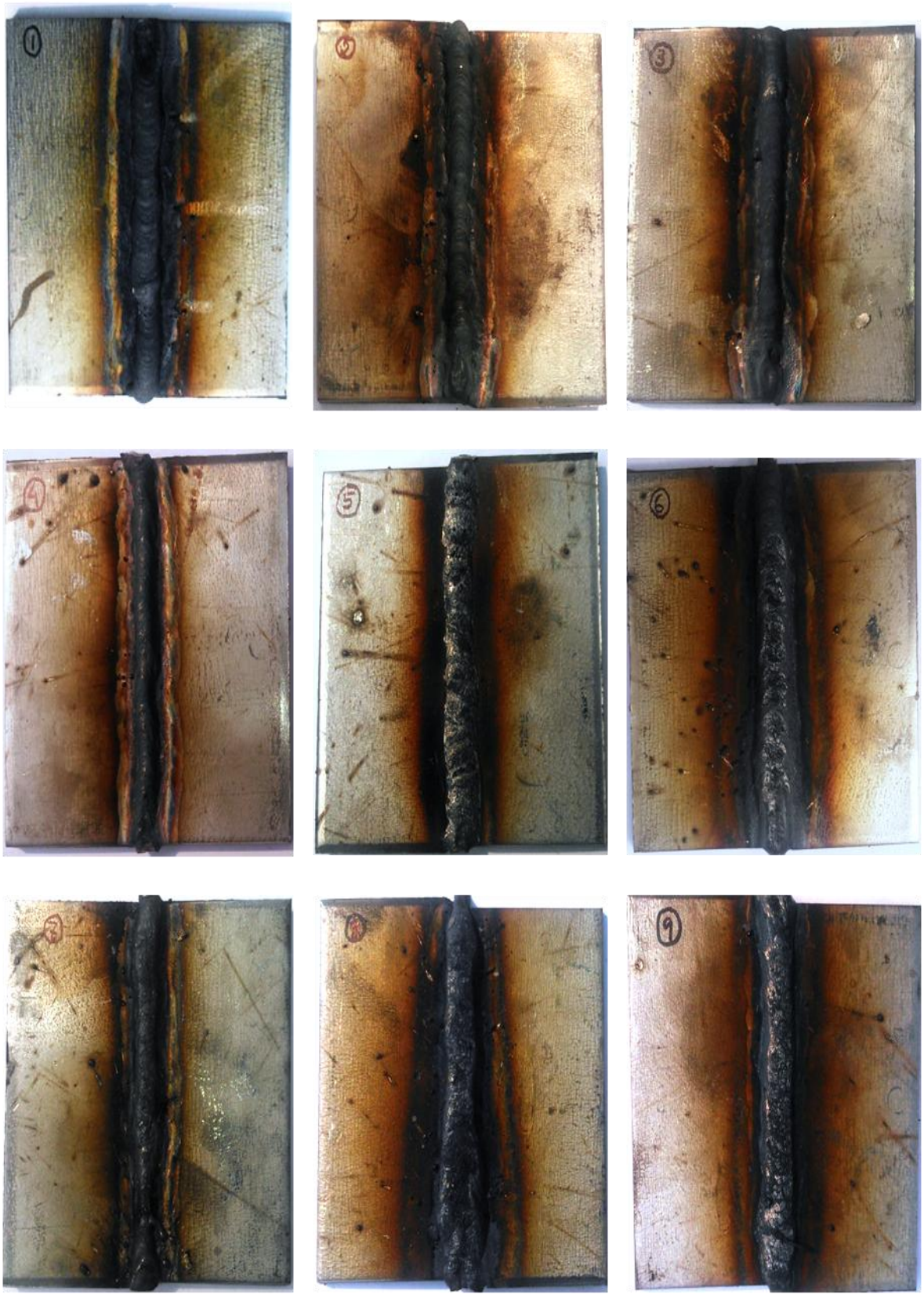

Figure 4.9: Specimens of AISI 304 stainless steel after GMAW

The specimens of AISI 304 stainless steel after welding are shown in the figure 4.10.

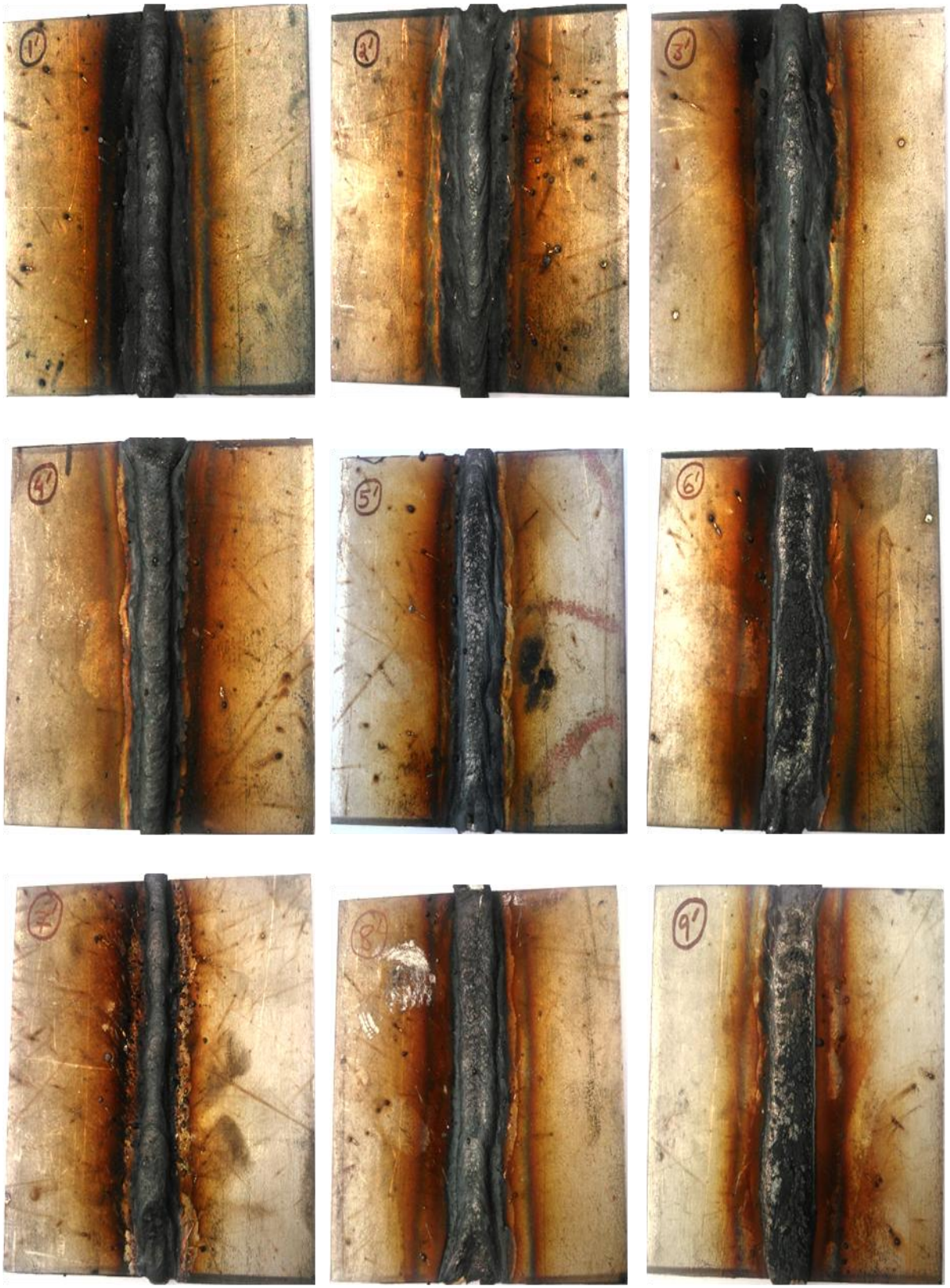

Figure 4.10: Specimens of AISI 316 stainless steel after GMAW

4.5 PREPERATION OF WELDED SPECIMENS FOR MECHANICAL TESTING AND MICROSTRUCTURE OBSERVATION

Weld bead was removed from all the specimens with the help of surface grinder for the purpose of testing of welded joints.

Figure 4.11: Weld bead removal on surface grinder
(**Courtesy**: Central Workshop Thapar University, Patiala)

Welded plates were marked for various tests after removing the weld bead from the specimens. A margin of 3 mm was left for each cut of the specimens on chop saw. The marking on welded specimens and cutting for different test is shown in the figure 4.12.

Table 4.9: Description of various portion marked on the specimens (refer figure 4.12)

S. No.	Purpose
1	Rejection at start and end of welded region
2	Specimen for impact test
3	Rejection at both sides of the specimens.
4	Specimen for X-Ray Diffraction and Scanning Electron Microscopy
5	Specimen for microhardness test

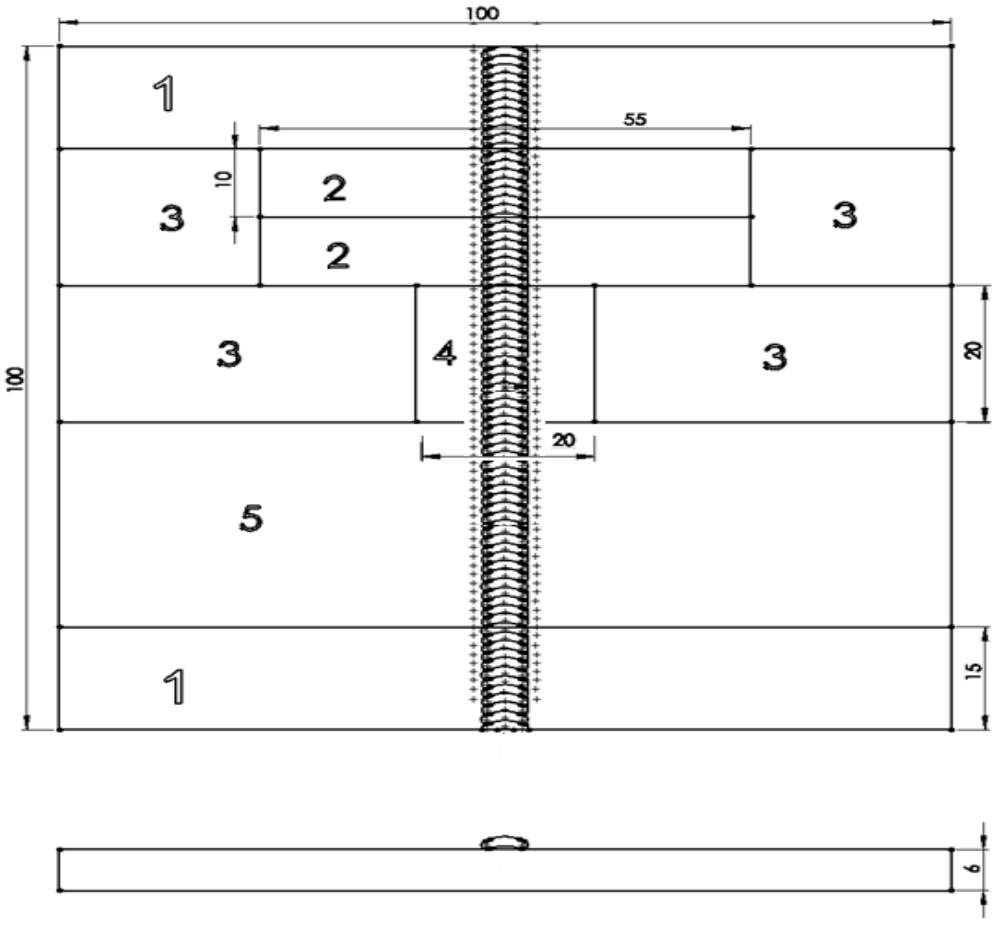

All dimensions are in mm

Figure 4.12: Marking and cutting of plates after welding

Figure 4.13: Cutting on chop saw
(**Courtesy:** Product Realisation Lab, Indian Institute of Technology, Ropar)

The welded specimens were cut as per the sizes mentioned above on chop saw (Make: Dewalt Industrial Tool Co.) as shown above in the figure 4.13. Water as coolant was used during cutting of specimens to ensure that temperature of the specimens did not rise and consequently change their properties. After cutting the specimens was ground on the surface grinder to make them of exact sizes as per ASTM standards A-370, 2010 [9]. V-notch on specimens for Impact test was prepared on shaping machine (Make: Cooper Engineering Ltd.) available at Central workshop Thapar University, Patiala.

Figure 4.14: Shaper machine used for making v-notch and impact test samples

4.6 TESTING METHODOLOGY

As proposed in this thesis work following tests and measurements were conducted on the weld specimens:

- Impact test
- Vickers Microhardness test
- X-Ray Diffraction test
- Scanning Electron Microscopy

4.6.1 Impact Test

Impact test of metals provides information on failure mode under high velocity loading conditions leading sudden fracture where a sharp stress raiser (notch) is present. The energy absorbed at fracture is generally related to the area under the stress-strain curve which is termed as toughness in some references. Impact test on the weld specimens was conducted on the impact testing machine (Make: Alfred J. Amsler & Co. Switzerland) having a range of 0-30 kg-m or 0-300 Joules as shown in the figure 4.17.

Figure 4.15: Impact testing machine
(**Courtesy:** Solid Mechanics Lab, MED, Thapar University, Patiala)

Specimens were prepared according to ASTM standard A-370 (2010) and having cross-section of 10 mm x 6 mm and length 55 mm for both the selected grades as shown in the figure 4.15.

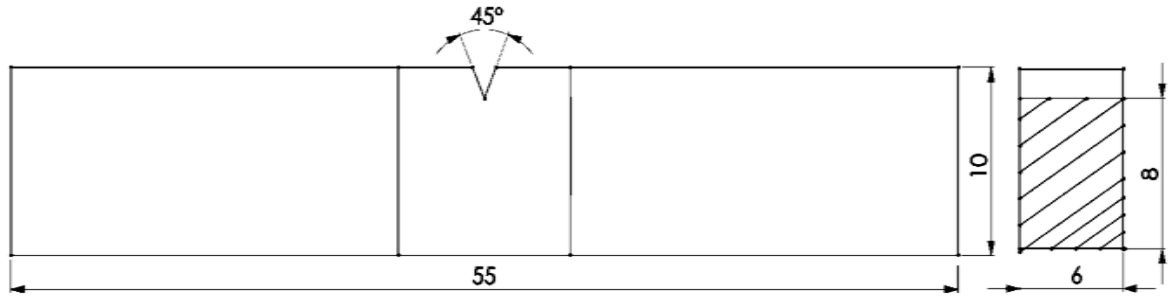

All dimensions are in mm

Figure 4.16: Standard size of impact test specimen according to ASTM standard A-370 [9]

Temperature of the specimens below room temperature (-20 °C) was generated by using liquid nitrogen and the specimens were put in the same for 5 minutes. An infrared thermometer was used for the measurement of temperature of the test specimens as shown in the figure 4.16.

Figure 4.17: Vacuum flask and infrared thermometer used for measurement of temperature

4.6.2 Vickers Microhardness Test

The samples for microhardness were ground on the belt grinder (Make: Chennai Metco Pvt. Ltd.), rubbed successively with emery paper grade no. 220, 400, 600, 800, 1000, 1500 and 2000. Finally polishing on disc polishing machine (Make: Frontier Techno Product Pvt. Ltd.) as shown in the figure 4.18. Microhardness of the weld region was measured by using the computer interfaced microhardness tester (Make: Metatech Industries, Pune, India) as shown in the figure 4.19. The measurement was dependent on the size of indentation on the samples. The diagonals of the indents formed by a pyramid shaped diamond indenter were measured with the help Quantimet software at 40X magnification, which gave a direct hardness Vickers Number (HVN) for microhardness. The load applied on the indenter was 500 gms and the dwell time was 20 sec.

Figure 4.18: Belt grinder and disc polishing machine
(**Courtesy:** Material Science Lab, Indian Institute of Technology, Ropar)

Figure 4.19: Microhardness testing machine
(**Courtesy**: Central Workshop Thapar University, Patiala)

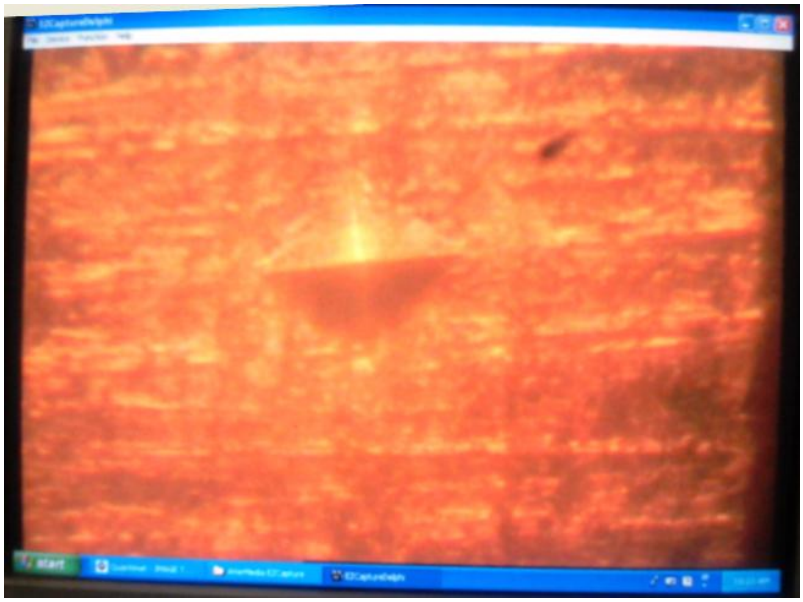

Figure 4.20: Diamond indent at 40X

4.6.3 X-Ray Diffraction (XRD) Test

X-ray diffraction method is generally used to distinguish between single crystal and polycrystalline or powder applications. About 95% of all solid materials can be described as crystalline. When x-rays interact with a crystalline substance (phase), one gets a diffraction pattern. An electron in an alternating electromagnetic field will oscillate with the same

frequency as the field. When an x-ray beam hits an atom, the electrons around the atom start to oscillate with the same frequency as the incoming beam. In almost all directions we will have destructive interference, that is, the combining waves are out of phase and there is no resultant energy leaving the solid sample. However the atoms in a crystal are arranged in a regular pattern, and in a very few directions we will have constructive interference. The waves will be in phase and there will be well defined x-ray beams leaving the sample at various directions. Hence, a diffracted beam may be described as a beam composed of a large number of scattered rays mutually reinforcing one another.

Figure 4.21: X-ray diffraction machine
(**Courtesy:** XRD Lab, Indian Institute of Technology, Ropar)

The samples used for doing XRD were cut into the proper dimension (20 x 20 x 6 mm) as discussed previously. The fixture used to hold the specimen in XRD machine was somewhat different as required for my samples. So a new fixture was designed on Solid Works designing software (see figure 4.23). The drawing was saved in STL format. The STL file was then transfered to the 3D printer (Make: Stratasys Ltd.) for a tangible fixture as shown in the figure 4.22 for accomplishing testing on XRD machine. The raw material used by the

printer was PVC. The printer achieved 100° C temperature before starting to make the fixture layer by layer. The 3D printer took 30 minutes to convert it into a tangible fixture.

Figure 4.22: 3D Printer
(**Courtesy:** Indian Institute of Technology, Ropar)

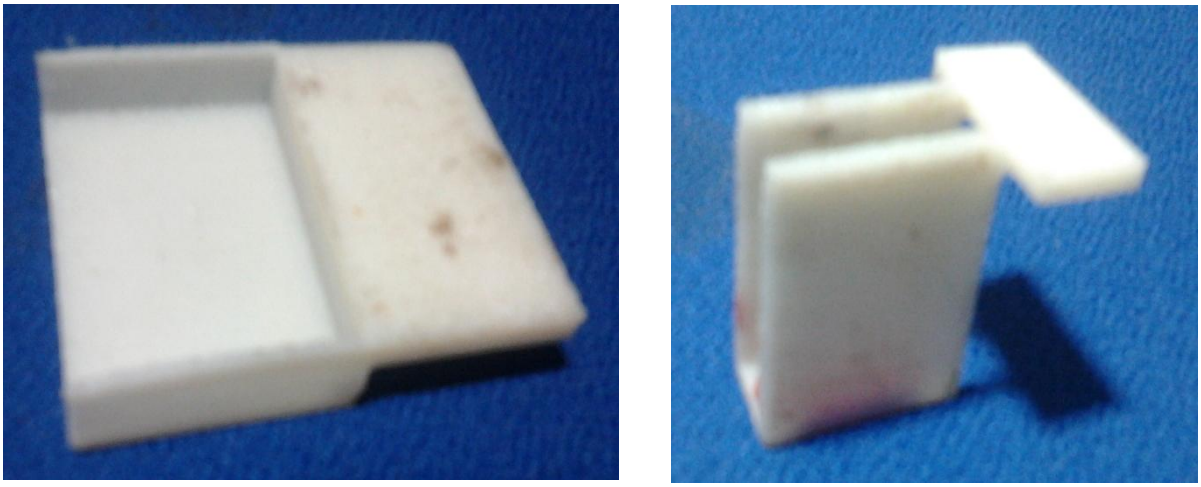

Figure 4.23: Fixtures for holding specimen on XRD machine

4.6.4 Scanning Electron Microscopy (SEM)

Scanning electron microscopy uses a focused electron probe to extract structural and chemical information point-by-point from a region of interest in the sample (see figure 4.25). The high spatial resolution of an SEM makes it a powerful tool to characterize a wide range of specimens at the nanometer to micrometer length scales.

Figure 4.24: Etchant for SEM specimens

The samples used for conducting scanning electron microscopy were cut into the proper dimensions (20 x 20 x 6 mm) using chop saw as discussed earlier. Before placing the samples into the machine all the samples were etched with cupric sulphate solution for two minutes as shown in the figure 4.24.

Figure 4.25: Scanning electron microscopy machine
(**Courtesy:** SEM Lab, Indian Institute of Technology, Ropar)

4.7 ANALYSIS OF RESULTS

ANOVA is a statistical tool that allows analyzing the variations of the test results into components that are contributed by different sources. This allows to partition total experiment variance to different factors, and even to combination to different factors.

$SS_T = SS_F + SS_E$

$$SS_T = \sum_{J=1}^{P} \left(\gamma_j - \gamma_m \right)^2$$

Where SS_T = Total sum of squared deviations about the mean.

γ_j = Mean response for j^{th} experiment.

γ_m = Grand mean of the response.

SS_F = Sum of squared deviations due to each factor.

SS_E = Sum of squared deviations due to error.

In the ANOVA table mean square deviation is defined as:

MS = Mean Square

$$MS = \frac{SS\ (\text{Sum of squared division})}{DOF\ (\text{Degree of Freedom})}$$

F-value of Fisher's F ratio (Variance ratio) is defined as:

$$F = \frac{\text{MS for a term}}{\text{MS for the error term}}$$

PC value (Percentage contribution) is calculated from the F value. F (critical) value is drawn from the table. If F-value for a factor appears greater than its F (critical) then it can be concluded that the effect of that factors is significant on the selected response. Significance of all the dependent variables has been evaluated using statistical software MINITAB 14. The dependent variables studied in this study are (1) Toughness at room temperature (2) Toughness at -20 °C (3) Microhardness (HVN).

In the ANOVA table the degrees of freedom are used to calculate the mean square (MS). In general the degrees of freedom measure how much 'independent' information is available to calculate each sum of squares (SS).

Total DOF = DOF for all factors + DOF for all interactions + DOF for error

Where n is the total number of observations used,

DOF for factor = K-1

Where K is the number of the factor levels.

DOF for Interaction = $(K_1-1) \times (K_2-1)$

Where K_1, K_2 are the number of levels of factor one and factor two respectively. The same rule applies to interactions of more than two factors. In the present study, the interaction of factors has not been studied. The sequential sum of squares for each term in the model (factors or interaction) measures the amount of variation in the response that is explained by adding each term to the model sequentially. Thus, the sequential sums of squares for terms are specific to the order of the terms specified in the linear model. The adjusted sum of squares for a term in the model (factor or interaction) measures the amount of additional variation in the response that is explained by the term, given that all the other terms are already in the model. Thus the levels for the adjusted sums of squares do not depend on the order of the terms listed under source. The adjusted mean square for a term is simply the adjusted sum of squares divided by the degrees of freedom.

For this experimental work, the following response characteristics have been studied:

1.	Response name	:	Toughness at room temperature (19 °C)
	Response type	:	Higher the better
	Units	:	Joule
2.	Response name	:	Toughness at room temperature (-20 °C)
	Response type	:	Higher the better
	Units	:	Joule
3.	Response name	:	Microhardness at weld region
	Response type	:	Higher the better
	Units	:	HVN

CHAPTER 5

RESULTS AND DISCUSSION

5.1 IMPACT TEST (AT ROOM TEMPERATURE)

Following the methodology as discussed in Chapter 4, impact test samples are prepared for parent metal and all welded samples. Impact test result for the both the parent metals (AISI 304 and AISI 316) at room temperature are given in table 5.1.

Table 5.1: Toughness test results for base metal

Base Metal	Toughness at room temperature (19 °C) (Joule)
AISI 304	62.784
AISI 316	53.955

5.1.1 Toughness test results for AISI 304 stainless steel

Impact test of all the welded samples of AISI 304 are carried out following similar methodology and given in table 5.2. The tested specimens after toughness test for AISI 304 are shown in the figure 5.1.

Table 5.2: Toughness values for various experiments on AISI 304 stainless steel

Experiment. No.	Toughness at room temperature (19 °C) (Joule)
1.	113.796
2.	83.385
3.	63.765
4.	53.955
5.	68.67
6.	112.815
7.	32.373
8.	103.005
9.	112.815

Figure 5.1: Specimens of AISI 304 stainless steel after toughness test

5.1.2 ANOVA for Toughness of AISI 304 stainless steel

Table 5.2 consists of the values of toughness at room temperature for the nine experiments conducted on AISI 304 stainless steel. The experimental results for toughness are analysed using ANOVA and is given in table 5.3. Since all DOF for factors are equal to DOF of L9 orthogonal array, no DOF are available for error. Thus to calculate the F-value and judge the relative significance of parameters, factors with lowest variance value is considered and added to obtain pooled error. Further, F-values of all remaining factors are calculated considering pooled error. The similar approach is used for ANOVA of all results during the present study. The results shows that welding speed is the most significant factor whereas voltage and gas flow rate is the least significant factor in effecting the toughness of AISI 304 stainless steel. Main effects plot for mean shows the variation in the toughness at room temperature with the change in the input factors i.e. welding current, voltage, speed and gas flow rate is shown in the figure 5.2. It is quite clear from the figure 5.2 that speed is the most significant factor for the toughness as the best results are obtained by using slowest welding speed. Best value of toughness is obtained as 113.796 J for experiment no. 1 (140 A, 20 V, 2.5 mm/s, 8 l/min.). Voltage and gas flow rate also affects the toughness considerably as

toughness as toughness is higher for lower value of voltage and also higher for the maximum gas flow rate. From ANOVA table for mean it can be seen that F value for speed is greater than its critical counterpart effecting toughness.

Table 5.3: Analysis of variance for means toughness for AISI 304 stainless steel

Source	Units	DOF	SS	Variance	F	% Contribution
Current	A	2	108.43	54.21	-	-
Voltage	V	2	1351.80	675.90	12.4681	19.01
Speed	mm/s	2	4528.87	2264.44	41.7716	63.71
Flow rate	l/min.	2	1118.91	559.45	10.3200	15.74
Residual error		0	0	0	-	-
Total		8	7108.00			100
Error pooled		2	108.43	54.21		1.52

(SS = Sum of Squares, F = F factor, factor with least variance value is considered for error pooling)

Table 5.4: Response table for mean toughness at room temperature for AISI 304

Level	Current	Voltage	Speed	Flow rate
1	86.98	66.71	109.87	98.43
2	78.48	85.02	83.39	76.19
3	82.73	96.46	54.94	73.58
Delta	8.50	29.76	54.94	24.85
Rank	4	2	1	3

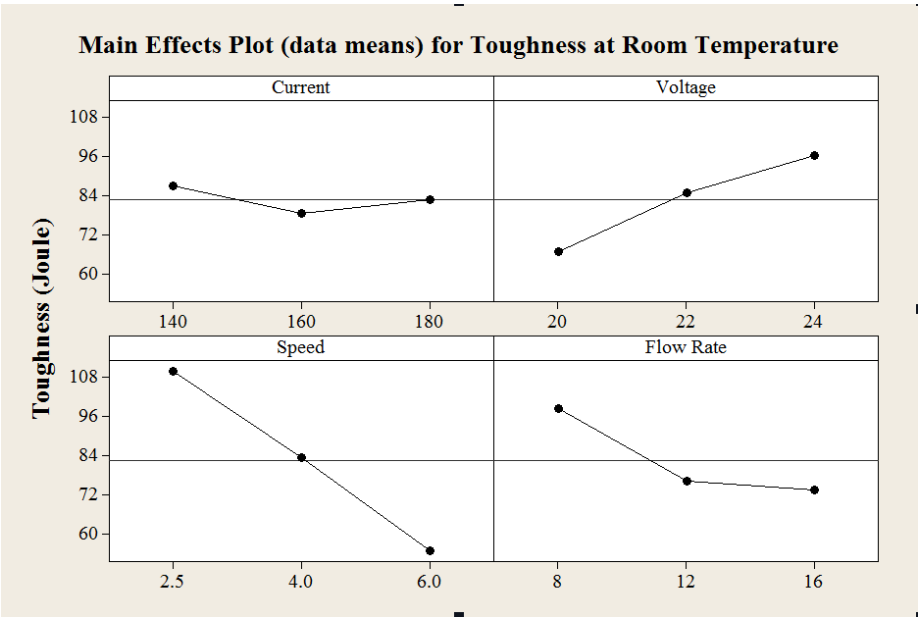

Figure 5.2: Main effects plot for means for toughness (at room temperature) of AISI 304 specimens

5.1.3 Toughness test results for AISI 316 stainless steel

Impact test of all the welded samples of AISI 316 are carried out following similar methodology and given in table 5.5. The tested specimens after toughness test for AISI 316 are shown in the figure 5.3.

Table 5.5: Toughness values for various experiments on AISI 316 stainless steel

Experiment. No.	Toughness at room temperature (19 °C) (Joule)
1.	56.898
2.	43.164
3.	58.86
4.	34.335
5.	60.822
6.	68.67
7.	34.335
8.	70.632
9.	73.575

Figure 5.3: Specimens of AISI 316 stainless steel after toughness test

5.1.4 ANOVA for Toughness of AISI 316 stainless steel

The results of toughness test carried out on experimental specimens of AISI 316 stainless steel are given in table 5.5. The results are analysed using ANOVA and the results are given in the form of tables 5.6 and 5.7. Main effects plot for mean given in figure 5.4 shows the variation in the toughness at room temperature with change in the input factors. Last column of table 5.6 shows the percentage contribution of each factor as the response. It can be seen from these values that voltage is significantly affects the response (53.85% contribution). Best values of toughness are obtained in the test results of experiments no. 8 and 9. In general it can be conclude that after welding the toughness value of welded joints has increased in comparison to the base metal for all the experiments except experiment no. 2, 4 and 7.

Table 5.6: Analysis of variance for means toughness for AISI 316 stainless steel

Source	Units	DOF	SS	Variance	F	% Contribution
Current	A	2	69.50	34.752	-	-
Voltage	V	2	979.26	489.628	14.0892	53.85
Speed	mm/s	2	424.94	212.468	6.1138	23.36
Flow rate	l/min.	2	344.74	172.370	4.9600	18.95
Residual error		0	0	0	-	-
Total		8	1818.43			100
Error pooled		2	69.50	34.752		3.82

(SS = Sum of Squares, F = F factor, factor with least variance value is considered for error pooling)

Table 5.7: Response table for mean toughness at room temperature for AISI 316

Level	Current	Voltage	Speed	Flow rate
1	52.97	41.86	65.40	63.77
2	54.61	58.21	50.36	48.72
3	59.51	67.04	51.34	54.61
Delta	6.54	25.18	15.04	15.04
Rank	4	1	2.5	2.5

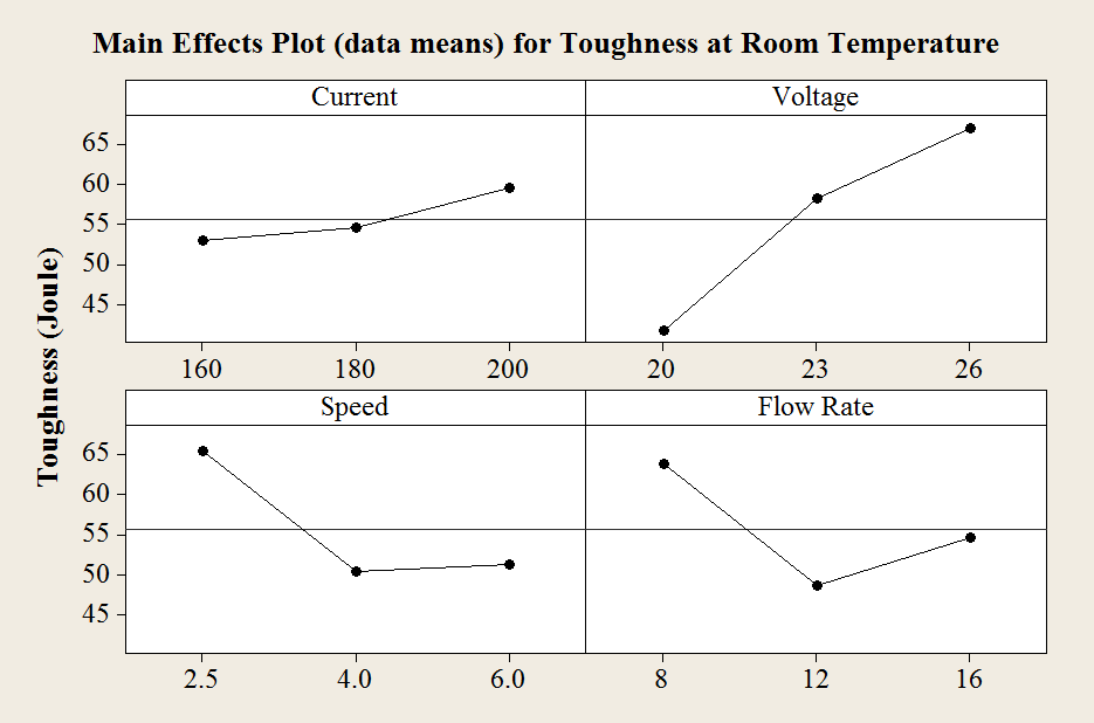

Figure 5.4: Main effects plot for means for toughness (at room temperature) of AISI 316 specimens

5.2 IMPACT TEST (AT -20 °C)

All samples dipped in liquid nitrogen and subsequently tested for impact test at -20 °C. Temperature of samples was measured using infrared thermometer and when samples temperature at -20 °C impact test carried out. Toughness of parent metals at -20 °C is given in table 5.8.

Table 5.8: Toughness test results for base metal

Base Metal	Toughness at -20 °C (Joule)
AISI 304	54.936
AISI 316	47.008

5.2.1 Toughness test results for AISI 304 stainless steel

Table 5.9 gives the value of toughness obtained for the specimens of AISI 304 stainless steel at -20 °C.

Table 5.9: Toughness values for various experiments on AISI 304 stainless steel

Experiment. No.	Toughness at -20 °C (Joule)
1.	73.575
2.	55.917
3.	53.955
4.	44.145
5.	66.708
6.	93.195
7.	19.62
8.	83.385
9.	73.575

5.2.2 ANOVA for Toughness of AISI 304 stainless steel

Experimental results are analysed using ANOVA and results are given in table 5.10 and 5.11. Main effects plot for mean is given in the figure 5.5 shows the variation in the toughness at room temperature with the change in the input factors i.e. welding current, voltage, speed and gas flow rate. Last column of table 5.10 shows the percentage contribution of each factor as the response. It can be seen from these values that welding speed is significantly affects the response (53.78% contribution). Best values of toughness are obtained in the test results of experiments no. 6 and 8. The result shows that voltage and gas flow rate is the least significant factor in effecting the toughness of AISI 304 stainless steel. In general it can be conclude that after welding the toughness value of welded joints has increased in comparison to the base metal for all the experiments except experiment no. 4 and 7.

Table 5.10: Analysis of variance for means toughness for AISI 304 stainless steel

Source	Units	DOF	SS	Variance	F	% Contribution
Current	A	2	136.23	68.11	-	-
Voltage	V	2	1320.57	660.29	9.6944	33.57
Speed	mm/s	2	2115.48	1057.74	15.5298	53.78
Flow rate	l/min.	2	360.78	180.39	2.6485	9.173
Residual error		0	0	0	-	-
Total		8	3933.06			100
Error pooled		2	136.23	68.11		3.45

(SS = Sum of Squares, F = F factor, factor with least variance value is considered for error pooling)

Table 5.11: Response table for mean toughness at -20 °C temperature for AISI 304

Level	Current	Voltage	Speed	Flow rate
1	61.15	45.78	83.38	71.29
2	68.02	68.67	57.88	56.24
3	58.86	73.57	46.76	60.50
Delta	9.16	27.79	36.62	15.04
Rank	4	2	1	3

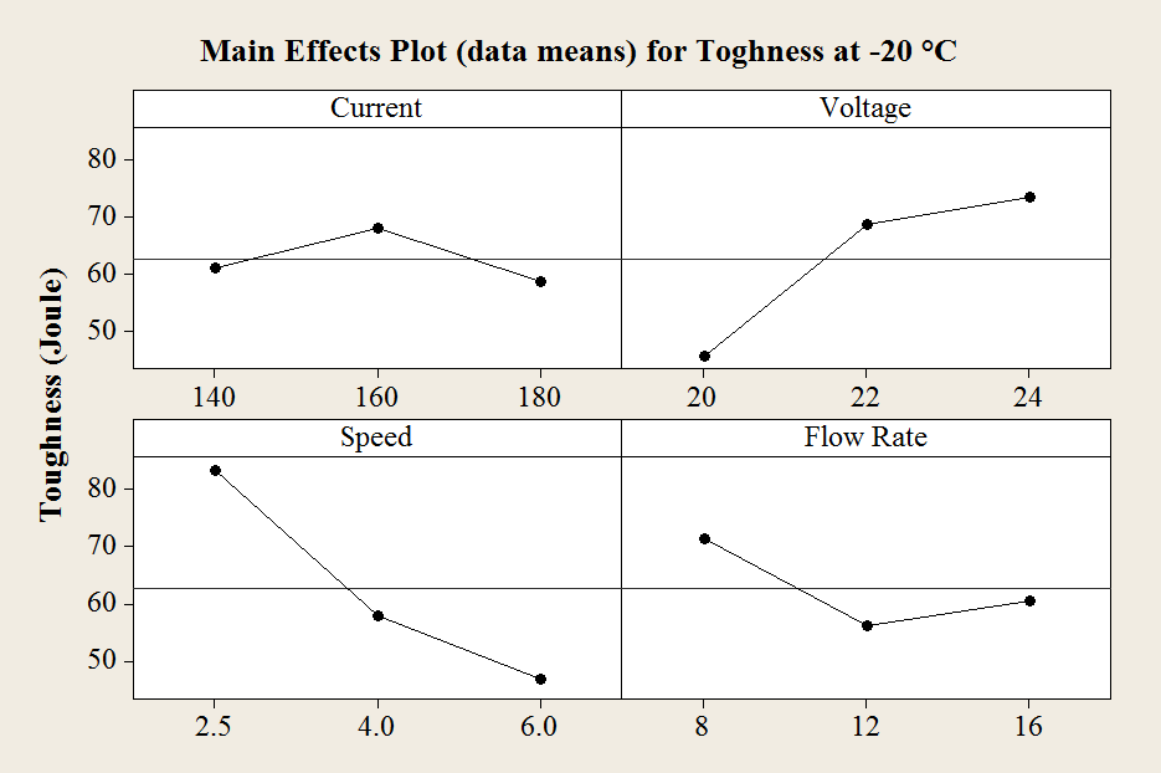

Figure 5.5: Main effects plot for means for toughness (at -20 °C temperature) of AISI 304 specimens

5.2.3 Toughness test results for AISI 316 stainless steel

Toughness of welded samples at -20 °C for AISI 316 stainless steel are completed and results are given in table 5.12.

Table 5.12: Toughness values for various experiments on AISI 316 stainless steel

Experiment. No.	Toughness at -20 °C (Joule)
1.	23.544
2.	39.24
3.	44.145
4.	29.43
5.	53.955
6.	39.24
7.	19.62
8.	56.898
9.	54.936

5.2.4 ANOVA for Toughness of AISI 316 stainless steel

Table 5.12 shows the value of toughness obtained for the specimens of AISI 316 stainless steel at -20 °C. Experimental results are analysed using ANOVA and results are given in table 5.13 and 5.14. It is clear from the table of ANOVA of means that voltage is the most significant factor among all followed by gas flow rate whereas welding current and speed are least significant factors. Graphs for main effects are plotted in figure 5.6 and shows that toughness increases with the increase in the values of the current and it is maximum for a voltage of 23 V and then decreases to a low value at 26 V. Maximum value of toughness is obtained as 56.898 Joules for experiment no. 8 (200 A, 23 V, 2.5 mm/s and 16 l/min.). It is clear from table of ANOVA for means that values of F for voltage and gas flow rate are greater than F (critical) so these both factors are statistically significant. Therefore it can be concluded from the response table for means that the optimal value for toughness at -20 °C is 50.03 Joules.

Table 5.13: Analysis of variance for means toughness for AISI 316 stainless steel

Source	Units	DOF	SS	Variance	F	% Contribution
Current	A	2	102.87	51.433	17.1786	6.77
Voltage	V	2	1162.75	581.373	194.1793	76.52
Speed	mm/s	2	5.99	2.994	-	-
Flow rate	l/min.	2	247.86	123.931	41.3931	16.31
Residual error		0	0	0	-	-
Total		8	1519.46			100
Error pooled		2	5.99	2.994		0.39

(SS = Sum of Squares, F = F factor, factor with least variance value is considered for error pooling)

Table 5.14: Response table for mean toughness at -20 °C temperature for AISI 316

Level	Current	Voltage	Speed	Flow rate
1	35.64	24.20	39.89	44.15
2	40.88	50.03	41.20	32.70
3	43.82	46.11	39.24	43.49
Delta	8.18	25.83	1.96	11.45
Rank	3	1	4	2

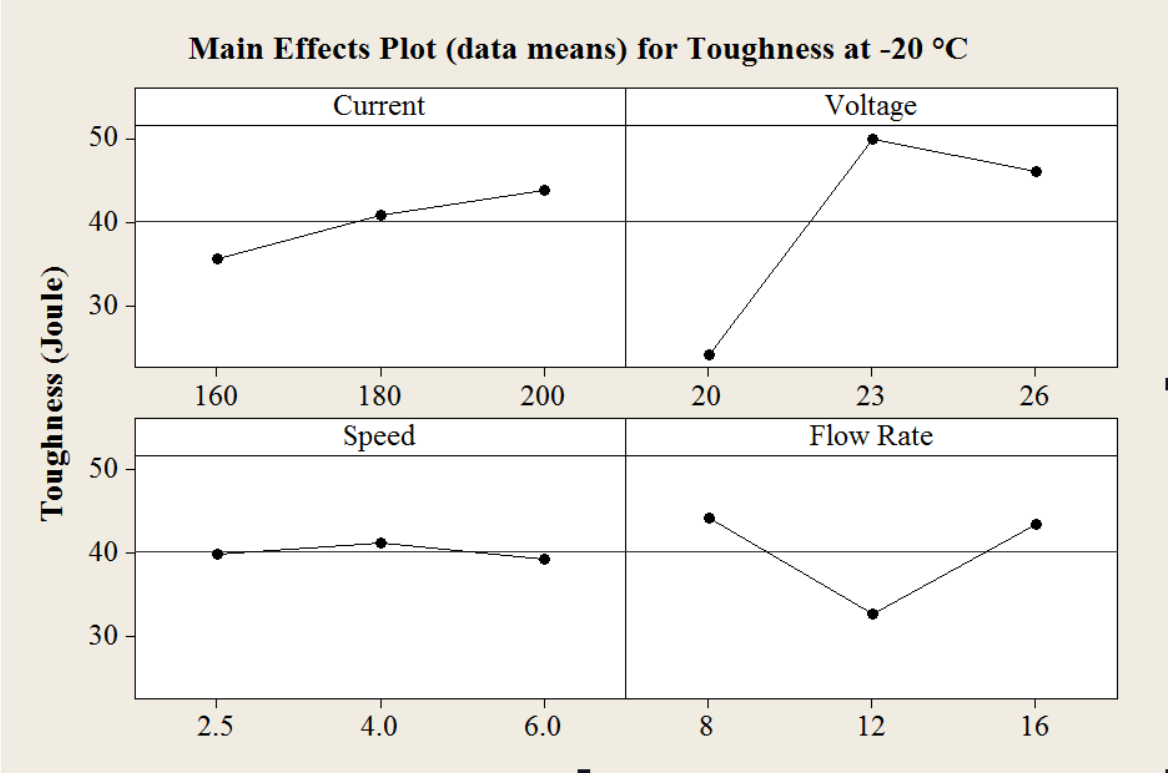

Figure 5.6: Main effects plot for means for toughness (at -20 °C temperature) of AISI 316 specimens

5.3 MICROHARDNESS

Vicker's microhardness test was conducted on all the welding samples including base metals of both AISI 304 and AISI 316 stainless steel. The measurement in microhardness is depended on indents formed in the shape of pyramid on the welded region of welded samples by the indenter were measured with Quantimet software using load of 500 grams for 20 seconds. The values of microhardness (HVN) for both the base metals are shown in table 5.15.

Table 5.15: Microhardness test results for base metal

S. No.	Metal	Microhardness Number (HVN)
1.	AISI 304	81.521
2.	AISI 316	74.261

5.3.1 Microhardness test results for AISI 304 stainless steel

Results for Vickers microhardness test for AISI 304 stainless steel are given in the table 5.16.

Table 5.16: Microhardness values for various experiments on AISI 304 stainless steel

Experiment. No.	Microhardness Number (HVN)
1.	98.791
2.	85.752
3.	87.480
4.	82.769
5.	97.166
6.	95.657
7.	86.537
8.	98.521
9.	81.852

5.3.2 ANOVA for microhardness of AISI 304 stainless steel

Table 5.16 gives all the values of microhardness for various experiments on AISI 304 stainless steel. The experiment results are analysed using ANOVA for identifying the significant factors affecting the performance at 95% confidence interval and the results are shown in table 5.17. It can be concluded from the ANOVA tables that welding speed is the most significant factor for the microhardness and others the factors like voltage and gas flow rate have some effects on the said response, whereas welding current is having negligible effect on microhardness. Main effects plot are shown in figure 5.7 and it can be concluded from the said figure that the values of microhardness is maximum at 2.5 mm/s welding speed. Maximum value of microhardness (HVN) is 98.791 for experiments no. 1 (140 A, 20 V, 2.5 mm/s, 8 l/min.). From ANOVA table of mean it can be concluded that the welding speed is statistically significant factor for the microhardness results and accordingly from the response table for means the optimum value of HVN is 97.66.

Table 5.17: Analysis of variance for means microhardness (HVN) for AISI 304 stainless steel

Source	Units	DOF	SS	Variance	F	% Contribution
Current	A	2	12.695	6.348	-	-
Voltage	V	2	50.919	25.460	4.010	13.190
Speed	mm/s	2	302.456	151.228	23.822	78.349
Flow rate	l/min.	2	19.962	9.981	1.572	5.171
Residual error		0	0	0	-	-
Total		8	386.033			100
Error pooled		2	12.695	6.348		3.288

(SS = Sum of Squares, F = F factor, factor with least variance value is considered for error pooling)

Table 5.18: Response table for mean microhardness (HVN) for AISI 304

Level	Current	Voltage	Speed	Flow rate
1	90.67	89.37	97.66	92.60
2	91.86	93.81	83.46	89.32
3	88.97	88.33	90.39	89.59
Delta	2.89	5.48	14.20	3.29
Rank	4	2	1	3

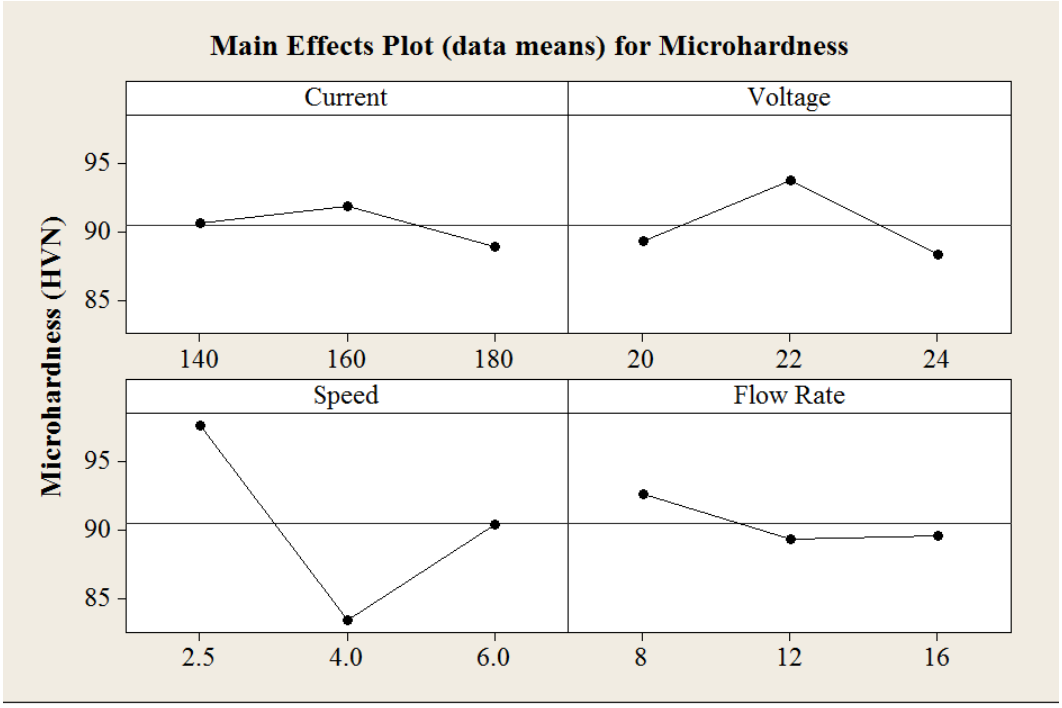

Figure 5.7: Main effects plot for means for microhardness (HVN) of AISI 304 specimens

5.3.3 Microhardness test results for AISI 316 stainless steel

Results for Vicker's microhardness test for AISI 316 stainless steel are given in table 5.19.

Table 5.19: Microhardness values for various experiments on AISI 316 stainless steel

Experiment. No.	Microhardness Number (HVN)
1.	83.991
2.	75.312
3.	81.253
4.	76.361
5.	88.592
6.	89.945
7.	86.476
8.	74.562
9.	78.268

5.3.4 ANOVA for microhardness of AISI 316 stainless steel

Values of microhardness for AISI 316 stainless steel are given in table 5.19. The results of microhardness are analysed using ANOVA for identifying the significant factors affecting the performance at 95% confidence interval are shown in the form of table 5.20. It can be concluded from the table that welding speed is the most significant factor for microhardness measurement and others factors like current and gas flow rate have some effects on the said response whereas voltage is having negligible effect on microhardness. Main effects plot are shown in figure 5.8. It is clear from the main effects plot that the value of microhardness is maximum at 6 mm/s welding speed. It increases with increase in the values of welding speed. Maximum value of HVN is 89.945 for experiment no. 6 (180 A, 26 V, 2.5 mm/s, 12 l/min.). From ANOVA table of means it can be concluded that the welding speed is statistically significant factor for the microhardness results and accordingly from response table for means the optimum value of HVN is 85.44.

Table 5.20: Analysis of variance for means microhardness (HVN) for AISI 316 stainless steel

Source	Units	DOF	SS	Variance	F	% Contribution
Current	A	2	50.041	25.0203	2.2759	18.14
Voltage	V	2	21.987	10.9934	-	-
Speed	mm/s	2	122.385	61.1926	5.5663	44.38
Flow rate	l/min.	2	81.334	40.6672	3.6992	29.49
Residual error		0	0	0	-	-
Total		8	275.747			100
Error pooled		2	21.987	10.9934		7.97

(SS = Sum of Squares, F = F factor, factor with least variance value is considered for error pooling)

Table 5.21: Response table for mean microhardness (HVN) for AISI 316

Level	Current	Voltage	Speed	Flow rate
1	80.19	82.28	82.83	83.62
2	84.97	79.49	76.65	83.91
3	79.77	83.16	85.44	77.39
Delta	5.20	3.67	8.79	6.52
Rank	3	4	1	2

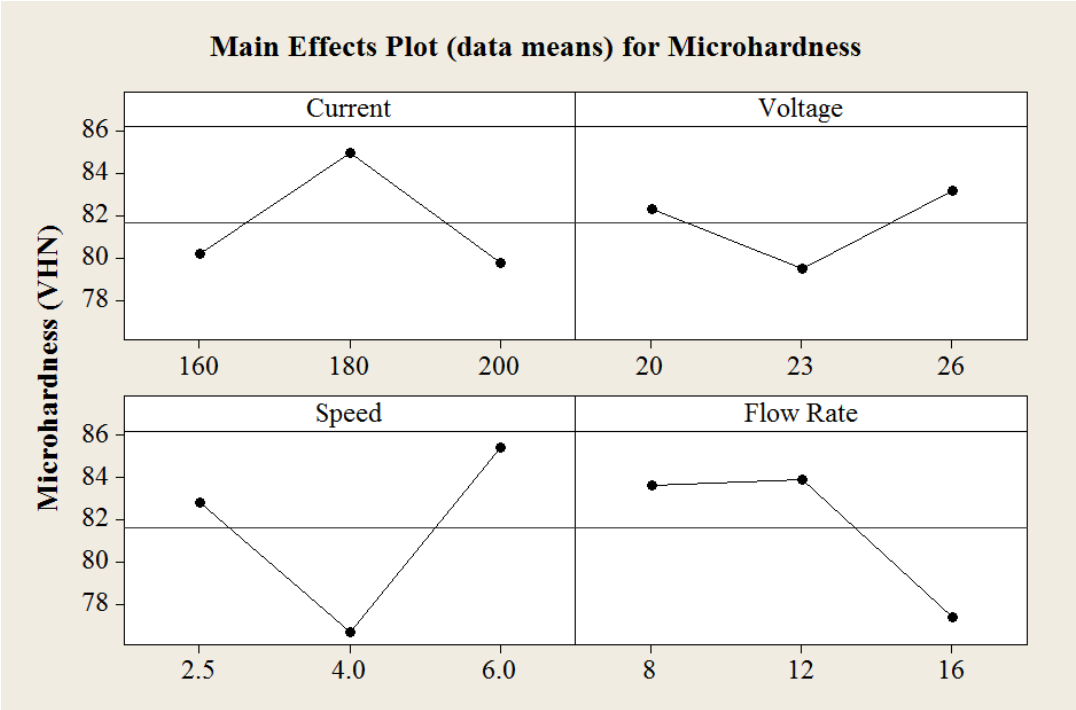

Figure 5.8: Main effects plot for means for microhardness (HVN) of AISI 316 specimens

5.4 METALLURGYCAL TESTING

Further analysis of the welded specimens after confirmation experiments is performed to find out surface composition and microstructure. Surface composition is determined with the help of XRD analysis and microstructural studies are carrying out on a scanning electron microscope.

5.4.1 X-Ray Diffraction results for AISI 304 stainless steel

During welding base metal and electrode metal mixed together due to intense heat and resulting change in properties of weld zone and heat affected zone. The materials mixed together and which forms various compounds. To analyses the modification workpiece is tested by XRD. The range of 2θ from the 20° to 120° is used at a scan speed of 5°/minute for each test.

The XRD pattern of sample 1 for welded specimen of AISI 304 stainless steel is shown in figure 5.9. Pattern list is given in table 5.22 which shows the percentage of the compound according to their score. The pattern shows the traces of carbon chromium iron, silicon chromium, iron nickel, and carbon. The XRD pattern shows that the traces of carbon have not formed any compound.

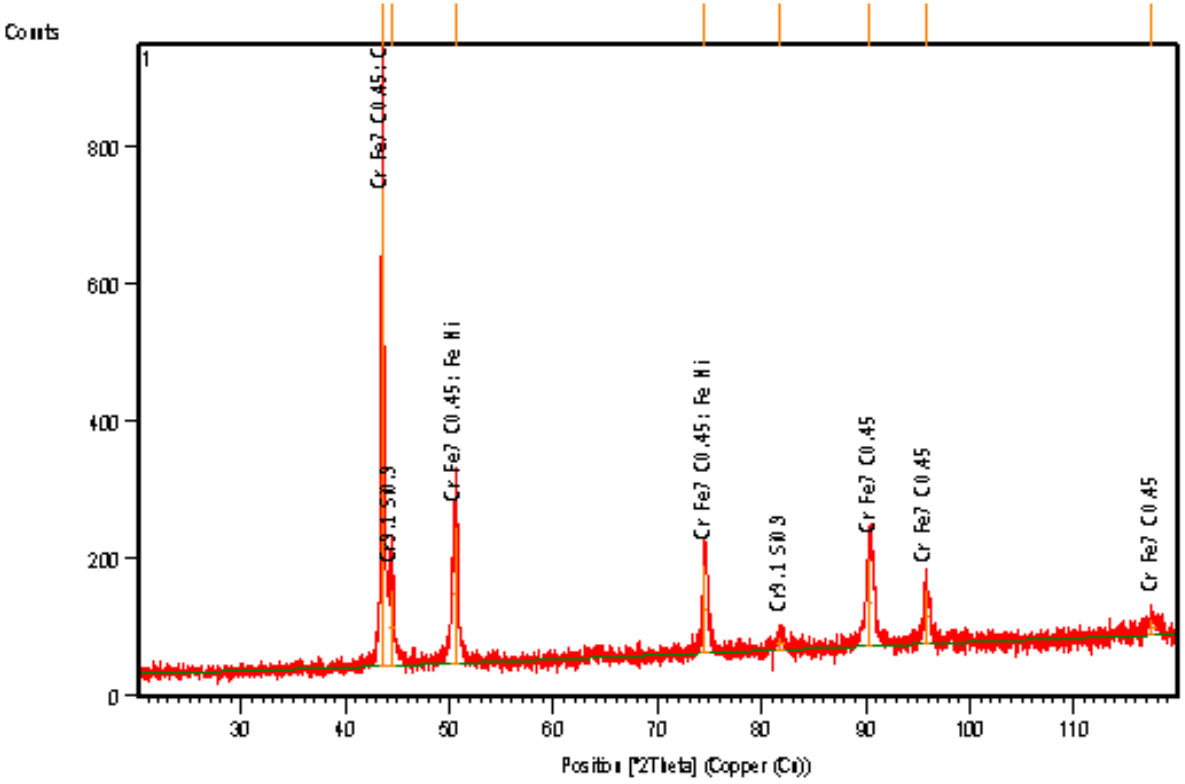

Figure 5.9: XRD pattern obtained for welded sample-1of AISI 304 stainless steel

Table 5.22: Patterns list of welded sample-1 of AISI 304 stainless steel

Ref. code	Score	Compound name	Scale factor	Chem. formula
03-065-9781	83	Carbon chromium iron	0.769	$Cr\ Fe_7\ C_{0.45}$
03-065-5355	44	Silicon chromium	0.170	$Cr_{9.1}\ Si_{0.9}$
00-003-1206	30	Iron nickel	0.119	Fe Ni
01-071-3649	30	Carbon	0.136	C

The XRD pattern of sample 2 for welded specimen of AISI 304 stainless steel is shown in figure 5.10. Pattern list is given in table 5.23 which shows the percentage of the compound according to their score. The pattern shows the formation of chromium nickel, chromium iron, iron manganese and manganese carbide.

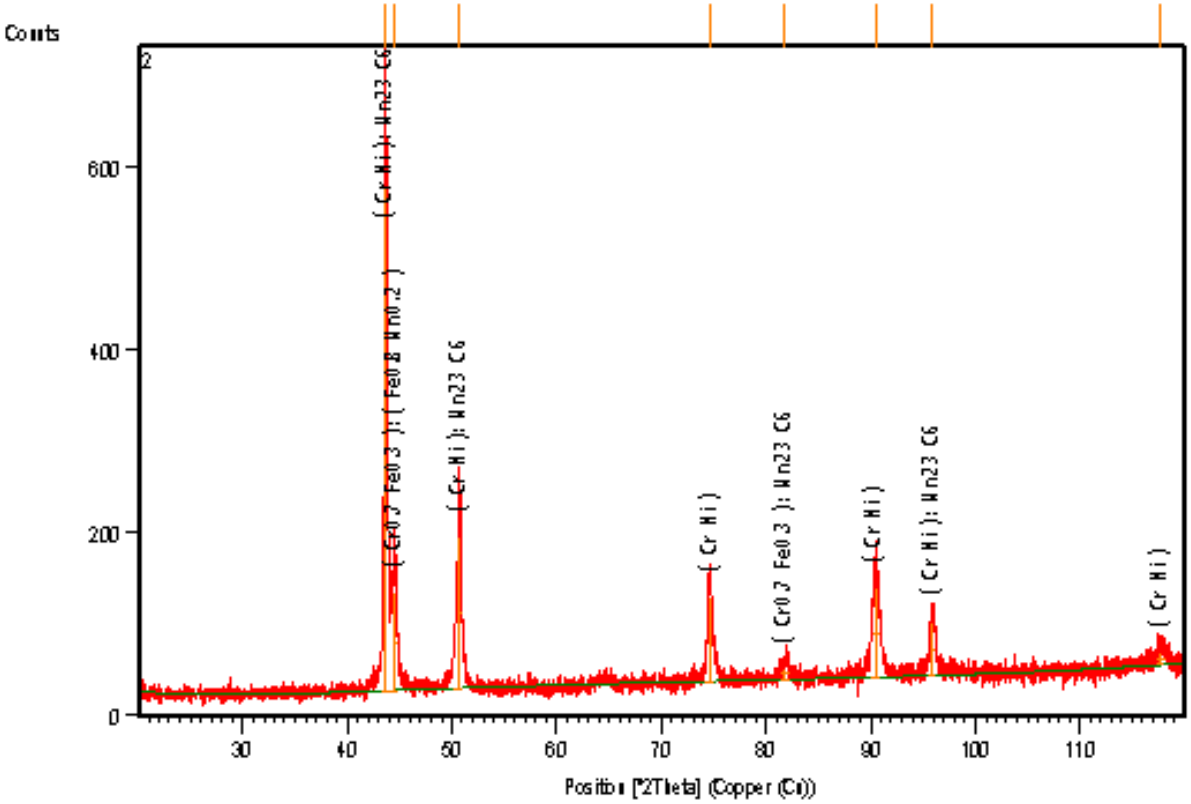

Figure 5.10: XRD pattern obtained for welded sample-2 of AISI 304 stainless steel

Table 5.23: Patterns list of welded sample-2 of AISI 304 stainless steel

Ref. code	Score	Compound name	Scale factor	Chem. formula
01-071-7594	76	Chromium nickel	0.900	Cr Ni
01-071-7537	33	Chromium iron	0.208	$Cr_{0.7}$ $Fe_{0.3}$
01-071-8286	20	Iron manganese	0.110	$Fe_{0.8}$ $Mn_{0.2}$
01-075-2662	21	Manganese carbide	0.487	Mn_{23} C_6

The XRD pattern of sample 3 for welded specimen of AISI 304 stainless steel is shown in figure 5.11. Pattern list is given in table 5.24 which shows the percentage of the compound according to their score. The pattern shows the presence of iron nickel, iron manganese, iron silicon, and iron nickel.

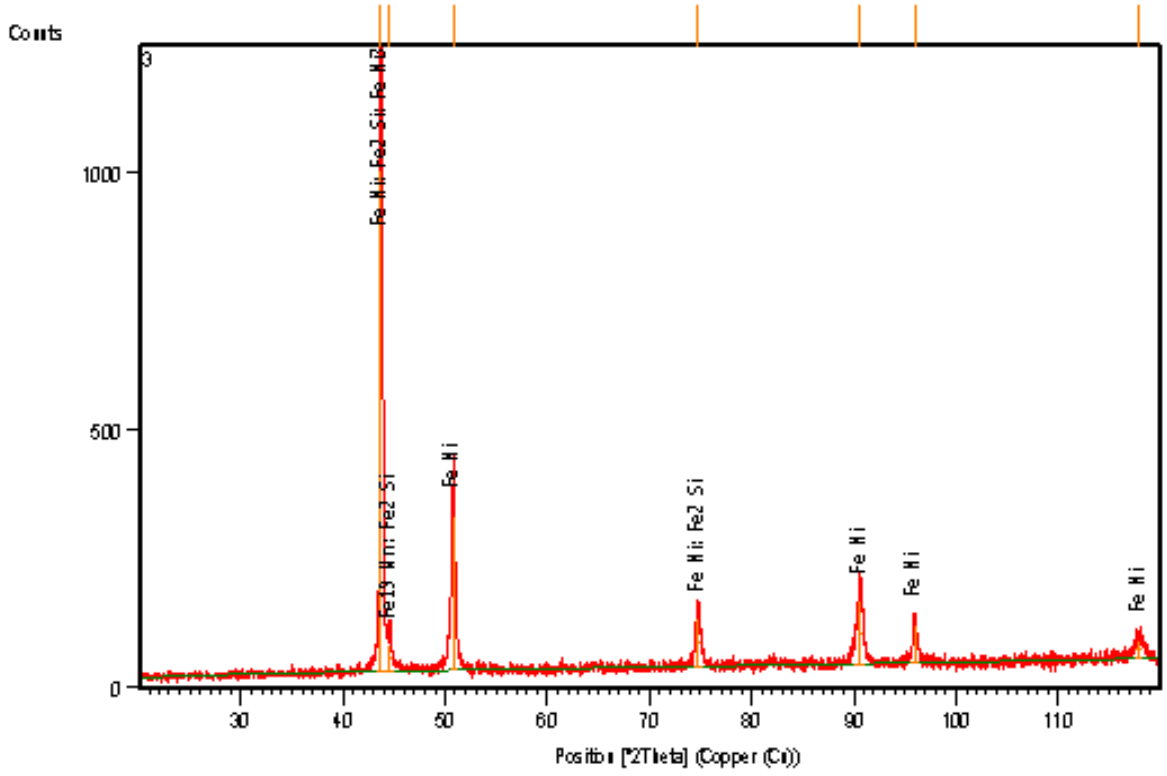

Figure 5.11: XRD pattern obtained for welded sample-3 of AISI 304 stainless steel

Table 5.24: Patterns list of welded sample-3 of AISI 304 stainless steel

Ref. code	Score	Compound name	Scale factor	Chem. formula
00-018-0646	73	Iron nickel	0.162	Fe Ni
03-065-7528	37	Iron manganese	0.069	Fe_{19} Mn
01-083-1259	18	Iron silicon	0.211	Fe_2 Si
01-074-5840	23	Iron nickel	0.211	Fe Ni_3

The XRD pattern of sample 4 for welded specimen of AISI 304 stainless steel is shown in figure 5.12. Pattern list is given in table 5.25 which shows the percentage of the compound according to their score. The pattern shows the traces of chromium iron carbide, iron silicon, carbon chromium and chromium iron.

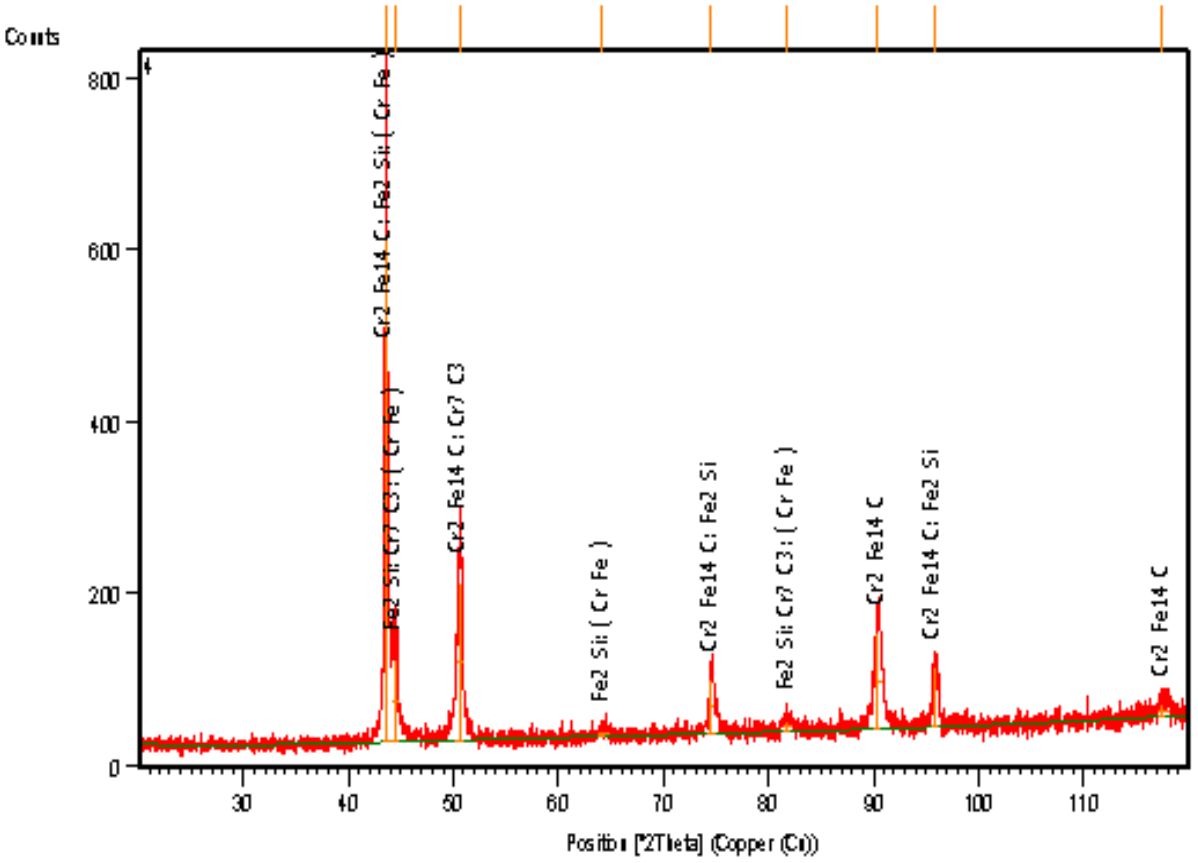

Figure 5.12: XRD pattern obtained for welded sample-4 of AISI 304 stainless steel

Table 5.25: Patterns list of welded sample-4 of AISI 304 stainless steel

Ref. code	Score	Compound name	Scale factor	Chem. formula
01-089-7245	79	Chromium iron carbide	0.702	$Cr_2 Fe_{14} C$
01-083-1259	48	Iron silicon	0.156	$Fe_2 Si$
00-006-0683	8	Carbon chromium	0.154	$Cr_7 C_3$
01-071-7534	36	Chromium iron	0.134	Cr Fe

The XRD pattern of sample 5 for welded specimen of AISI 304 stainless steel is shown in figure 5.13. Pattern list is given in table 5.26 which shows the percentage of the compound according to their score. The pattern shows the traces of chromium iron carbide, silicon chromium, carbon and iron nickel. The XRD pattern shows that the traces of carbon have not formed any compound.

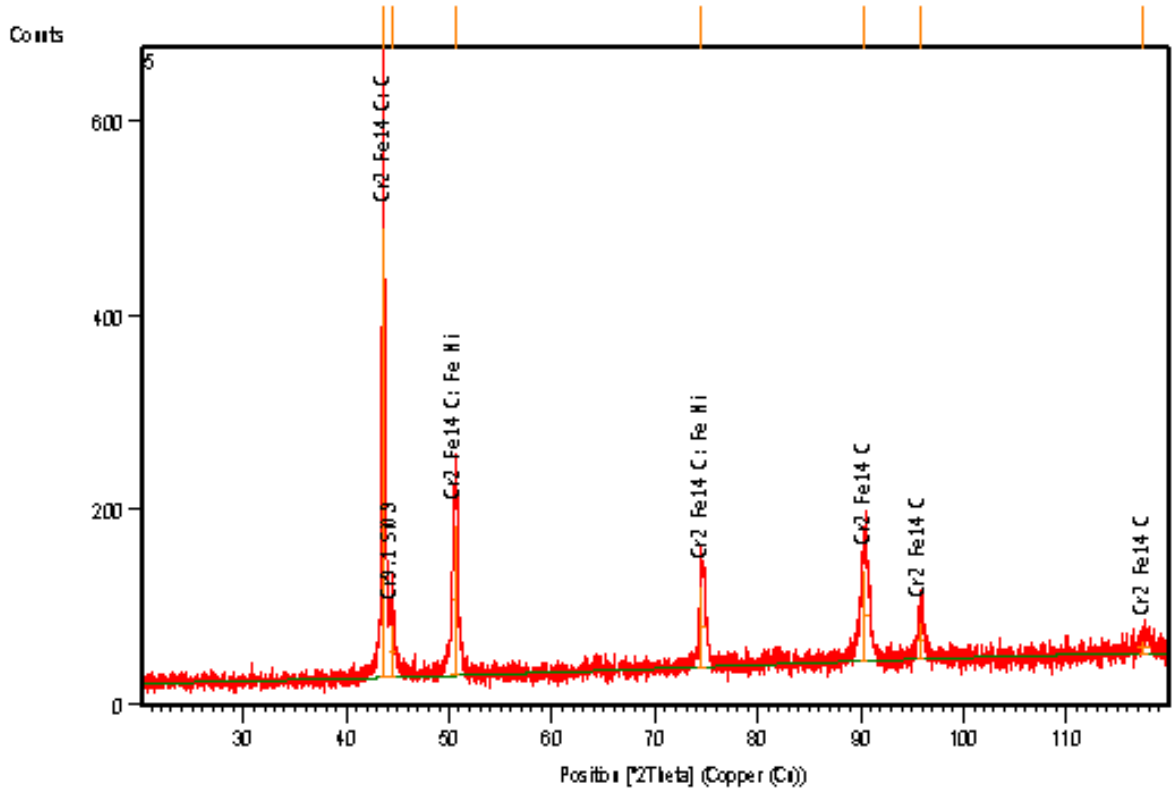

Figure 5.13: XRD pattern obtained for welded sample-5 of AISI 304 stainless steel

Table 5.26: Patterns list of welded sample-5 of AISI 304 stainless steel

Ref. code	Score	Compound name	Scale factor	Chem. formula
01-089-7245	77	Chromium iron carbide	0.707	$Cr_2 Fe_{14} C$
03-065-5355	37	Silicon chromium	0.155	$Cr_{9.1} Si_{0.9}$
01-075-0465	22	Carbon	0.172	C
00-003-1207	33	Iron nickel	0.119	Fe Ni

The XRD pattern of sample 6 for welded specimen of AISI 304 stainless steel is shown in figure 5.14. Pattern list is given in table 5.27 which shows the percentage of the compound according to their score. The pattern shows the traces of iron nickel, chromium nickel, chromium carbide and manganese carbide.

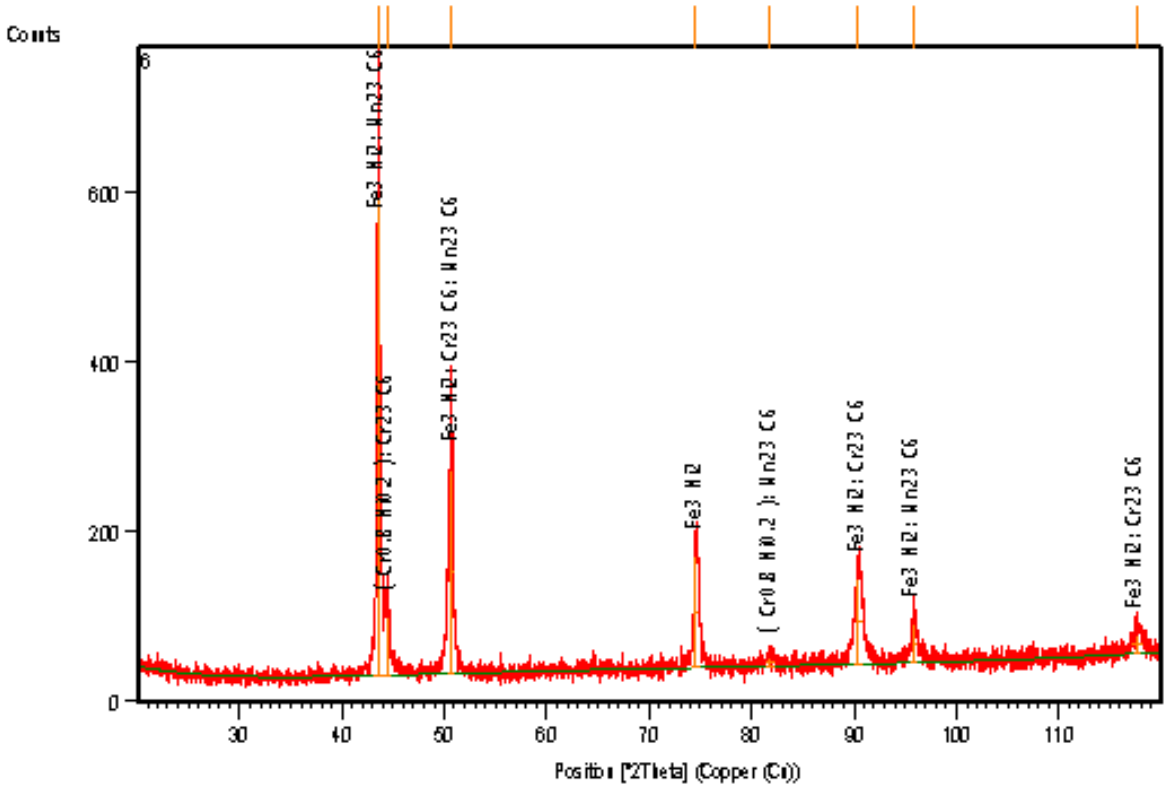

Figure 5.14: XRD pattern obtained for welded sample-6 of AISI 304 stainless steel

Table 5.27: Patterns list of welded sample-6 of AISI 304 stainless steel

Ref. code	Score	Compound name	Scale factor	Chem. formula
03-065-5131	81	Iron nickel	0.977	$Fe_3 Ni_2$
01-071-7597	26	Chromium nickel	0.097	$Cr_{0.8} Ni_{0.2}$
01-071-0552	8	Chromium carbide	0.186	$Cr_{23} C_6$
01-075-2662	16	Manganese carbide	0.271	$Mn_{23} C_6$

The XRD pattern of sample 7 for welded specimen of AISI 304 stainless steel is shown in figure 5.15. Pattern list is given in table 5.28 which shows the percentage of the compound according to their score. The pattern shows the traces of chromium iron carbide, chromium manganese, iron nickel and chromium silicon.

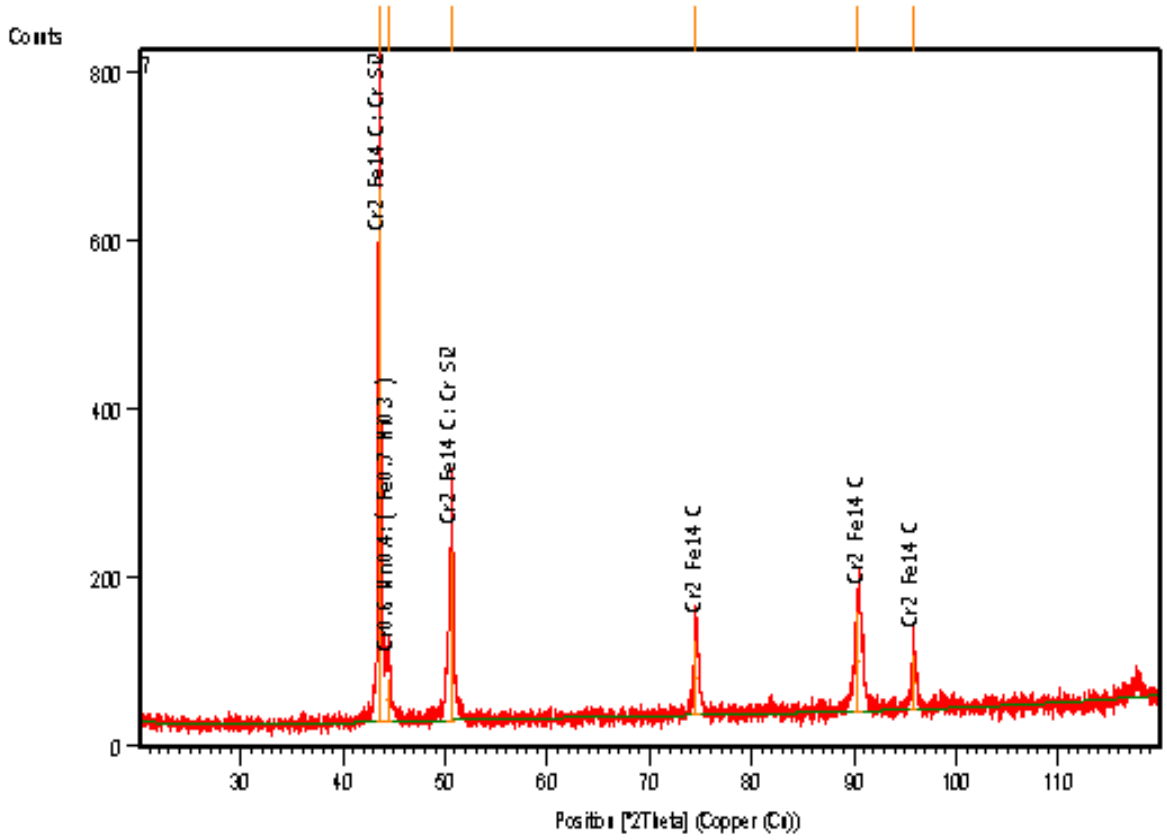

Figure 5.15: XRD pattern obtained for welded sample-7 of AISI 304 stainless steel

Table 5.28: Patterns list of welded sample-7 of AISI 304 stainless steel

Ref. code	Score	Compound name	Scale factor	Chem. formula
01-089-7245	89	Chromium iron carbide	0.841	$Cr_2\ Fe_{14}\ C$
01-074-5721	34	Chromium manganese	0.089	$Cr_{0.6}\ Mn_{0.4}$
01-071-8326	14	Iron nickel	0.050	$Fe_{0.7}\ Ni_{0.3}$
00-012-0596	19	Chromium silicon	0.112	$Cr\ Si_2$

The XRD pattern of sample 8 for welded specimen of AISI 304 stainless steel is shown in figure 5.16. Pattern list is given in table 5.29 which shows the percentage of the compound according to their score. The pattern shows the traces of chromium nickel, chromium, iron nickel and carbon iron. The XRD pattern shows that the traces of chromium have not formed any compound.

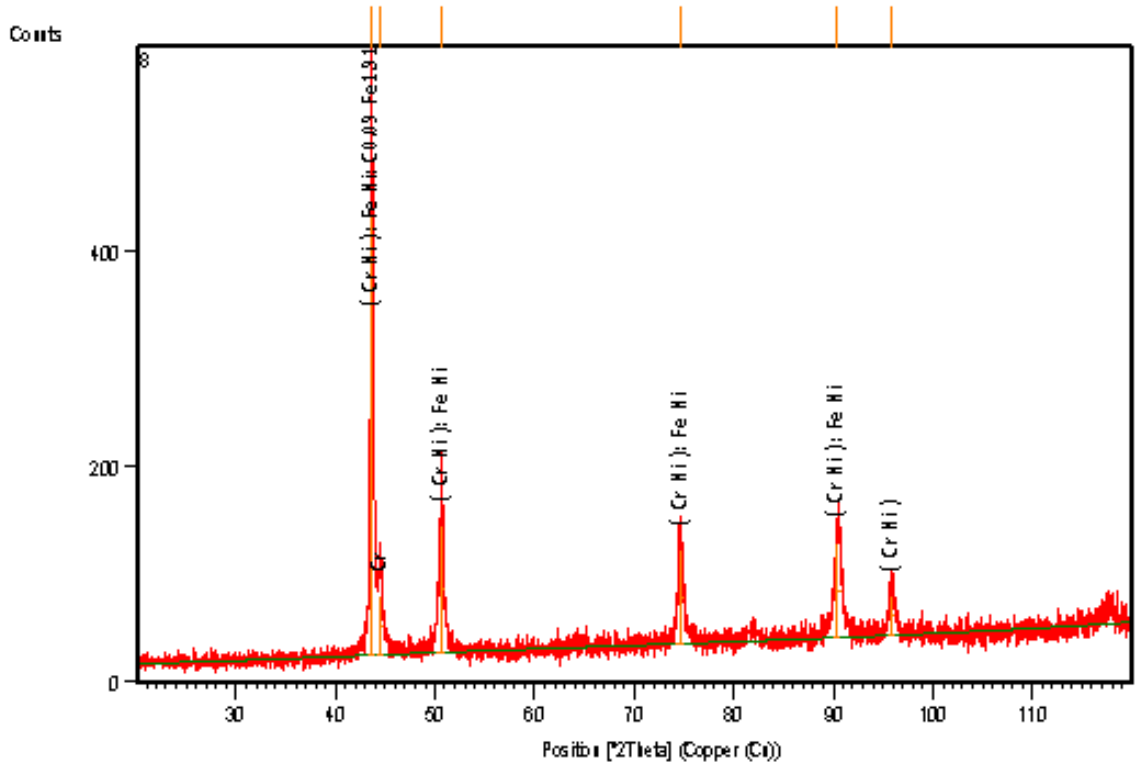

Figure 5.16: XRD pattern obtained for welded sample-8 of AISI 304 stainless steel

Table 5.29: Patterns list of welded sample-8 of AISI 304 stainless steel

Ref. code	Score	Compound name	Scale factor	Chem. formula
01-071-7594	81	Chromium nickel	0.875	Cr Ni
01-085-1336	40	Chromium	0.141	Cr
00-003-1016	43	Iron nickel	0.217	Fe Ni
00-044-1292	16	Carbon iron	0.270	$C_{0.09}$ $Fe_{1.91}$

The XRD pattern of sample 9 for welded specimen of AISI 304 stainless steel is shown in figure 5.17. Pattern list is given in table 5.30 which shows the percentage of the compound according to their score. The pattern shows the traces of manganese nickel, chromium nickel, chromium and manganese carbide. The XRD pattern shows that the traces of chromium have not formed any compound.

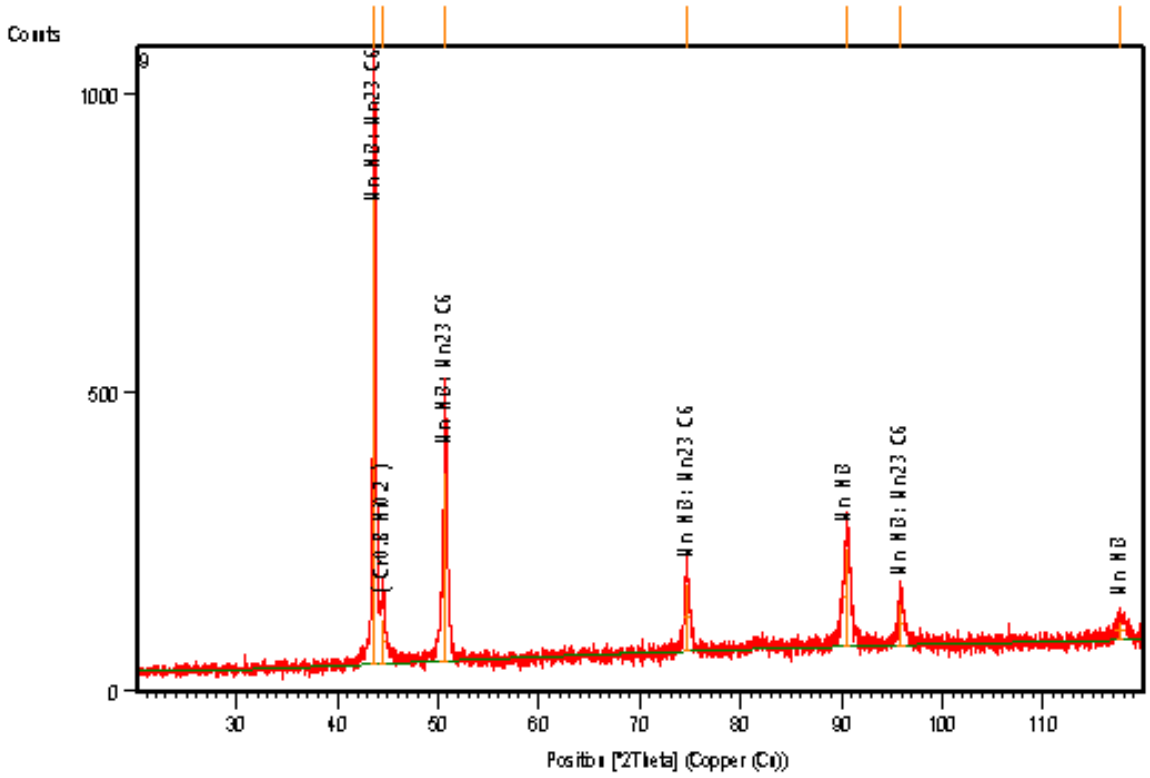

Figure 5.17: XRD pattern obtained for welded sample-9 of AISI 304 stainless steel

Table 5.30: Patterns list of welded sample-9 of AISI 304 stainless steel

Ref. code	Score	Compound name	Scale factor	Chem. formula
01-071-9645	79	Manganese nickel	0.828	$Mn\ Ni_3$
01-071-7597	36	Chromium nickel	0.130	$Cr_{0.8}\ Ni_{0.2}$
01-073-2771	20	Chromium	0.096	Cr
01-075-2662	19	Manganese carbide	0.552	$Mn_{23}\ C_6$

5.4.2 X-Ray Diffraction results for AISI 316 stainless steel

The XRD pattern of sample 1 for welded specimen of AISI 316 stainless steel is shown in figure 5.18. Pattern list is given in table 5.31 which shows the percentage of the compound according to their score. The pattern shows the traces of manganese nickel, manganese silicon, iron nickel and molybdenum nickel.

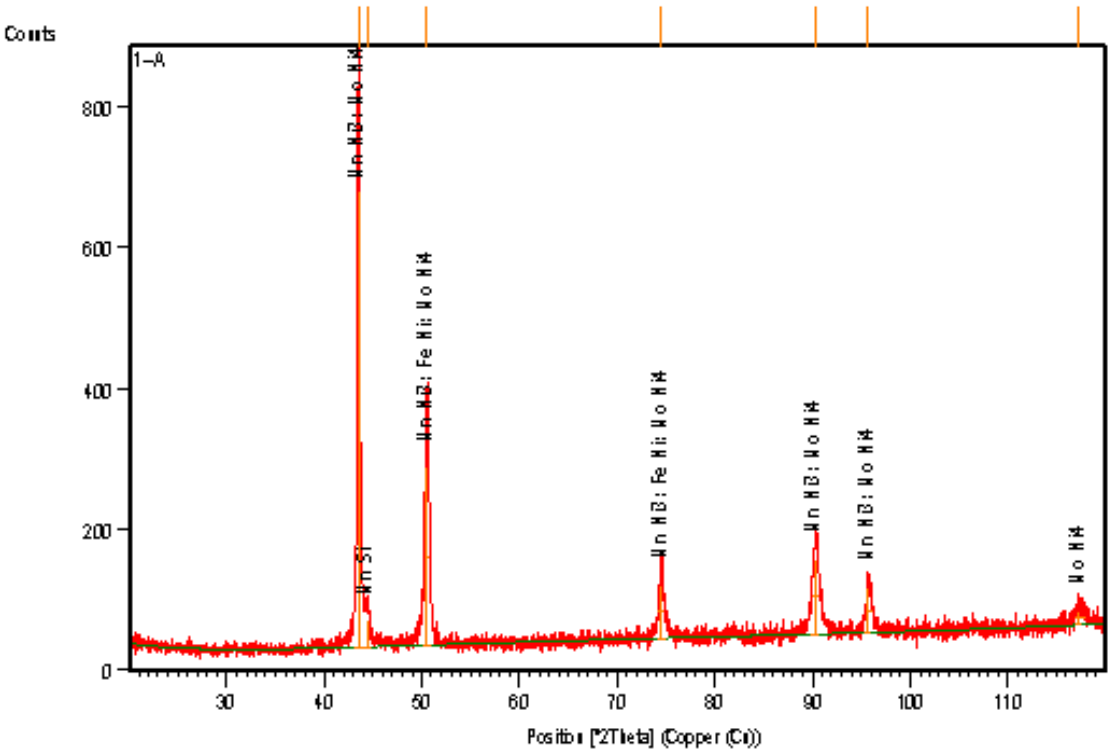

Figure 5.18: XRD pattern obtained for welded sample-1 of AISI 316 stainless steel

Table 5.31: Patterns list of welded sample-1 of AISI 316 stainless steel

Ref. code	Score	Compound name	Scale factor	Chem. formula
01-071-9645	65	Manganese nickel	0.753	$Mn\ Ni_3$
00-042-1487	18	Manganese silicon	0.075	Mn Si
00-003-1206	29	Iron nickel	0.122	Fe Ni
03-065-1533	65	Molybdenum nickel	0.923	$Mo\ Ni_4$

The XRD pattern of sample 2 for welded specimen of AISI 316 stainless steel is shown in figure 5.19. Pattern list is given in table 5.32 which shows the percentage of the compound according to their score. The pattern shows the traces of manganese nickel, silicon chromium, manganese carbide and iron carbide.

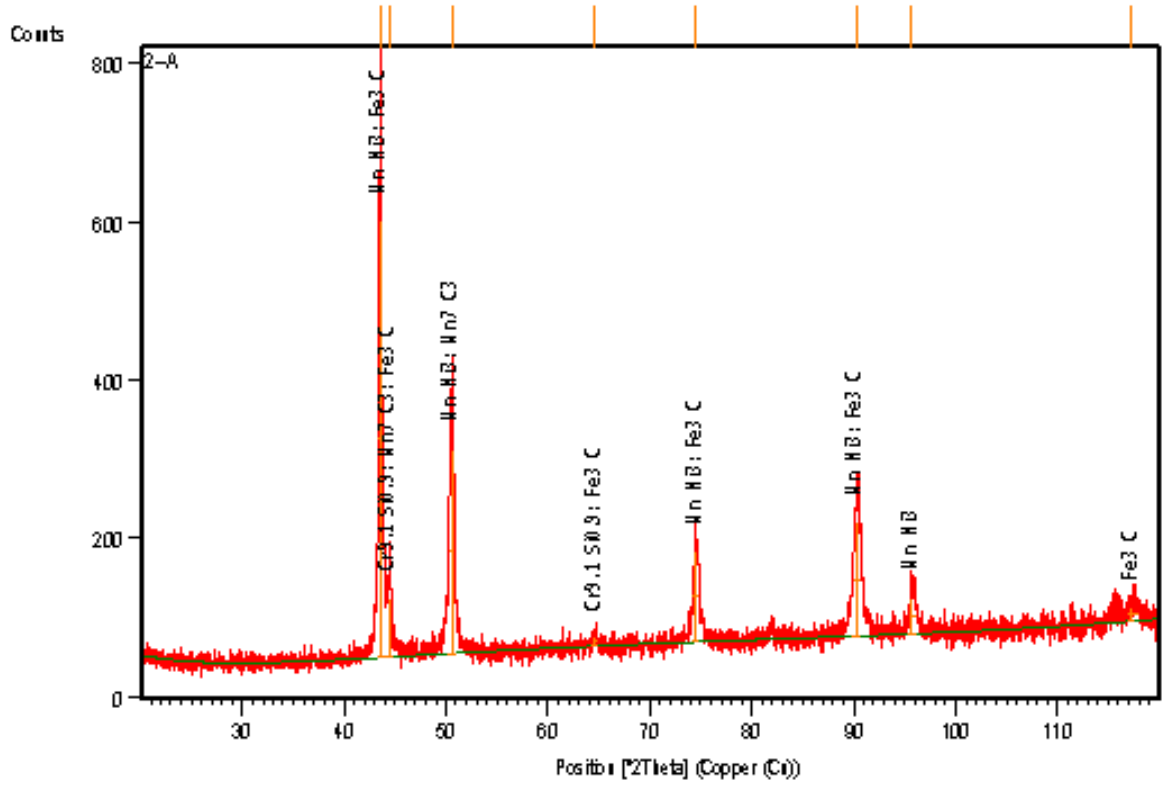

Figure 5.19: XRD pattern obtained for welded sample-2 of AISI 316 stainless steel

Table 5.32: Patterns list of welded sample-2 of AISI 316 stainless steel

Ref. code	Score	Compound name	Scale factor	Chem. formula
01-071-9645	66	Manganese nickel	0.839	$Mn\ Ni_3$
03-065-5355	47	Silicon chromium	0.181	$Cr_{9.1}\ Si_{0.9}$
00-036-1269	12	Manganese carbide	0.091	$Mn_7\ C_3$
01-074-3835	3	Iron carbide	0.332	$Fe_3\ C$

The XRD pattern of sample 3 for welded specimen of AISI 316 stainless steel is shown in figure 5.20. Pattern list is given in table 5.33 which shows the percentage of the compound according to their score. The pattern shows the traces of chromium iron carbide, iron nickel and iron carbon.

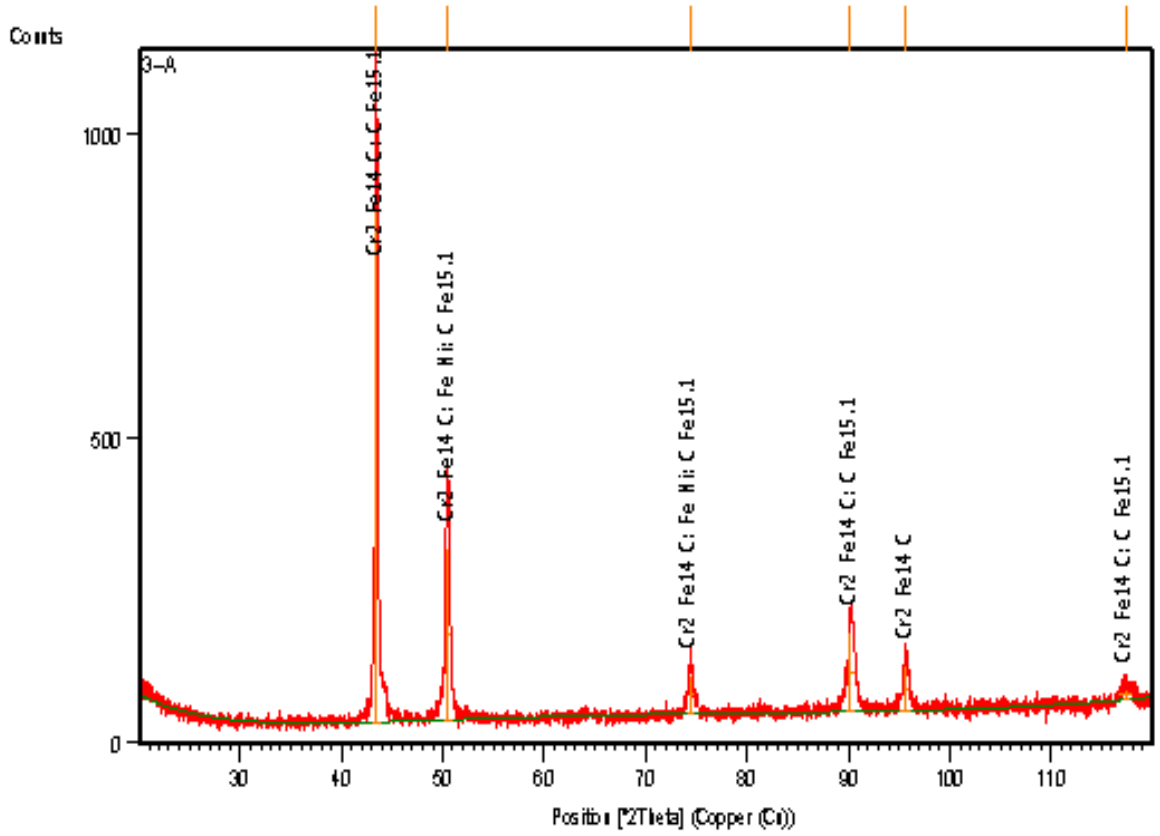

Figure 5.20: XRD pattern obtained for welded sample-3 of AISI 316 stainless steel

Table 5.33: Patterns list of welded sample-3 of AISI 316 stainless steel

Ref. code	Score	Compound name	Scale factor	Chem. formula
01-089-7245	65	Chromium iron carbide	0.751	$Cr_2 Fe_{14} C$
00-003-1207	26	Iron nickel	0.170	Fe Ni
00-052-0512	53	Iron carbon	0.445	$C Fe_{15.1}$

The XRD pattern of sample 4 for welded specimen of AISI 316 stainless steel is shown in figure 5.21. Pattern list is given in table 5.34 which shows the percentage of the compound according to their score. The pattern shows the traces of iron nickel, nickel silicon, chromium iron and chromium nickel.

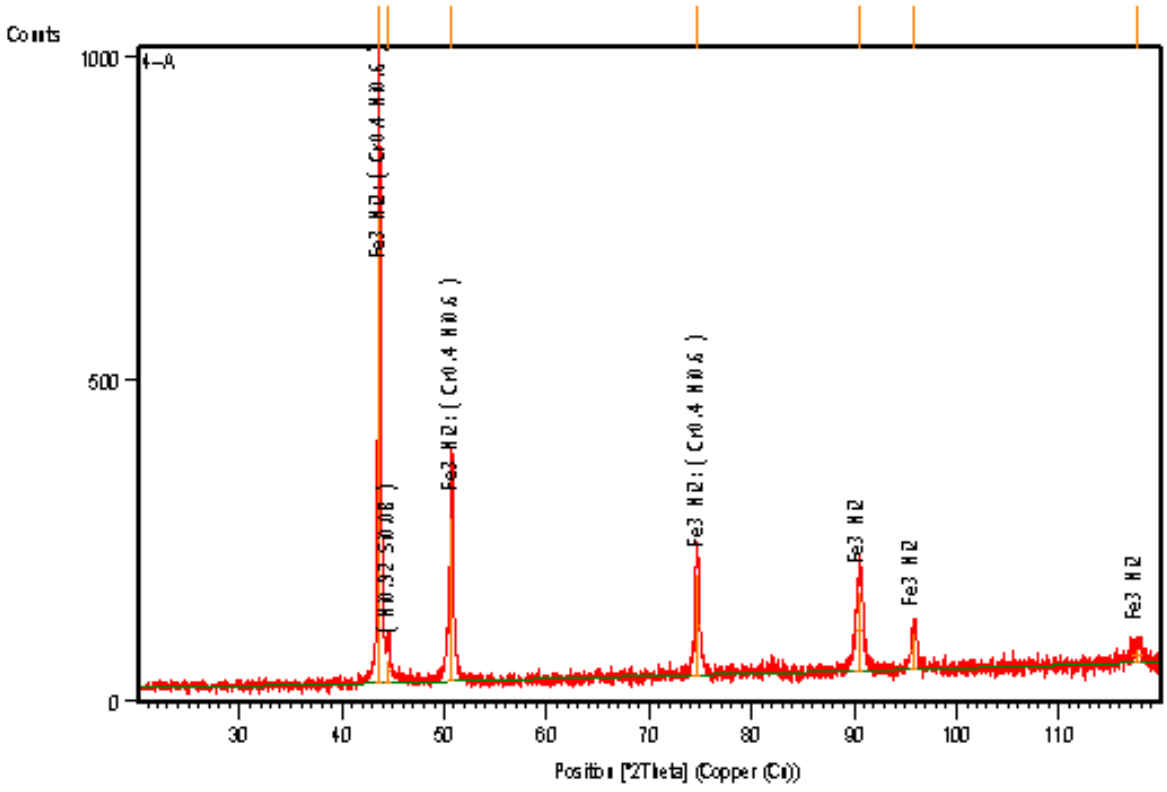

Figure 5.21: XRD pattern obtained for welded sample-4 of AISI 316 stainless steel

Table 5.34: Patterns list of welded sample-4 of AISI 316 stainless steel

Ref. code	Score	Compound name	Scale factor	Chem. formula
03-065-5131	78	Iron nickel	0.595	$Fe_3 Ni_2$
01-072-2550	27	Nickel silicon	0.062	$Ni_{0.92} Si_{0.08}$
01-071-7534	19	Chromium iron	0.067	Cr Fe
01-071-7596	40	Chromium nickel	0.591	$Cr_{0.4} Ni_{0.6}$

The XRD pattern of sample 5 for welded specimen of AISI 316 stainless steel is shown in figure 5.22. Pattern list is given in table 5.35 which shows the percentage of the compound according to their score. The pattern shows the traces of chromium iron carbide, iron nickel, silicon oxide and chromium. The XRD pattern shows that the traces of chromium have not formed any compound.

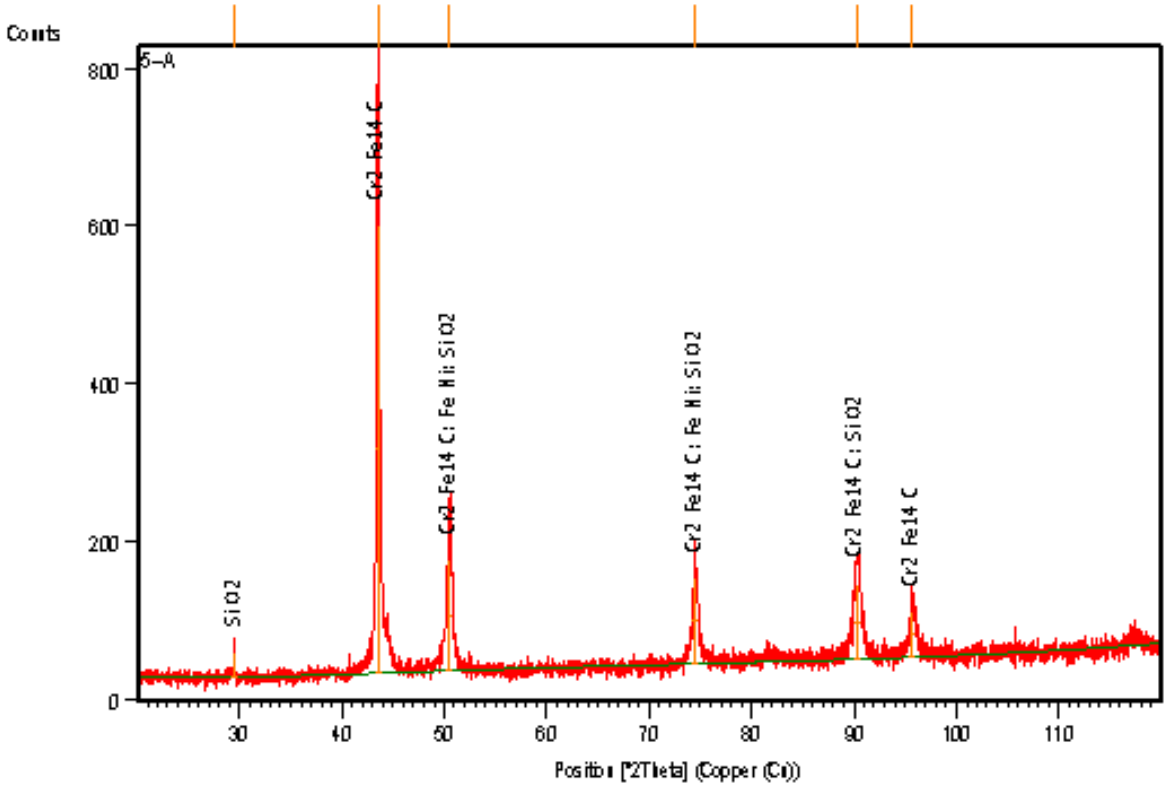

Figure 5.22: XRD pattern obtained for welded sample-5 of AISI 316 stainless steel

Table 5.35: Patterns list of welded sample-5 of AISI 316 stainless steel

Ref. code	Score	Compound name	Scale factor	Chem. formula
01-089-7245	77	Chromium iron carbide	0.925	$Cr_2 Fe_{14} C$
00-003-1206	34	Iron nickel	0.114	Fe Ni
01-075-4411	19	Silicon oxide	0.051	$Si O_2$
01-085-1336	18	Chromium	0.082	Cr

The XRD pattern of sample 6 for welded specimen of AISI 316 stainless steel is shown in figure 5.23. Pattern list is given in table 5.36 which shows the percentage of the compound according to their score. The pattern shows the traces of iron nickel, silicon chromium, molybdenum nickel and chromium carbide.

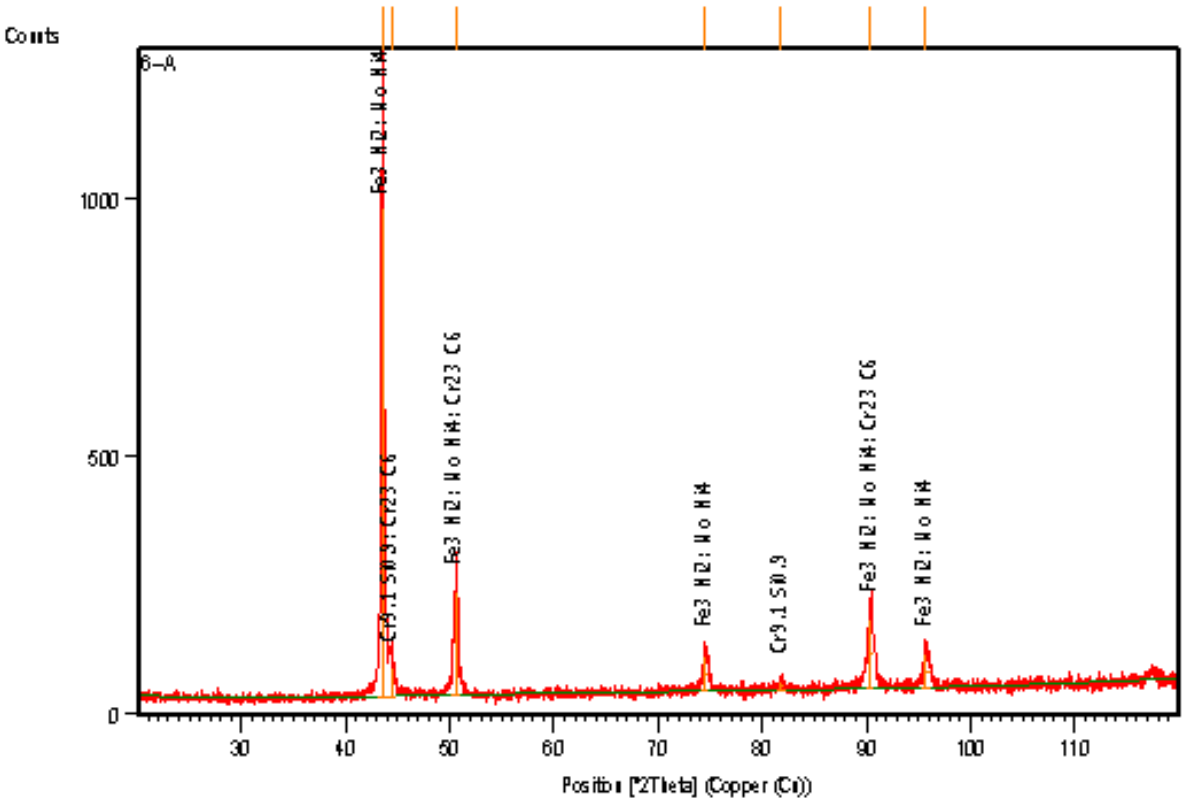

Figure 5.23: XRD pattern obtained for welded sample-6 of AISI 316 stainless steel

Table 5.36: Patterns list of welded sample-6 of AISI 316 stainless steel

Ref. code	Score	Compound name	Scale factor	Chem. formula
03-065-5131	74	Iron nickel	0.901	$Fe_3 Ni_2$
03-065-5355	48	Silicon chromium	0.072	$Cr_{9.1} Si_{0.9}$
03-065-5480	47	Molybdenum nickel	0.904	$Mo Ni_4$
00-035-0783	10	Chromium carbide	0.107	$Cr_{23} C_6$

The XRD pattern of sample 7 for welded specimen of AISI 316 stainless steel is shown in figure 5.24. Pattern list is given in table 5.37 which shows the percentage of the compound according to their score. The pattern shows the traces of chromium nickel, iron nickel, iron carbide and chromium iron carbide.

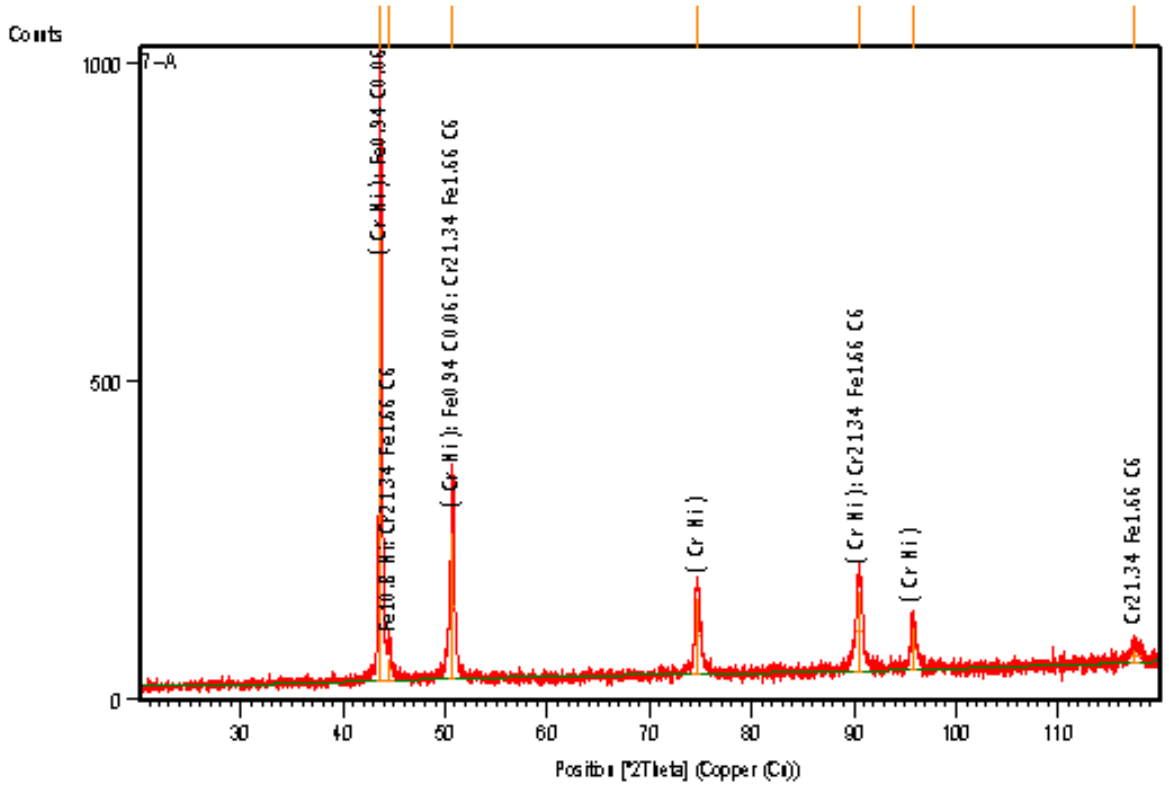

Figure 5.24: XRD pattern obtained for welded sample-7 of AISI 316 stainless steel

Table 5.37: Patterns list of welded sample-7 of AISI 316 stainless steel

Ref. code	Score	Compound name	Scale factor	Chem. formula
01-071-7594	78	Chromium nickel	0.790	Cr Ni
03-065-7753	36	Iron nickel	0.057	$Fe_{10.8}$ Ni
01-074-5520	24	Iron carbide	0.090	$Fe_{0.94}$ $C_{0.06}$
01-078-1500	6	Chromium iron carbide	0.144	$Cr_{21.34}$ $Fe_{1.66}$ C_6

The XRD pattern of sample 8 for welded specimen of AISI 316 stainless steel is shown in figure 5.25. Pattern list is given in table 5.38 which shows the percentage of the compound according to their score. The pattern shows the traces of iron nickel, iron molybdenum, chromium iron and chromium nickel.

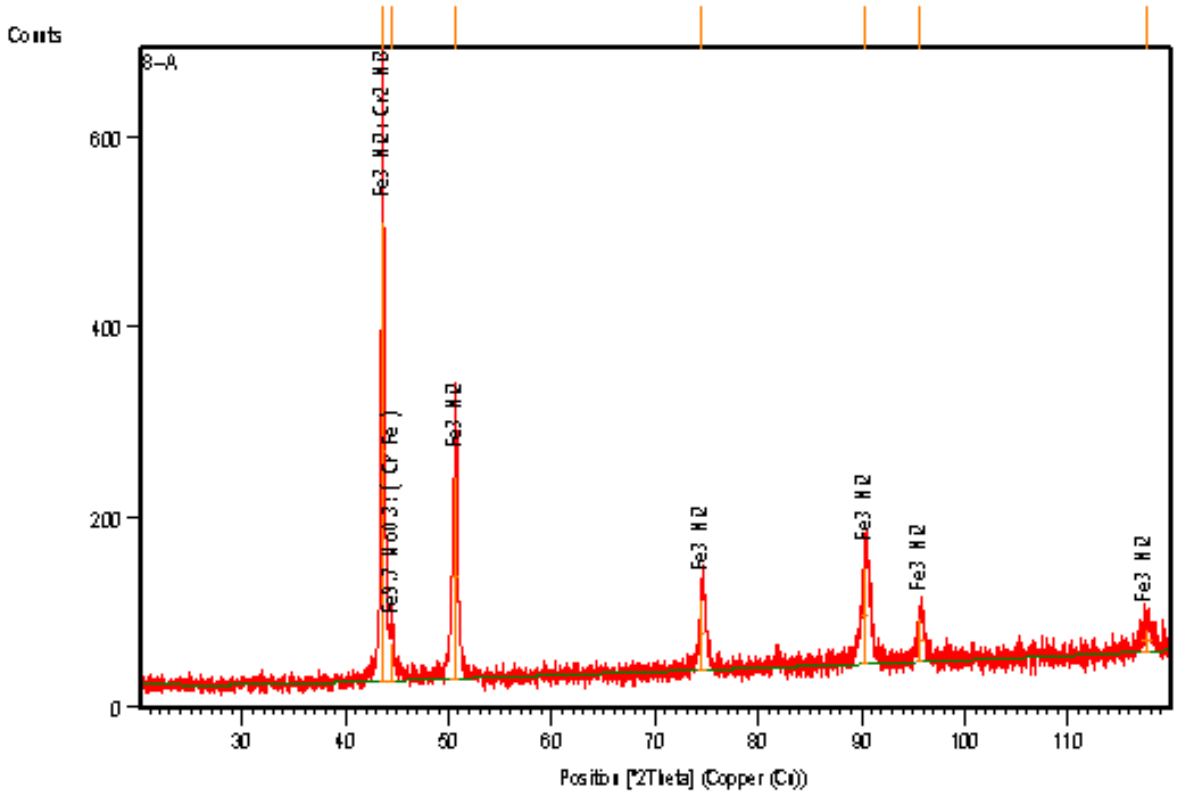

Figure 5.25: XRD pattern obtained for welded sample-8 of AISI 316 stainless steel

Table 5.38: Patterns list of welded sample-8 of AISI 316 stainless steel

Ref. code	Score	Compound name	Scale factor	Chem. formula
03-065-5131	78	Iron nickel	0.816	$Fe_3 Ni_2$
03-065-7296	39	Iron molybdenum	0.090	$Fe_{9.7} Mo_{0.3}$
01-071-7534	19	Chromium iron	0.091	Cr Fe
03-065-6291	41	Chromium nickel	0.466	$Cr_2 Ni_3$

The XRD pattern of sample 9 for welded specimen of AISI 316 stainless steel is shown in figure 5.26. Pattern list is given in table 5.39 which shows the percentage of the compound according to their score. The pattern shows the traces of chromium, iron and iron nickel. The XRD pattern shows that the traces of carbon have not formed any compound.

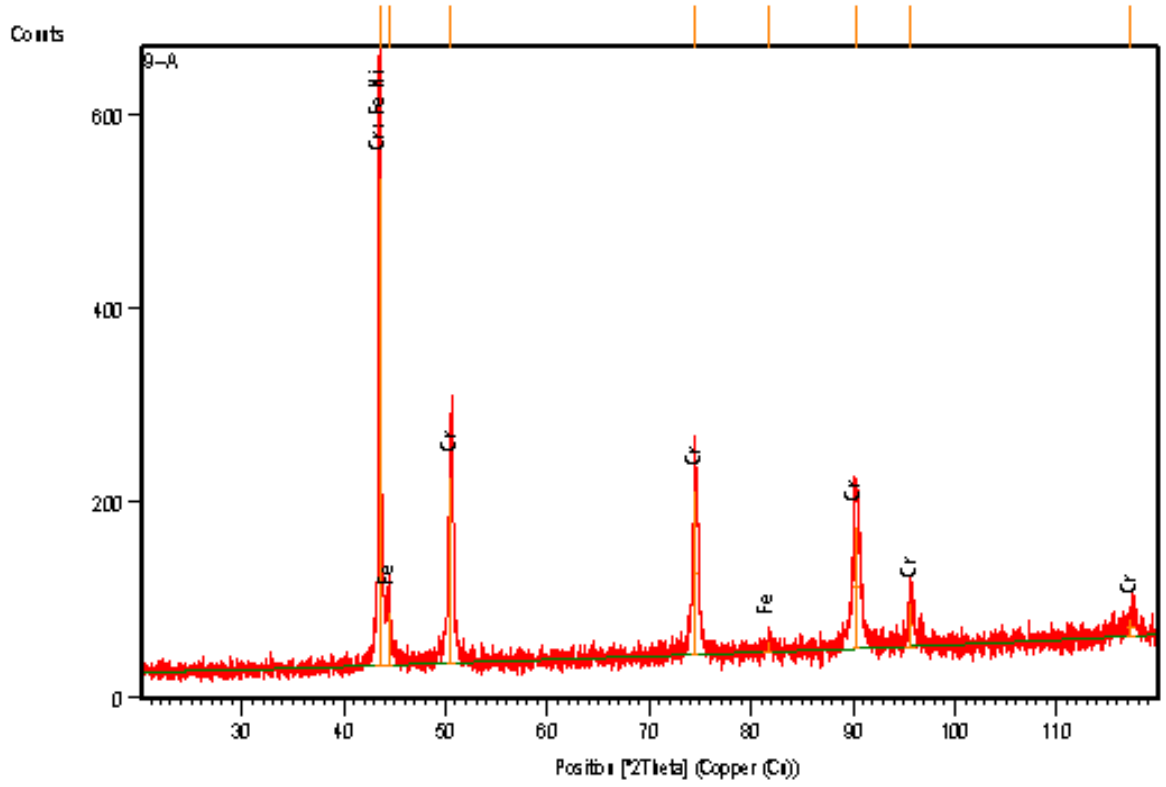

Figure 5.26: XRD pattern obtained for welded sample-9 of AISI 316 stainless steel

Table 5.39: Patterns list of welded sample-9 of AISI 316 stainless steel

Ref. code	Score	Compound name	Scale factor	Chem. formula
01-088-2323	72	Chromium	0.895	Cr
01-085-1410	50	Iron	0.132	Fe
01-071-8321	29	Iron nickel	0.193	Fe Ni

5.4.3 Scanning Electron Microscopy results for AISI 304 stainless steel

Microstructure analysis is carried out on welded specimens using scanning electron microscope to study the change in the microstructure after welding. The samples are prepared as per the standards before SEM analysis on three different magnifications namely 250X, 1000X and 2000X. Samples of AISI 304 stainless steel used for performing SEM are shown in figure 5.27.

Figure 5.27: Samples for scanning electron microscopy

Table 5.40: SEM results of AISI 304 stainless steel

SN	SEM Micrograph at 250x of Fusion Boundary	SEM Micrograph at 1000x of HAZ (A)	SEM Micrograph at 2000x of Weld Zone (B)
1	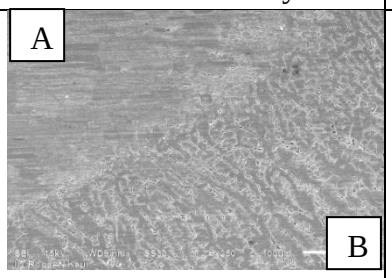	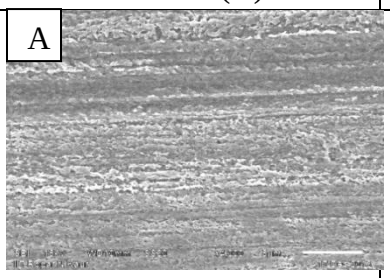	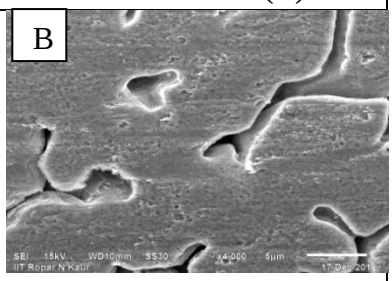
(140 A, 20 V, 2.5 mm/s, 8 l/min.) Heat input = 1120 J/mm			
2	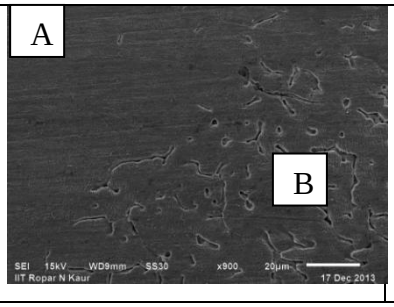	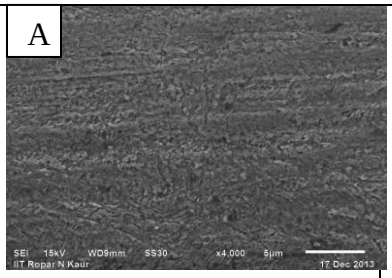	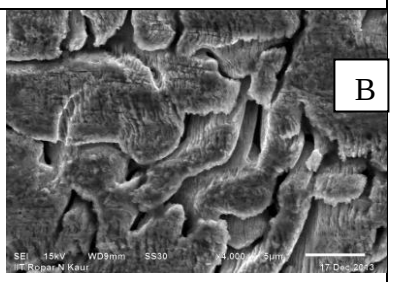
(140 A, 22 V, 4 mm/s, 12 l/min.) Heat input = 1232 J/mm			
3	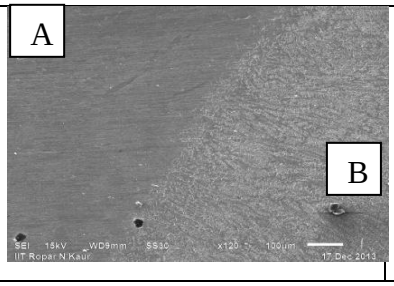	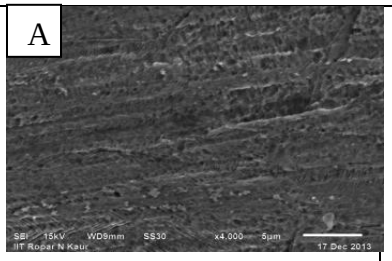	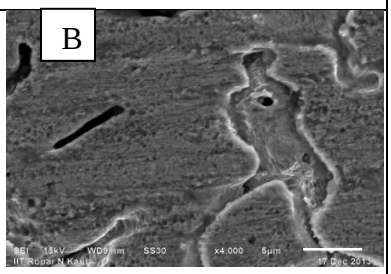
(140 A, 24 V, 6 mm/s, 16 l/min.) Heat input = 560 J/mm			
4	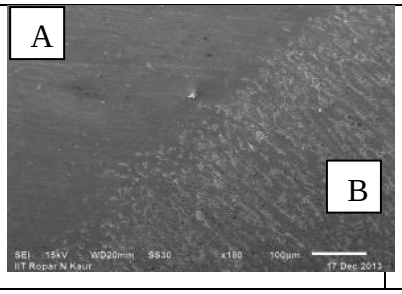	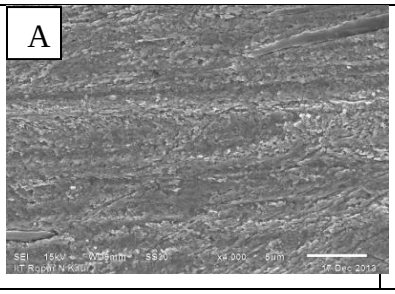	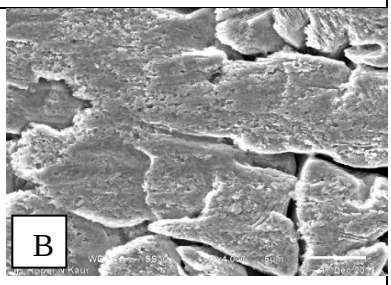
(160 A, 20 V, 4 mm/s, 16 l/min.) Heat input = 800 J/mm			
5	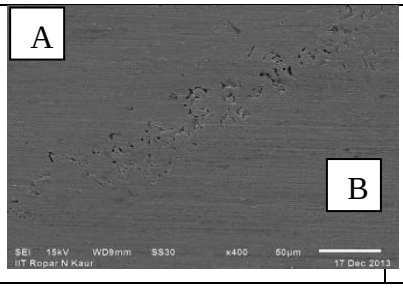	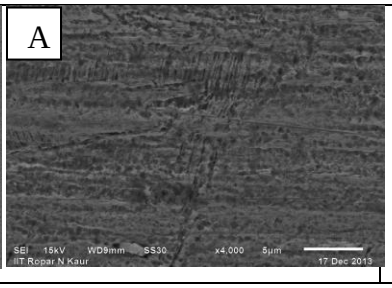	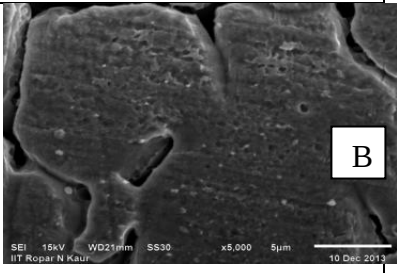
(160 A, 22 V, 6 mm/s, 8 l/min.) Heat input = 587 J/mm			

S N	SEM Micrograph at 250x of Fusion Boundary	SEM Micrograph at 1000x of HAZ (A)	SEM Micrograph at 2000x of Weld Zone (B)
6	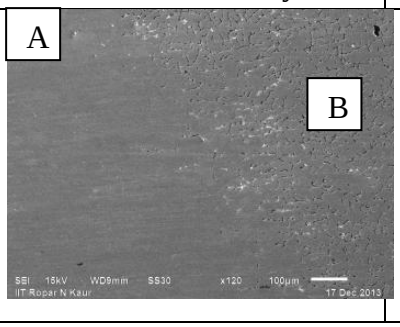	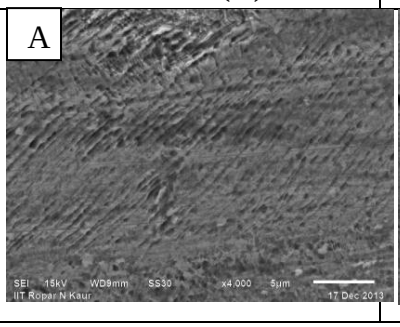	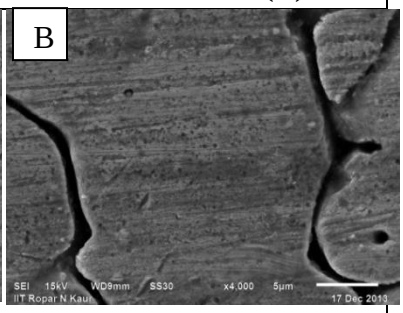
(160 A, 24 V, 2.5 mm/s, 12 l/min.) Heat input = 1536 J/mm			
7	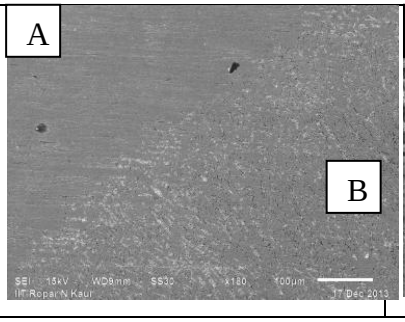	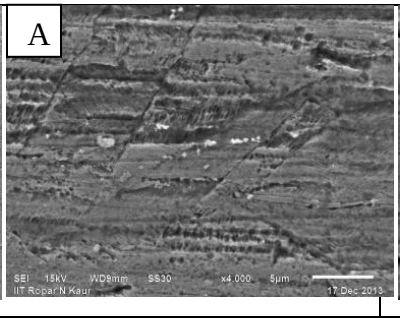	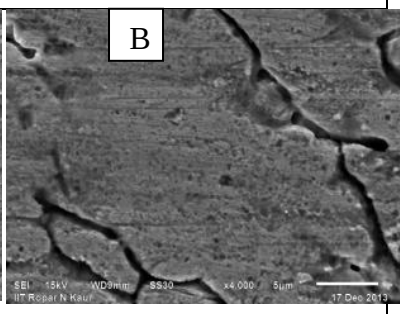
(180 A, 20 V, 6 mm/s, 12 l/min.) Heat input = 600 J/mm			
8	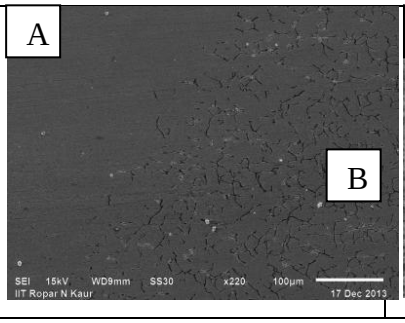	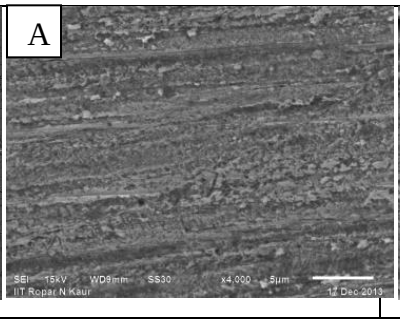	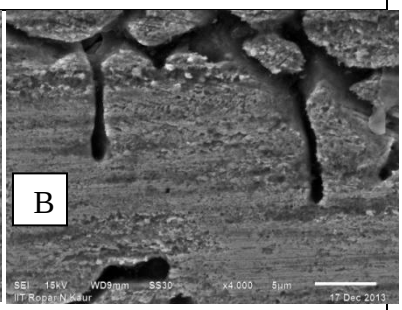
(180 A, 22 V, 2.5 mm/s, 16 l/min.) Heat input = 1584 J/mm			
9	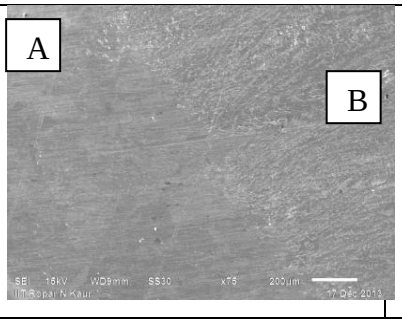	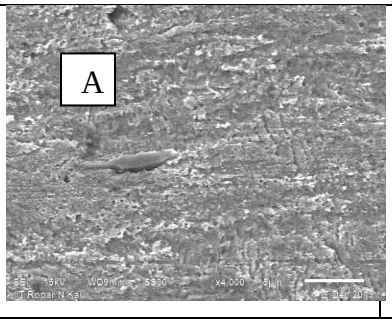	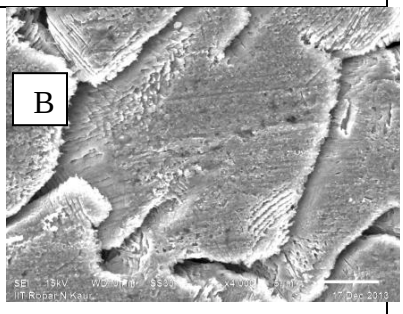
(180 A, 24 V, 4 mm/s, 8 l/min.) Heat input = 1080 J/mm			

The SEM results of all welded specimens of AISI 304 stainless steel is given in table 5.40. The first column of the table shows the boundary of weld zone and heat affected zone of different welded specimens. Similarly in second and third column of the table shows the zoomed HAZ and weld zone respectively at different welding parameters. Adjacent to the weld zone the heat affected zone composed of parent metal heated enough that different grain growth occurred in AISI 304 stainless steel shown in third column of the table 5.40. Depending upon the different welding parameters and solidification rates, the different cellular or dendrite growth of weld zone can be seen in second column of the table 5.40. The fine grain microstructure exhibit greater yield stresses than coarse grain structure. The heat input due to different welding parameters is different in all the specimens and given below the SEM micrographs. It can be concluded from the table 5.40 that the heat input is maximum in sample-6 (1536 J/mm) and consequently the grain size was maximum.

5.4.4 Scanning Electron Microscopy results for AISI 316 stainless steel

Different SEM results of welded specimens of AISI 316 stainless steel are given in table 5.41.

Table 5.41: SEM results of AISI 316 stainless steel

S N	SEM Micrograph at 250x of Fusion Boundary	SEM Micrograph at 1000x of HAZ (A)	SEM Micrograph at 2000x of Weld Zone (B)
1	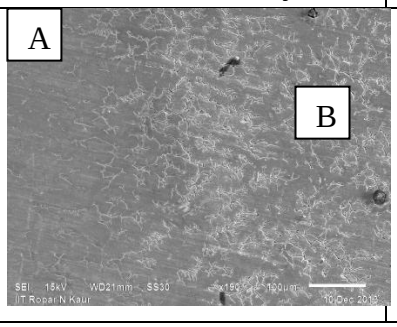	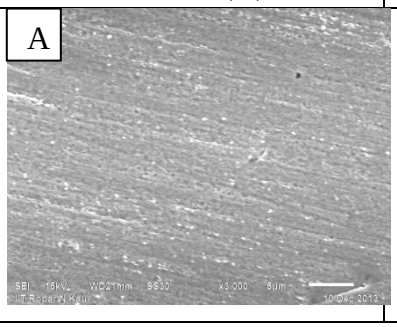	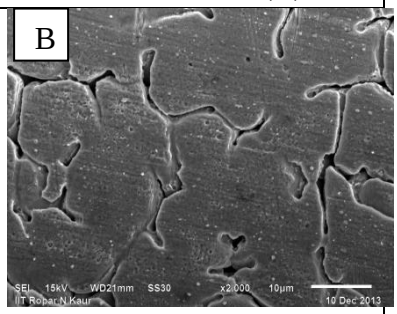
(160 A, 20 V, 2.5 mm/s, 8 l/min.) Heat input = 1280 J/mm			
2	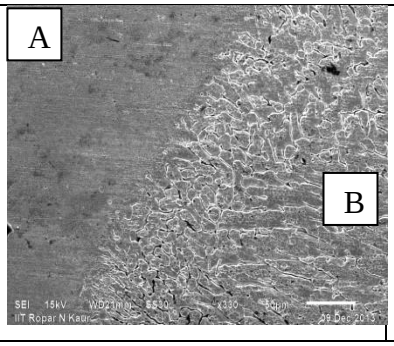	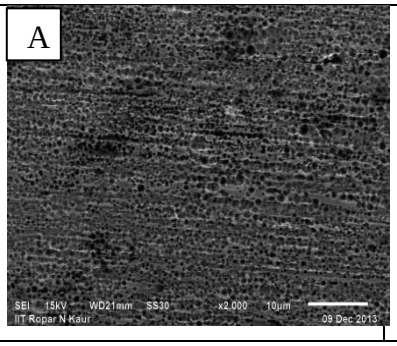	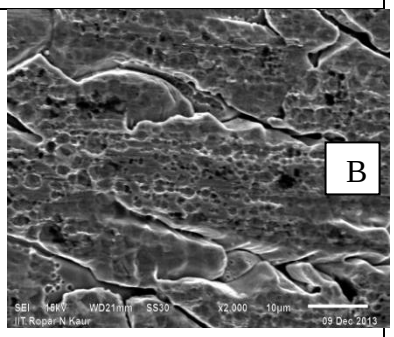
(160 A, 23 V, 4 mm/s, 12 l/min.) Heat input = 920 J/mm			
3	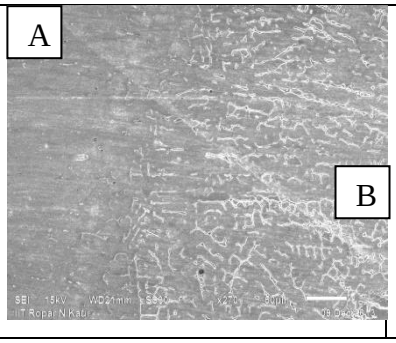	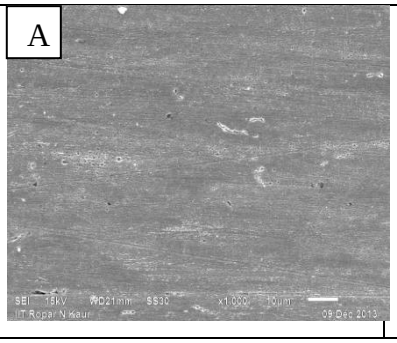	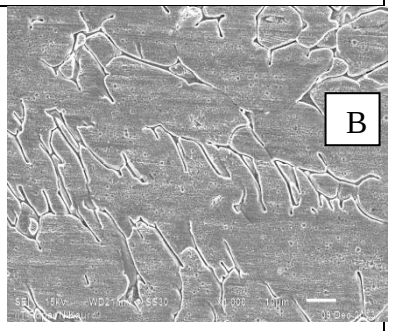
(140 A, 26 V, 4 mm/s, 16 l/min.) Heat input = 910 J/mm			
4	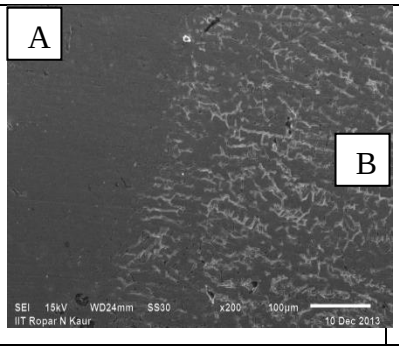	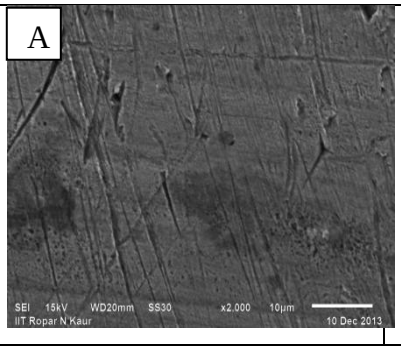	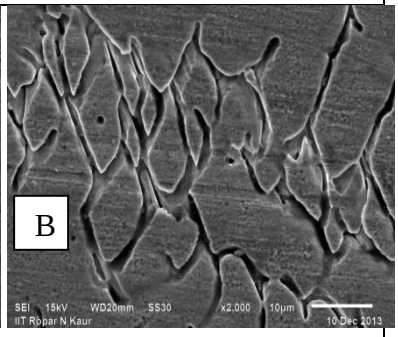
(180 A, 20 V, 4 mm/s, 16 l/min.) Heat input = 900 J/mm			

S N	SEM Micrograph at 250x of Fusion Boundary	SEM Micrograph at 1000x of HAZ (A)	SEM Micrograph at 2000x of Weld Zone (B)
5	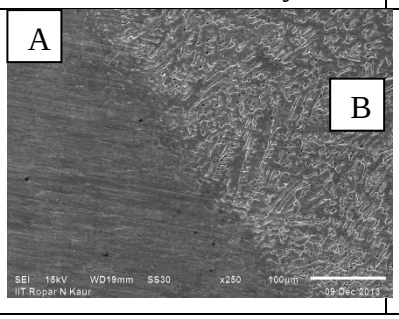	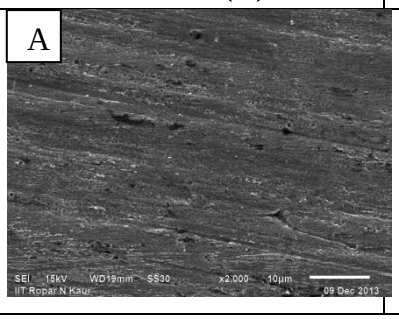	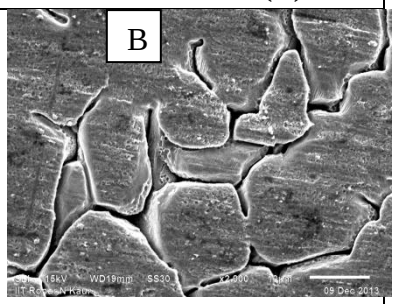
(180 A, 23 V, 6 mm/s, 8 l/min.) Heat input = 690 J/mm			
6	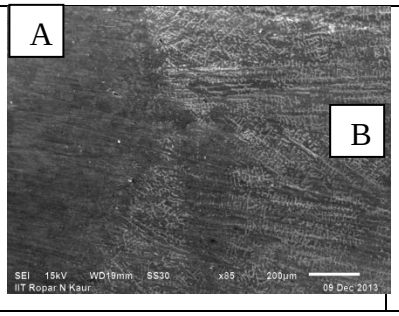	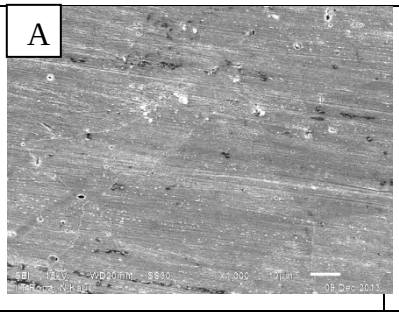	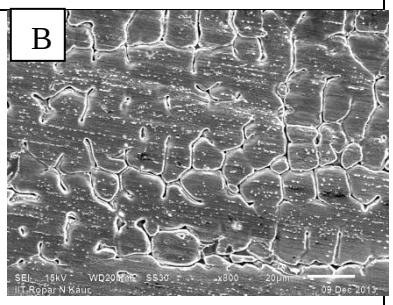
(180 A, 26 V, 2.5 mm/s, 12 l/min.) Heat input = 1872 J/mm			
7	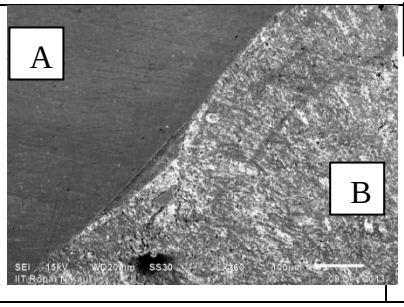	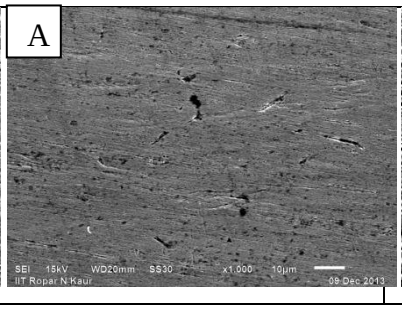	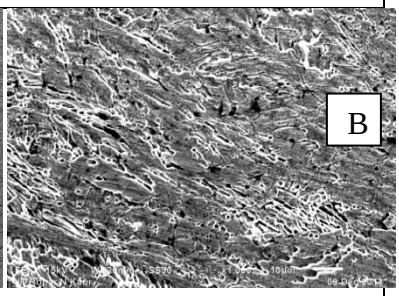
(200 A, 20 V, 6 mm/s, 12 l/min.) Heat input = 667 J/mm			
8	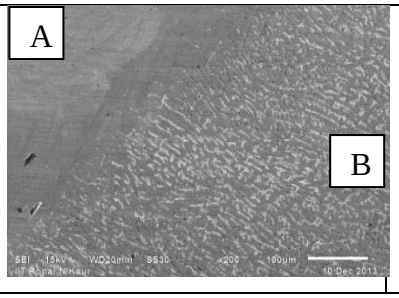	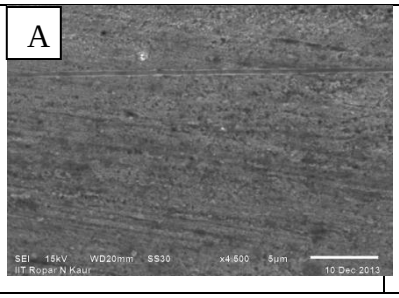	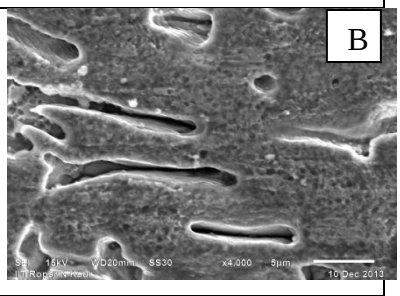
(200 A, 23 V, 2.5 mm/s, 16 l/min.) Heat input = 1840 J/mm			
9	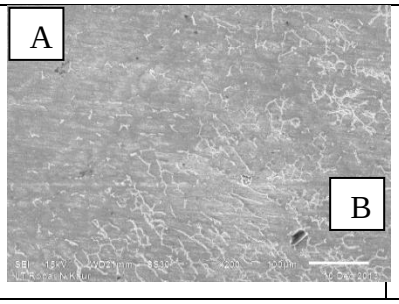	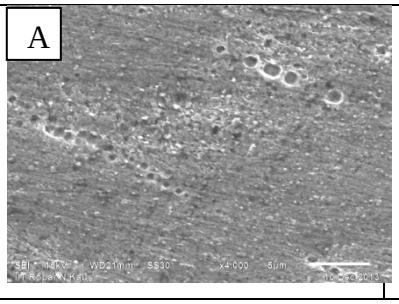	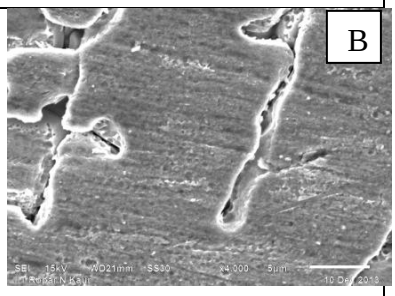
(200 A, 26 V, 4 mm/s, 8 l/min.) Heat input = 1300 J/mm			

Table 5.41 consists of SEM results of all welded specimens of AISI 316 stainless steel. The first column of the table shows the boundary of weld zone and heat affected zone of different welded specimens. Similarly in second and third column of the table shows the zoomed HAZ and weld zone respectively at different welding parameters. Heat affected zone is that portion of the base metal whose mechanical properties and microstructure altered by the heat of welding as it can be seen in second column of the table 5.41. Different microstructure of the weld zone depending on the different welding parameters and cooling rates are shown in the third column of the table 5.41. At high temperature the grain boundaries become weaken due to more heat input. The heat input due to different welding parameters is different in all the specimens and given below the SEM micrographs. It can be concluded from the table 5.41 that at maximum value of current, the grain size of the microstructure increases significantly as in the case of sample-9.

CHAPTER 6

CONCLUSION AND SCOPE FOR FUTURE WORK

6.1 CONCLUSION

It is intended to develop a simple and inexpensive single direction automatic GMAW setup. The present setup is used to deposited bead on plates and deposited bead is compared with manually deposited bead. Some of the conclusion are drawn and listed below:

- The constant gap between contact tube and workpiece is possible with the use of automatic setup.
- Uniform weld bead is obtained from the setup.
- Straight weld is possible as compared to manual one.
- Uniform deposition of weld metal gave good appearance.
- Uniform bead width as automatic setup move with guides.
- Low spatters are become possible with the present automatic setup.

Using the present fabricated setup effect of input parameters i.e. welding current, voltage, speed and gas flow rate on toughness microhardness and microstructural properties are observed. The following conclusions are drawn from the study:

- Impact test results for AISI 304 stainless steel shows that toughness at room temperature mainly depends on the value of welding speed. Toughness value is higher at lower welding speed and increases with the increase in value of voltage.
- Impact test results for AISI 304 at -20 °C shows that it mostly depends on the speed followed by voltage. Toughness value is maximum on and after 2.5 mm/s welding speed. Current has no effect on toughness value at this temperature.
- Impact test results for AISI 316 at room temperature shows that toughness increases as well as decreases in welded specimens as compare to base metal. Toughness is increases with the increase of voltage value up to the highest voltage (26 V).
- Impact test results for AISI 316 at -20 °C shows that it mostly depends on the voltage. Toughness value is maximum at 23 V welding voltage. Welding speed has no effect on toughness value at this temperature.

- Microhardness test results for AISI 304 stainless steel shows that there is slight increase in the value of microhardness for most of the welding combinations. HVN value first increases with increase in the value of voltage and then decrease. Lowest value of welding speed can provide maximum hardness.
- Microhardness test results for AISI 316 stainless steel shows that maximum value of microhardness is obtained at maximum welding speed. Welding speed is the most important parameter in effecting the value of said response and the maximum value of HVN is obtained for 6 mm/s.

6.2 SCOPE FOR FUTURE WORK

- In present study the automatic setup with single degree of freedom is fabricated and the same may be modified upto two or three degree of freedom so that parts with complicated shapes conveniently welded.
- Different ferrous and non ferrous may be welded by using to observe the improvement in weld quality.
- Similar and dissimilar metal may be welded to study the effect of different welding parameters on their microstructural and mechanical properties with the help of automatic fabricated setup.
- Shielding gas composition may be carried to study its effect on various properties of the steel.
- Tensile test, bending and reverse bending test etc. may also be carried along with other non-destructive tests like radiography, ultrasonic testing etc.

REFERENCES

1. B.S. Raghuwanshi, “A Course in Workshop Technology”, Dhanpat Rai and Company (P) Limited, 2009.
2. http://www.google.co.in/url?sa=t&rct=j&q=lincoln%20electric%20ppt&source=web&cd=1&cad=rja&sqi=2&ved=0CCsQFjAA&url=http%3A%2F%2Fwww.lincolnelectric.com%2Fen-us%2Feducation center%2FDocuments%2FArcWeldingBasics.ppt&ei=TBOXUdq-LsvIrQea-ICoDg&usg=AFQjCNFegT3sBfQDoG2sDGSyX3sX825OkA&bvm=bv.46751780,d.bmk
3. http://www1.gantep.edu.tr/~oyilmaz/Lecture%20Notes/ME%20473/Welding%20Processes_PartI.pdf
4. https://boc.com.au/boc_sp/au/downloads/reference_manuals/industrial/BOC_IPRM_S04-WeldProcesses.pdf
5. http://www.lincolnelectric.com/assets/global/Products/Consumable_MIGGMAWWires-SuperArc-SuperArcLA-75/c4200.pdf
6. https://www.google.co.in/search?q=schaeffler+diagram&espv=210&es_sm=93&source=lnms&tbm=isch&sa=X&ei=igW3UtmsOMGHrQeAy4G4AQ&ved=0CAkQ_AUoAQ&biw=1241&bih=583#facrc=_&imgdii=_&imgrc=G7Q5IwEACnIo5M%3A%3BQNe8wzQkid5A7M%3Bhttp%253A%252F%252Fwww.nhml.com%252Fimages%252Fresources_NHML_Martensite-Austenitic-Stainless_fig1.jpg%3Bhttp%253A%252F%252Fwww.nhml.com%252Fmartensite-in-austenitic-stainless-steel-welds.cfm%3B650%3B420
7. John Norrish, “Advanced welding Processes”, Woodhead Publishing Limited, 2006.
8. V.M. Radhakrishnan, “Welding Technology & Design”, New Age International publishers, 2008.
9. ASTM standard A-370 – standard testing methods and definitions for mechanical testing of steel products.
10. T.Kannan, J.Yoganandh, Effect of process parameters on clad bead geometry and its shape relationships of stainless steel claddings deposited by GMAW, International Journal Advance Manufacturing Technology, 2010, Vol. 47, pp. 1083–1095.
11. A.Ibrahim, S.A. Mohamat, A. Amir1, A. Ghalib, The Effect of Gas Metal Arc Welding (GMAW) processes on different welding parameters, Procedia Engineering, 2012, Vol. 41, pp. 1502–1506.

12. E. Karadeniz, U. Ozsarac, C. Yildiz, The effect of process parameters on penetration in gas metal arc welding processes, Materials and Design, 2007, Vol. 28, pp. 649–656.
13. L. Grad, J. Grum, I. Polajnar, J.M. Slabe, Feasibility study of acoustic signals for on-line monitoring in short circuit gas metal arc welding, International Journal of Machine Tools & Manufacture, 2004, Vol. 44, pp. 555–561.
14. P.J. Modenesi, R.I. Reis, A model for melting rate phenomena in GMA welding, Journal of Materials Processing Technology, 2007, Vol. 189, pp. 199–205.
15. G. Tham, M.Y. Yaakub, S.K. Abas, Y. Manurung, B.A. Jalil, Predicting the GMAW 3F T-Fillet Geometry and Its Welding Parameter, Procedia Engineering, 2012, Vol. 41, pp. 1794 – 1799.
16. S. Nansaarng, C. Chaisang, Influence of Parameters of Gas Metal Arc Welding on Macrostructures and Mechanical Properties of Austenitic Stainless Steels, WSEAS International Conference on system science and simulation in engineering, 2007, Vol. 21-23, pp. 144-152.
17. S. Kaewkuekool, B. Amornsin, A Study of Parameters Affecting to Mechanical Property of Dissimilar Welding between Stainless Steel (AISI 304) and Low Carbon Steel, WSEAS International Conference on materials science, 2008, pp. 105-109.
18. R. Sudhakaran, V. Vel-Murugan, P.S. Sivasakthivel, Effect of Process Parameters on Depth of Penetration in Gas Tungsten Arc Welded (GTAW) 202 Grade Stainless Steel Plates Using Response Surface Methodology, 2012, Vol. 9, pp. 64-79.
19. P.K. Giridharan, N. Murugan, Optimization of pulsed GTA welding process parameters for the welding of AISI 304L stainless steel sheets, International Journal of Advance Manufacturing Technologies, 2009, Vol. 40, pp. 478–489.
20. M. Vasudevan, M.V. Kuppuswamy, A.K. Bhaduri, Optimising process parameters for gas tungsten arc welding of an austenitic stainless steel using genetic algorithm, Transactions of The Indian Institute of Metals, 2010, Vol. 63, pp. 1-10.
21. J. Shang, K. Wang, Q. Zhou, D. Zhang, J. Huang, G. Li, Microstructure characteristics and mechanical properties of cold metal transfer welding Mg/Al dissimilar metals, Materials and Design, 2012, Vol. 34, pp. 559–565.
22. Y. Ruan, X.M. Qiu, W.B. Gong, D.Q. Sun, Y.P. Li, Mechanical properties and microstructures of 6082-T6 joint welded by twin wire metal inert gas arc welding with the SiO2 flux, Materials and Design, 2012, Vol. 35, pp. 20–24.

23. E. Zumelzu, J. Sepulveda, M. Ibarra, Influence of microstructure on the mechanical behaviour of welded 316 L SS joints, Journal of Materials Processing Technology, 1999, Vol. 94, pp. 36–40.
24. A. Klimpel, L.A. Dobrzanski, D. Janicki, A. Lisiecki, Abrasion resistance of GMA metal cored wires surfaced deposits, Journal of Materials Processing Technology, 2005, Vol. 164–165, pp. 1056–1061.
25. A.M. Torbati, R.M. Miranda, L. Quintino, S. Williams, D. Yapp, Optimization procedures for GMAW of bimetal pipes, Journal of Materials Processing Technology, 2011, Vol. 211, pp. 1112–1116.
26. R. Yilmaz, H. Uzun, Mechanical properties of austenitic stainless steels welded by GMAW and GTAW, Journal of Marmara for Pure and Applied Science, 2002, Vol. 18, pp. 97-113.
27. K. Sittichai, N. Santirat, P. Sompong, A Study of Gas Metal Arc Welding Affecting Mechanical Properties of Austenitic Stainless Steel AISI 304, World Academy of Science, Engineering and Technology, 2012, Vol. 61, pp. 402-405.
28. X.H. Ha, S.W. Jang, W.H. Bang, U. Yoon, K.H. Oh, Texture Evolution in Weld Regions of SUS-304 Stainless Steel and TRIP Steel, Materials Science Forum, 2002, Vol. 408-412, pp. 1377-1382.
29. E.S. Puchi-Cabrera, R.A. Saya-Gamboa, J.G. La Barbera-Sosa, M.H. Staia, V. Ignoto Cardinale, J.A. Berríos-Ortiz, G. Mesmacque, Fatigue life of AISI 316L stainless steel welded joints, obtained by GMAW, Welding International, 2009, Vol. 23, pp. 778-788.
30. J. Choi, J. Mazumder, Numerical and experimental analysis for solidification and residual stress in the GMAW process for AISI 304 stainless steel, Journal of Materials Science, 2002, Vol. 37, pp. 2143 – 2158.
31. H.J. Aval, A. Farzadi, S. Serajzadeh, A.H. Kokabi, Theoretical and experimental study of microstructures and weld pool geometry during GTAW of 304 stainless steel, International Journal of Advance Manufacturing Technologies, 2009, Vol. 42, pp. 1043-1051.
32. H.J. Aval, S. Serajzadeh, A.H. Kokabi, Prediction of Grain Growth Behaviour in HAZ During Gas Tungsten Arc Welding of 304 Stainless Steel, *Journal* of Materials Engineering and Performance, 2009, Vol. 18, pp. 1193–1200.
33. J. Feng, L.Li, Y. Chen, Z. Lei, H. Qin, Y. Li, Effects of welding velocity on the impact behavior of droplets in gas metal arc welding, Journal of Materials Processing Technology, 2012, Vol. 212, pp. 2163– 2172.

34. P.K. Ghosh, L. Dorn, S. Kulkarni, F. Hofmann, Arc characteristics and behaviour of metal transfer in pulsed current GMA welding of stainless steel, Journal of Materials Processing Technology, 2009, Vol. 209, pp. 1262–1274.
35. K. Luksa, Influence of weld imperfection on short circuit GMA welding arc stability, Journal of Materials Processing Technology, 2006, Vol. 175, pp. 285–290.
36. A. Gulenc, K. Develi, N. Kahraman, A. Durgutlu, Experimental study of the effect of hydrogen in argon as a shielding gas in MIG welding of austenitic stainless steel, International Journal of Hydrogen Energy, 2005, Vol. 30, pp. 1475 – 1481.
37. A.Y. Kang, Y.K.D.V. Prasad, M.J. Kang, H.J. Kim, I.S. Kim, Characteristics of alternate supply of shielding gases in aluminium GMA welding, Journal of Materials Processing Technology, 2009, Vol. 209, pp. 4716–4721.
38. R.E. Trevisan, E. Braga, H.C. Fals, Effects of nitrogen and pulsed mean welding current in AISI 316 austenitic steel solidification cracks, Welding International, 2003, Vol. 17, pp. 298-302.
39. R.S. Parmar, "Welding processes and technology", Khanna Publishers, 1997.
40. P.N. Rao, "Manufacturing Technology- Vol. 1", 3rd edition., Tata Mc-Graw Hill, New Delhi, 2009.